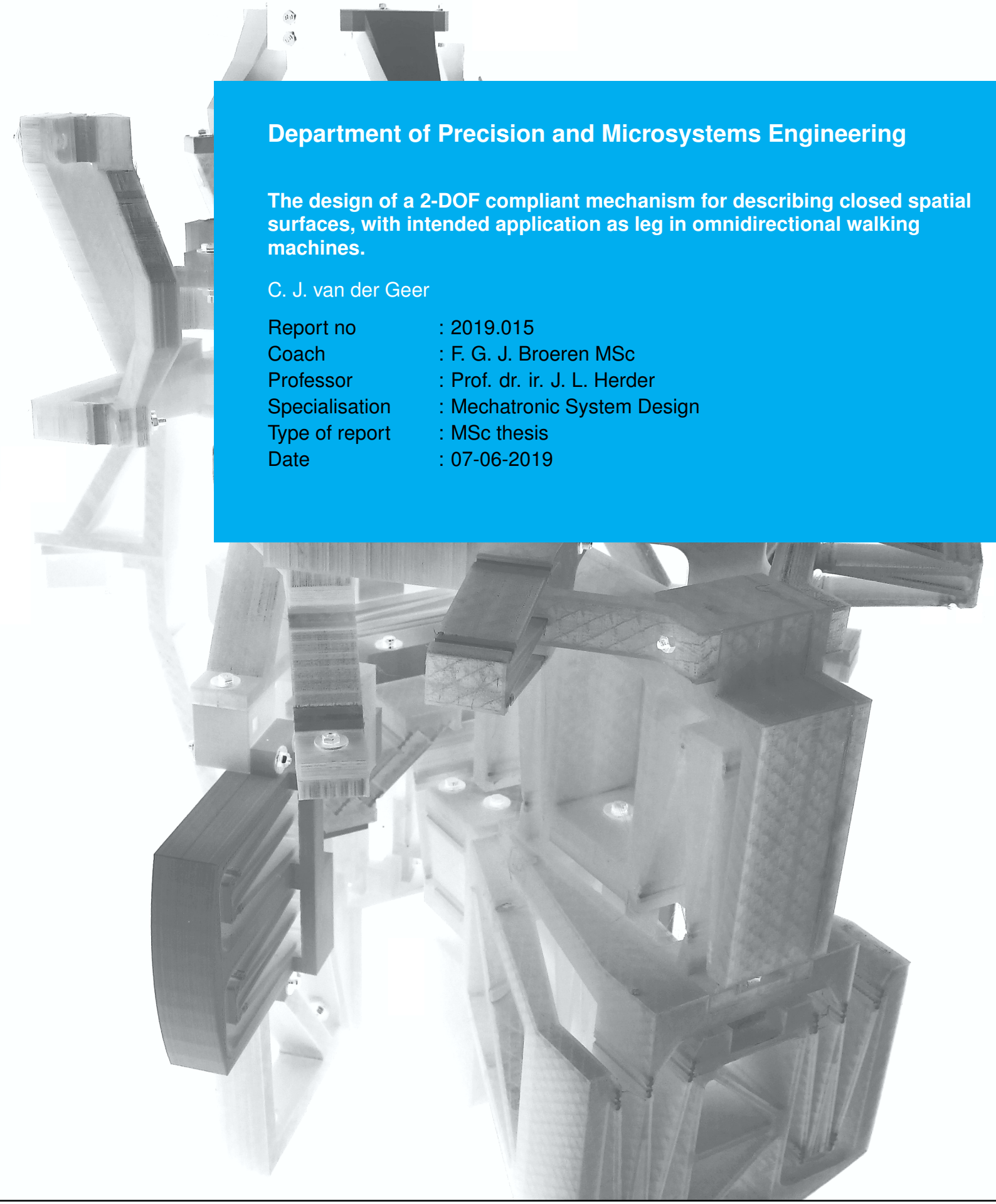

Department of Precision and Microsystems Engineering

The design of a 2-DOF compliant mechanism for describing closed spatial surfaces, with intended application as leg in omnidirectional walking machines.

C. J. van der Geer

Report no	: 2019.015
Coach	: F. G. J. Broeren MSc
Professor	: Prof. dr. ir. J. L. Herder
Specialisation	: Mechatronic System Design
Type of report	: MSc thesis
Date	: 07-06-2019

TU Delft Delft University of Technology

Challenge the future

Preface

This report presents a literature review, accompanied by the design of a spatial compliant mechanism. The literature review presents a quantitative analysis on the field of walking machines. By assuming these devices are limited to planar degrees of freedom, a categorization and analysis of a considerable sample size provides an insight into the more and less frequently occurring types of designs. The consecutively presented work is the design of a 2-DOF compliant mechanism for describing closed spatial surfaces. This mechanism finds use as leg in an omnidirectional walking machine, of which its rarity is stated by the literature review. Next to the kinematic and physical design of the leg itself, a conceptual design of the coupling of such a device is also presented, proving its applicability to walking machines.

I would hereby like to thank the people that have supported and inspired me in the process of this project. First of all Just Herder for supporting my initially rather under defined description of the project, granting me the trust and opportunity to explore this field of research. Secondly, a big thanks to Freek Broeren for his availability, his time and energy spent on the support of this project. Thirdly, the lab-support for providing the space, help and tools in the production phase of the mechanism.

A little less obvious, but I would also like to thank my friends for their generous mental support, my dad for inspiring me to chase any ambition and my mom for her persisting love and interest.

Delft, The Netherlands
June, 2019

C.J. van der Geer

Contents

Chapter 1

Introduction

1.1 Background

Walking Machines (WMs) are and have been an active field of research and design. Over the past decades various researchers and designers have been adding their knowledge and creativity to the field. Each of them focussing on various aspects and forms of application of these machines. One can define several categories: Machines designed for dexterity on uneven surfaces, machines with a focus on simplicity and efficiency and statically stable machines, with relatively little actuation. Notable contributions in the first direction include the work on the Adaptive Suspension Vehicle in the 1980s, by Song and Waldron [143], the Dante II project [9] and Big Dog by Boston Dynamics [118]. In another side of the field, with a focus on simplicity and efficiency, notable contributions were made by T. McGeer in the 1990s [96] on a two dimensional passive-dynamic walking robot, and S. H. Collins, M. Wisse and A. Ruina with their work on a three-dimensional version [26]. Next to these two, examples of statically stable walking machines involve Dutch artist Theo Jansen his Strandbeest [71] and a more optimized variant by A. Ghassei [42]. Machines based on the linkage by J. Klann [69] and Chebyshev [80] also belong to this area.

Looking at WMs more abstractly, one could say these machines are bound to their supporting surface and thus be considered to be limited to three planar degrees of freedom. Having stated this, one can accordingly categorize walking machines by their degrees of freedom (DOFs) and levels of actuation. This previously undiscussed categorization leads to new insights. As will be seen from the literature study in chapter 2, it appears that relatively little of current WM designs can be categorized as *fully actuated, TT* in this manner. These are walking machines which have two actuators to translate themselves in any direction at any point in time and are in that sense perfectly, or fully actuated.

The definition of a WM here, is taken to be: "A device able to propagate along a(n) (almost) horizontal plane, making use of a single or multiple supporting mechanisms which are intermittently in contact with the supporting surface. The support mechanisms or 'legs' in contact with the surface support the structure under the influence of gravity, while the (centre of mass of the) machine is allowed to move parallel with respect to the plane.".

With the advances in the field of additive manufacturing, the production of complex structures and mechanisms is continuously becoming less problematic. Knowing that walking machines are inherently more complex than their wheeled counterparts, designing for additive manufacturing seems ideal. More precisely, a monolithic design seems ideal since this means that no assembly would be needed. With this, conventional hinging elements would need to be substituted by compliant mechanisms (CMs).

The idea of a compliant walking machine is not new. M. Plecnik has presented the world an example of such a device already [113]. Just as well as J. Mantzel [91] has presented the design and production of a rather effective fully actuated TT WM. However, up until now there has been no report of a fully actuated, compliant, TT walking machine. This is the main reason for the design of a mechanism suitable for use as leg for such a walking machine was designed, and presented in this thesis.

In order for such a device to be competitive with one of its closest relatives; machines utilizing (omnidirectional) wheels for their locomotion, an important requirement would be for the machine to show little displacement of its centre of mass (COM) in the direction perpendicular to its supporting surface. This produces stability and a comparable motion behaviour. To obtain this, a strategy is applied which focusses on the leg mechanism producing

an approximately straight line, or planar surface during the support phase. Consequently, the influence of the leg path on the vibrations of the COM will be limited. Furthermore, since the leg mechanisms should per definition intermittently contact the supporting surface, a proper coupling of a multitude of these mechanisms is required. This report will therefore shortly elaborate on a conceptual manner of coupling the presented mechanism as well.

Concluding, although WMs are and have been an active field of research, no report of a fully actuated compliant walking machine capable of holonomically translating in any direction has surfaced up until now. With the advances in additive manufacturing and the advantages of compliant mechanisms, the design and fabrication of such an inherently complex mechanism becomes feasible and seemingly advantageous. Therefore, this report will present a kinematic and physical design of a mechanism and conceptual coupling thereof, capable of describing a closed spatial surface. This can find use as leg in such an omnidirectional walking machine.

The analysis of a kinematic model will prove the functioning of the device, measurements on the physical design will qualitatively confirm its performance and a further analysis will indicate the most prominent improvement directions. This is done without taking into account external loads.

1.2 Report structure

The report is structured by means of two individual papers providing the main contents. This part is concluded with an extended discussion, which provides additional insights into the design process and proposes directions for future work. In the added appendices a more detailed overview of the processes and their results are given. The first paper, a literature review in chapter 2, indicates a gap in the types of WM designs currently reported of. The second paper in chapter 3 presents the work done on "The design of a 2-DOF compliant mechanism for describing closed spatial surfaces, with intended application as leg in omnidirectional walking machines". This works towards filling the indicated gap in literature.
The appendices broadly follow the design process which is displayed in figure fig. 1.1. Each of the steps displayed in this figure are elaborated on in their respective appendix. Appendix G provides enlarged versions of figures as earlier presented in the papers as well as additional visual material of the project.
Shortly walking through the process, the project definition involved setting up the general design objectives and lists of requirements. With the kinematic design of the simplified mechanism several iterations and abstraction steps were done. This to eventually be able to come up with a set of functions, strategies and solution directions as displayed in the abstraction appendix. Next, the kinematic design of the final mechanism was performed. In order to verify the design and its performance, this design was converted into a physical compliant system and tested as presented in appendices E and F.

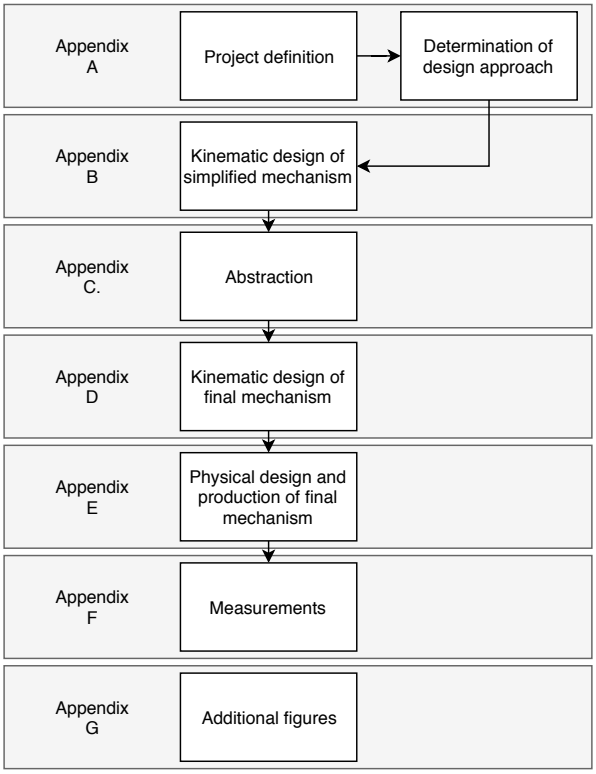

Figure 1.1: Design flowchart with a general overview of the design steps.

Chapter 2

A quantitative analysis in the field of walking machines.

A categorization based upon the view that these machines are limited to planar DOFs.

2.1 Abstract

Walking machines are and have been studied intensively. Several reviews have already been executed on this subject [60, 83, 87]. Plenty of these walking machines described in literature are said to be able to better handle 'rough' terrain than their wheeled counterparts [142, 43, 90, 83, 59, 51, 3, 137]. This is seen as an advantage of walking machines over wheeled machines. However, other research has also been done on for instance passive walking machines [26, 96], where the focus is a bit different. As the definition of a walking machine seems rather under defined, this paper firstly introduces a precise description of such a machine. Secondly, it briefly orders and elaborates on the current and past research directions and used terms to identify the machine under study. Finally, a new way of categorizing walking machines is proposed and put to practice. This categorization is based upon the view that walking machines are bound to their supporting surface and can thus be considered to be limited to three planar degrees of freedom. After categorization of a considerable sample size, we point out under-represented classes of walking machines which could benefit from further study.

2.2 Introduction

The vast amount of research and design on walking machines (*WMs*) is broadly speaking done in three main directions or categories. The first of these has a focus on machines with dexterity on uneven surfaces, the second has a focus on simplicity and efficiency, utilizing a passive dynamic walking motion and a third category comprises statically stable machines with relatively little actuation. Notable contributions on the first category include the work on the Adaptive Suspension Vehicle in the 1980s, by Song and Waldron [143], the Dante II project [9] and Big Dog by Boston Dynamics [118]. In the field of passive walking machines, notable contributions were made by S. H. Collins, M. Wisse and A. Ruina with their work on a three-dimensional passive-dynamic walking robot with two legs and knees[26] inspired by the work of McGeer in the 1990s [96] on a two dimensional version, which formed the inspiration of the previous. Examples of the statically stable machines involve the Strandbeest by Dutch artist Theo Jansen [71] and a more optimized variant by A. Ghassei [42]. Of course machines based on the linkage by J. Klann [69] and Chebyshev [72] also belong to this area.

As no all-embracing or specific enough definition of the concept of walking machines was found, the definition this report adheres to is taken to be the following:

"Devices able to propagate along a(n) (almost) horizontal plane, making use of a single or multiple supporting mechanisms which are intermittently in contact with the supporting surface. The support mechanisms or 'legs' in contact with the surface support the structure under the influence of gravity, while the (center of mass of the) machine is allowed to move parallel with respect to the plane."

In this paper, first the currently used terms to define and distinguish walking machines will be briefly discussed. Secondly, a new categorization is proposed and put into practice using a considerable number of *WM* examples. From this an insight is created regarding more or less common types of *WMs*. This categorization is based upon the view that *WMs* are bound to their supporting surface. Herewith, the maximum degrees of freedom (*DOFs*) of such a machine are three planar *DOFs*. By matching the *DOFs* of the system with the number of actuators present in the system, one can determine the according level of actuation of the machine. This is a bit different from the common practice as in general, the degrees of freedom and the level of actuation of the discussed *WMs* are related to the number of joints, links and actuators present in the system.
Additionally, possibly due to a too unspecific general definition of *WMs*, plenty of the machines in the dataset were named walking machine or the like, but had wheels incorporated in their designs. For this reason, an additional section is devoted to 'wheeled walking machines'. These wheeled machines are categorized in the same manner as the non-wheeled.

Finally, we analyse the results and discuss the findings, indicating which categories are well-represented and which are not.

2.3 Methods

2.3.1 Search methods

A literature and patent search were executed. For both, the used search terms were a combination of *walking* or *legged* and *machine*, *mechanism*, *robot*, *vehicle* or *device*. Relevant patents and papers were selected and their references explored.

2.3.2 Categorization

Firstly, an overview of the current categories and identifiers of *WMs* was made based on the collected literature. Secondly, in order to find out a more general underlying connection between the machines under consideration, an attempt to more abstractly formulate the purpose of *WMs* was made. This created the proposed vision and thus method of categorizing *WMs*. After putting the categorization into practice, various insights into the more and less common types of *WMs* were gained.

2.4 Overview

2.4.1 Existing categories

Currently, *WMs* commonly get classified based upon three properties. One depends on the type of stability of the machine. The second on the number of legs and the third upon the type of actuation. We will discuss each of these one by one.

Stability type

Firstly, *WMs* can be classified as being statically stable or dynamically stable. Statically stable *WMs* are in line with the definition for static stability in "ideal legged locomotion machines" as by McGhee [97]:

"An ideal legged locomotion machine is statically stable at time t if all legs in contact with the support plane at the given time remain in contact with that plane when all legs of the machine are fixed at their locations at time t and the translational and rotational velocities of the resulting rigid body are simultaneously reduced to zero."

This can be achieved by making sure the vertical projection of the centre of gravity is within the so called support pattern. This is defined by the area between the points in contact with the (horizontal) supporting surface [97]. McGhee also states that for the same "ideal legged locomotion machine, the minimum number of legs required to achieve a gait with a strictly positive static stability margin at all times is equal to three. If the time required to transfer a leg contact point to a new position is greater than zero, the number is four." This is based on the definition of the "ideal legged locomotion machine":

"An ideal legged locomotion machine is a rigid body to which are attached a specified number n of massless legs. The length of each leg is arbitrarily controllable. Each leg contacts the supporting surface at a point and can exert an arbitrary force directed into this surface. Arbitrary moments can be applied to the body by any leg subject only to the constraint that no moment be applied to the supporting surface at any leg contact point."[97]

This definition of an ideal legged motion machine shows strong resemblance with the definition of a walking machine as proposed within this study. However, it is not all-embracing considering that for some machines it holds that the physical legs are not adequately modelled as single point contacts. These hold the name of walking machine nevertheless. Thus, the devices described by McGhee exclude several machines deemed relevant in this study.
In a dynamically stable *WM*: "compensation of tipping motions takes place over time." [125]. So the centre of mass can be outside of the support pattern, but the tipping motion this induces has to continuously be compensated.

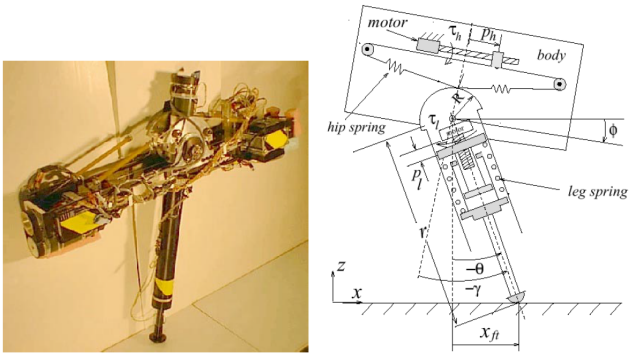

Figure 2.1: ARL monopod II as by Buehler, 2001 [17]

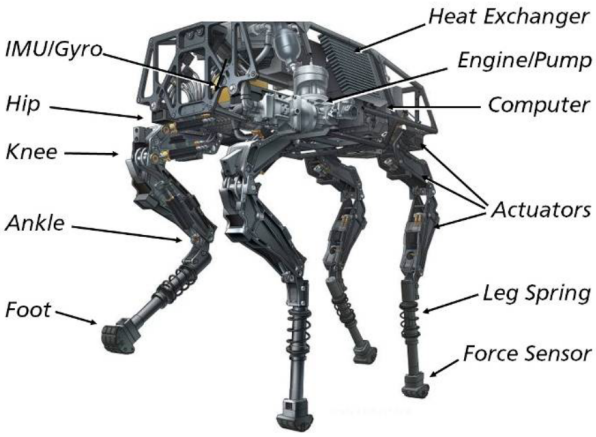

Figure 2.2: Active Quadruped WM "BigDog" by Boston Dynamics, Raibert et al. [118]

Figure 2.3: One of Theo Jansen his "Strandbeesten" [71] with a large number of legs.

Number of legs

It is also common practice to define the type of *WM* by the number of legs it possesses. This can be a single up to a grand multitude of legs. As an example for a single legged *WM*, take the ARL monopod as displayed in figure 2.1. A machine with a larger number of legs, as designed and created by Dutch artist Theo Jansen is displayed in figure 2.3. Referring to the monopod, this system can not be statically stable due to its single leg design and thus has to be dynamically stable in order to function.

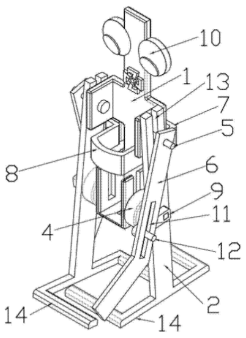

Figure 2.4: Biped WM as by Z. Nan [104]

Leg designs as for instance by Z. Nan [104], as displayed in figure 2.4 indicate the need for a wider definition of the term leg. Due to the large contact area with the supporting surface with respect to the body size, the physical legs of the machine can not be accurately modelled to have a single contact point with the supporting surface. This study desires to include these type of machines nevertheless and therefore deviates from the definition of an ideal legged locomotion machine as by McGhee. A more famous example of these surface contact footed *WMs* is for instance ASIMO by Honda[131].

Actuation type

Concerning the actuation type, in general two types can be distinguished: passive and active *WMs*. Passive *WMs* are mechanisms for which "gravity and natural dynamics alone generate the walking cycle"[96]. Active *WMs* are then walking machines for which this does not hold. Passive *WMs* are generally explicitly named to be passive. An example of a passive system is given in figure 2.5, which was said to function best on a five meter ramp with an inclination of 3.1 degrees [26]. One example of an active/actuated walking machine is the earlier discussed monopod (figure 2.1), but a representative example of such a machine with more legs is for instance BigDog by Boston Dynamics, see figure 2.2 as from the paper by Raibert et al. [118] Machines like this are designed for static and dynamic stability, depending on the gait.

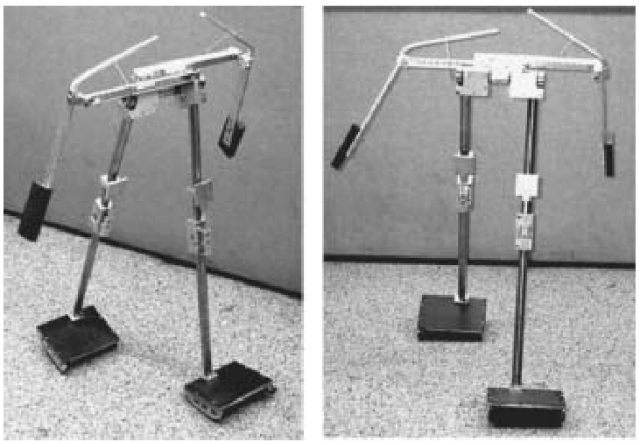

Figure 2.5: Passive biped WM as by Collins et al. [26]

2.4.2 Categorization

This section proposes a categorization and presents the gathered designs in their corresponding categories.

Definition

In addition to a system being active, a more precise categorization can be made. As with (actuated) mechanisms in general, a *WM* can be categorized as follows:

- over-actuated
- fully actuated
- under-actuated
- passive (un-actuated)

To determine the level of actuation a light has to be shed upon the degrees of freedom of walking machines. As stated by Westervelt et al. (p. 11 [162]), "Bipeds are typically high degree of freedom (DOF) mechanisms but the task of biped walking is inherently a low DOF task - transportation of the robot's center of mass (COM) from one point to another.". This was also briefly mentioned by Waldron and Mcghee, [158].

Approaching Westervelt's quote from a fundamental point of view, it is taken that the task of *WMs* in general is to transport the COM of the system from one point to another, parallel to its supporting surface. With this assumed, the minimum movement can be a single translation of the COM. A single rotation does not induce transportation of the COM along the supporting plane, so is only considered in combination with a translational DOF. The maximum number of movements in this point of view can be two respective translations *T*, parallel to the supporting plane, combined with a rotation *R* around a normal vector of the supporting plane. See the top view of a representation of a machine and its DOFs in figure 2.6. Now, the rotation becomes relevant as it adjusts the path of the machine. All possible combinations are represented in table 2.1.

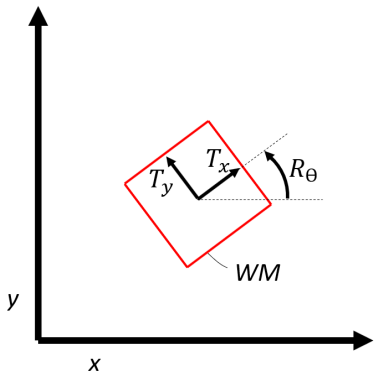

Figure 2.6: Schematic top view of WM, showing the degrees of freedom (T_x, T_y and R_θ) under the unilateral surface constraint.

As, according to this view, *WMs* can be designed for each of the in the table given combinations of DOFs,

the actuation level depends on the DOFs of the actual machine under the surface constraint. Here, over-actuation describes the *WMs* having more actuators than the degrees of freedom the walking machine possesses, being limited by the surface constraint. Fully actuated and under-actuated *WMs* respectively have as many actuators as the machine has DOFs and less actuators. Un-actuated *WMs* have no actuators mounted.

DoFs	Combinations	
1	*T*	
2	*TR*	*TT*
3	*TTR*	

Table 2.1: Degrees of freedom of the entire machine.

Combining the DOFs with the level of actuation in a single table lists all possible categories, see table 2.2. In relation with the active vs passive categorization as commonly used, un-actuated *WMs* are passive and the other levels split up the "active" category in three. An additional note is that with one degree of freedom, the T_P category equals T_U as underactuation with one DOF automatically means no actuators are present.

DoFs	Passive	Under-actuated	Fully actuated	Over-actuated
1, T		$T_{P,U}$	T_F	T_O
2, TT	TT_P	TT_U	TT_F	TT_O
2, TR	TR_P	TR_U	TR_F	TR_O
3, TTR	TTR_P	TTR_U	TTR_F	TTR_O

Table 2.2: Categorization of walking machines.

In this table the lettering indicates the DOFs of the *WM* and the subscripts indicate the actuation category. All found machine designs deemed *WM* can be categorized in either one of the groups indicated in this table.

Interestingly enough, the definition of a walking machine as introduced in section 2.2 does not necessarily exclude the use of wheels in the machine designs. This was also reflected in the titles of the found documents, where machines with incorporated wheels were named *WM* just as well as machines without. Therefore, a categorization of purely legged *WMs* and wheeled 'walking machines' is made.
In addition, to indicate another distinguishing element between *WMs* in the view of this categorization, systems which rely on a velocity differential which rely on steering are indicated. With the devices being referred to as a 'differential' and 'steering' *WM* or the like respectively.

2.4.3 Results

Counting purely legged walking machines

Table 2.3 shows the number of purely legged, *WMs* that have been found in this study, for each category. As can be seen in this table, the T_F, TR_O and TTR_O are well represented. Furthermore, an absence of designs in the multi-DOF, passive and under-actuated categories and the TTR_F category becomes clear.

DOFs	Passive	Under-actuated	Fully actuated	Over-actuated
1, T		3	31	8
2, TT	0	0	1	1
2, TR	0	0	14	40
3, TTR	0	0	0	38

Table 2.3: Number of patents and in literature described WMs found in this study, in the corresponding category.

The machines in table 2.3 within the TR category, are machines that depend on a difference in velocity of the two respective sides of the *WM* to rotate.The *WMs* using steering are listed in table 2.4, since a steering mechanism induces a rotation, the purely translational systems are left out of the table. For a graphical indication of the two respective systems see figures 2.10,2.11 and 2.13. For an example of a T_P system see figure 2.5, an example of a T_F system is given in figures 2.3 and 2.7 and an example of a T_O system is given in figure 2.1. A note on this last system is that during operation, it is constrained in sideways (T_y [fig. 2.6]) direction. Both TT systems are visualized in figures 2.8 and 2.9, for a broader explanation of the working principle reference is made to their sources [91, 144]. Lastly, one finds an example of the TTR_O systems in figure 2.2. Note that, in this study, literature describing leg designs with the purpose of being part of a walking machine are also taken into account in this categorization. Only though, if it can be determined in what category the machine would ultimately fall.

DoFs	Passive	Under-actuated	Fully actuated	Over-actuated
2, TR			[54, 89] [129]	[5] [14]
3, TTR				

Table 2.4: Patents and in literature described WMs found in this study, in the corresponding category.

T_F example

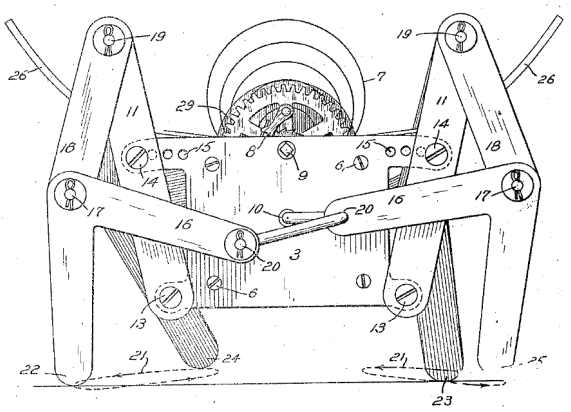

Figure 2.7: "Quadruped walking mechanism" as by Dunshee, 1926 [32]. A T_F WM.

TT_F example

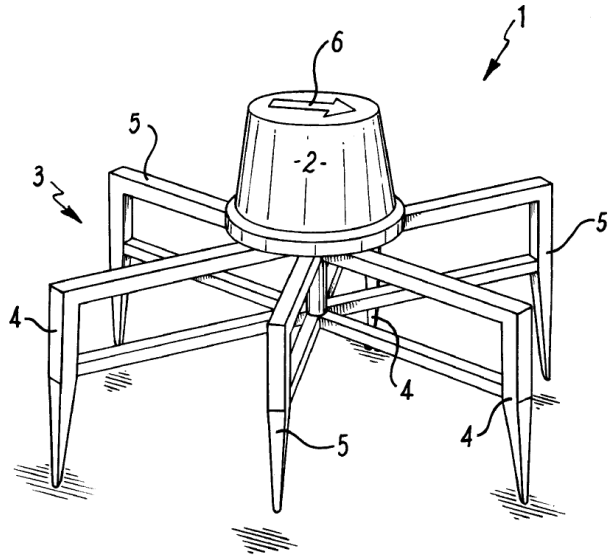

Figure 2.8: "Walking machine" as by Mantzel, 2014 [91]. A TT_F WM.

TT_O example

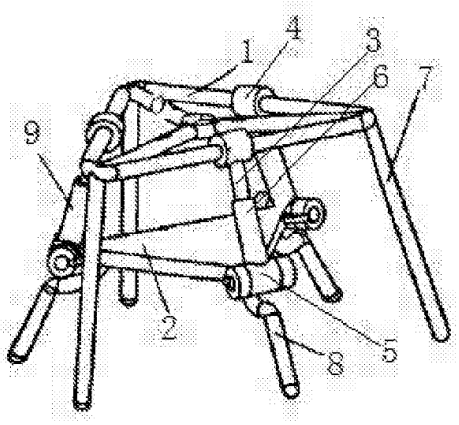

Figure 2.9: "Multi-legged walking robot based on 3-RPC parallel mechanism" as by Songhao, 2017 [144]. A TT_O WM.

TR_F examples

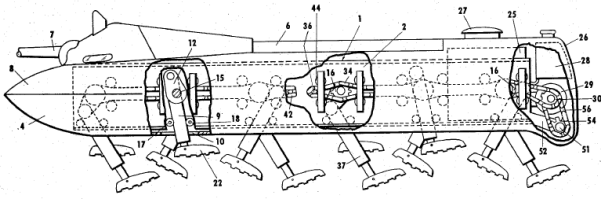

Figure 2.10: Side view of "Amphibious walking vehicle" as by Barr, 1959 [12]. An example of a TR_F Walking Machine.

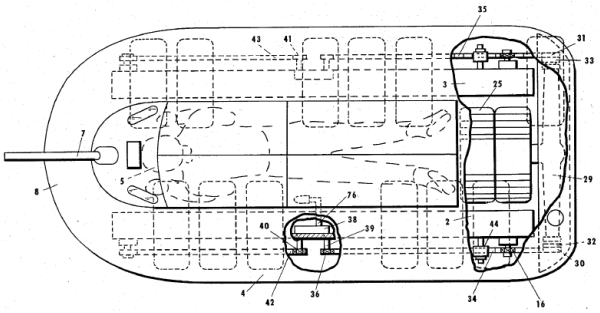

Figure 2.11: Top view of "Amphibious walking vehicle" as by Barr, 1959 [12]. An example of a TR_F Walking Machine.

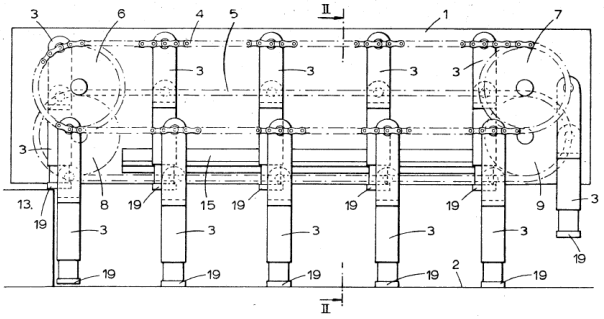

Figure 2.12: "Walking machine" as by Thring, 1970 [151].

TR_F Steering example

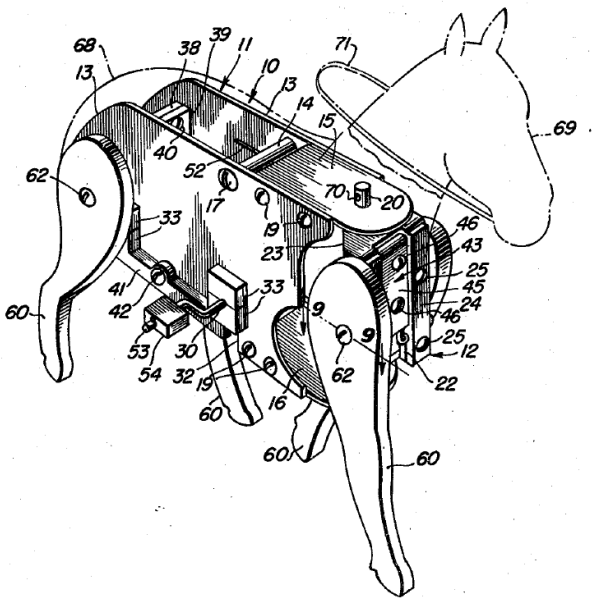

Figure 2.13: "Mechanical walking animal" as by Manfredi, 1948 [89]. A TR_F WM with implemented steering.

Counting wheeled 'walking machines'.

Various 'walking machine' designs incorporating wheels for their locomotion were also found. Categorizing these in the same manner as before gives table 2.5. The examples of these machines are given in figures 2.15, 2.14, 2.17 and 2.16. A significant difference within the category of these wheeled machines concerns whether the legs support the weight of the machine or not. The machines with non-supporting legs were excluded from table 2.5 as these are not in line with the definition of a *WM* in section 2.2, an example of such a non-supporting leg mechanism is given in figure 2.18. Also excluded from table 2.5 are machines like described in [37], as displayed in figure 2.19. Although the title of the patent reads "Walking wheeled vehicle", the emphasis for propelling the vehicle lies with the wheels instead of the 'leg mechanism'. The main goal of the walking behaviour of the machine is to overcome obstacles larger that the wheels allow.

DoFs	Passive	Under-actuated	Fully actuated	Over-actuated
1, T			[21, 116, 74] [36, 68]	
2, TT				
2, TR			[34, 146, 152] [93, 128, 61] [122, 99, 109] [78]	[165]
3, TTR				

Table 2.5: Wheeled 'Walking Machines' in their corresponding category, partialy wheeled systems (as in figures 2.16 and 2.17) are underlined. All found TR-systems depend on steering for their rotation.

T_F Wheeled example

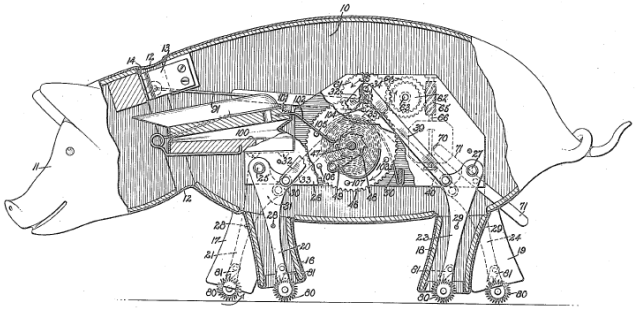

Figure 2.15: "Figure wheeled toy" as by Cardinal, 1917 [21]. An example of a T_F wheeled 'walking machine'.

TR_O Partially wheeled Steering example

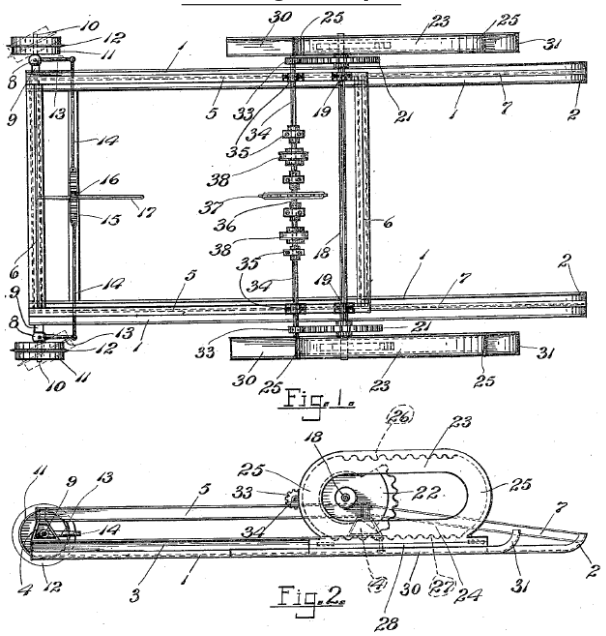

Figure 2.16: "Walking machine" as by Wilson, 1918 [165]. An example of a TR_O partially-wheeled steering 'Walking Machine'.

TR_F Wheeled steering example

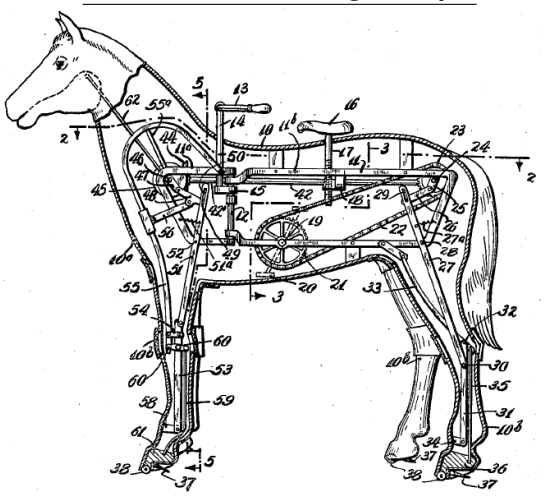

Figure 2.14: "Mechanical animal" as by Kurelic, 1938 [78]. An example of a TR_F wheeled steering 'Walking Machine'.

TR_F Partially wheeled Steering example

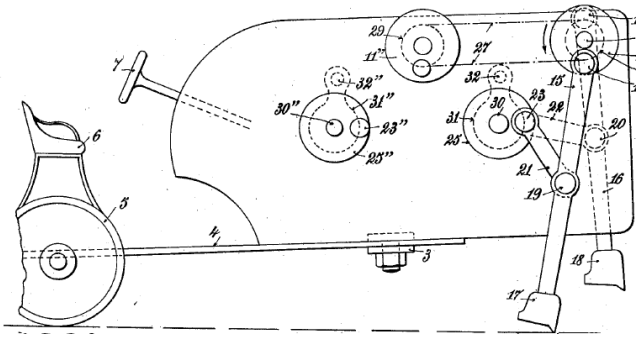

Figure 2.17: "Motor tractor with propulsive levers" as by Mauger, 1921 [93]. An example of a TR_F partially-wheeled steering 'Walking Machine'.

Machines considered irrelevant

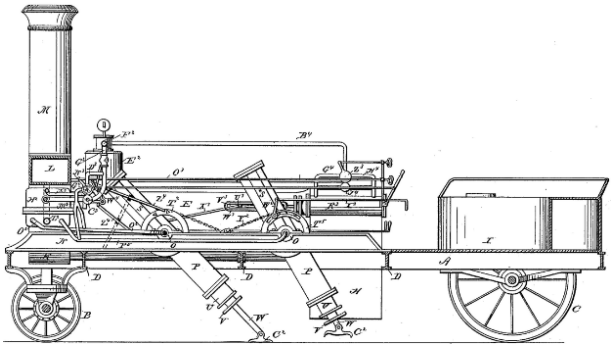

Figure 2.18: "Traction engine" as by Richardson, 1883 [124]. A machine showing strong resemblance with a wheeled WM, but without supporting legs.

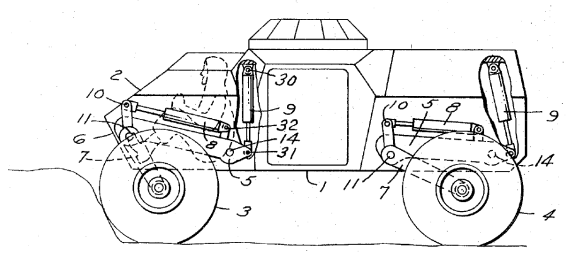

Figure 2.19: "Walking wheeled vehicle" as by Williams et al., 1974 [37]. An example of a TR_O wheeled (steering) machine with too little focus on walking locomotion to be considered relevant.

2.5 Discussion

Where other reviews [60, 83, 87] remain rather conceptual or qualitative, this study attempts to provide an more quantitative analysis of the distribution of *WM*-type designs within the set framework of categories.

2.5.1 Discussion of results

Various conclusions can be drawn from the results. For references, see tables 2.3 and 2.6. What stands out is that within the found set of machines, T_F, TR_O and TTR_O category machines are well represented. All found T_F machines are designed for static stability. This might indicate a focus on systems with little complexity, for the machines in this category. In addition, the intended application field of the designs are largely of low technical demand as for instance toys. One could hypothesize that these machines serve less of a practical use, but instead focus more on visualizing walking locomotion.

On the other side of the spectrum seem to be the TTR_O and TR_O machines. The mentioned advantage of walking machines being more capable of handling rough terrain than wheeled vehicles seems to be the focus of these designs. The over-actuation improves the dexterity on rough terrain and is thus a logical choice for these designs.

Another conclusion is that TT systems have received little to no attention, as with TR_P, TR_U, TTR_P,TTR_U and TTR_F.

A possible reason for the little effort on TT *WM* designs could be the limitation the rotational constraint imposes in the general functioning of the device. One could hypothesize for instance that the desired functions of a practical walking machine should include a rotation.

The absence of documentation on TR_U and TTR_U machines is noteworthy as under-actuation in general is a well established field of research. The absence of found research in the TTR_F category might imply the little interest in simplicity of the design in the TTR group. This strengthens the hypothesis mentioned earlier, that TTR designs focus on dexterity on rough terrain.

As seen in section 2.4.2, tables 2.3 and 2.4 a sub-categorization is made by separating differential and steering designs. From this it can be concluded that the number of steering designs is far less than the differential designs. Furthermore, within the steering designs, only fully and over-actuated TR designs are represented.

2.5.2 Discussion of methods

First off, as the number of *WM* designs available is vast, an attempt was made to gather a representative sample. However, the randomness of this sample might be slightly influenced by search terms, following references and search engine indexing not being completely random.

Secondly, as indicated in section 2.4.2 a grey area still exists in what is to be called a walking machine, even though an attempt was made to make the definition of a *WM* as comprehensive and specific as possible. This grey area holds for both purely legged *WMs* and wheeled 'walking machines'.

To elaborate on an example, Thring's machine as indicated in figure 2.12 shows strong resemblance with tracked vehicles. Although the machine fits the definition of a *WM* as mentioned in section 2.2 and is named "Walking machine", due to the serial connection of the legs this machine might also fit the description of a tracked vehicle. This is an example of a design which might not be fully in line with the intended goal of the definition of a *WM* as defined earlier. To resolve at least this unclarity, added to the definition of a *WM* could for instance be that all legs have to be independently connected to the base frame. This will influence the results. Concerning wheeled 'walking machines': It is in first place doubtful if the machines within the section of wheeled 'walking machines' can be categorized as walking machines. The mechanisms involved show strong resemblance with purely legged *WMs*, but wheels play a definite roll in the functioning of the device. Since the number of designs with wheels within the sample is significant, a separate section for these devices was deemed appropriate. However, the contribution level of the wheels remains an opaque separation line distinguishing wheeled machines from wheeled 'walking machines'.

To elaborate on this, machines incorporating mechanisms able to intermittently support (part of) the weight of the machine and propel it in a way as indicated in figures 2.17 and 2.16, should be called walking machines as by the definition in section 2.2. However, it is clear that wheels are used to fulfil a similar supporting function as the 'legs'. Furthermore, machines as given by figure 2.15 do have mechanisms that show great similarity with the legs of non-wheeled *WMs*. Also, they are named for instance "walking toy" or "walking toy figure" [36, 68]. Nevertheless, it is questionable if the legs intermittently support the vehicle, as contact with the supporting surface seems likely to be remained.

Thirdly, the categorization is based upon the assumption of allowed slip at the contact surface allowing for a rotation based upon different speeds of the relative sides of the *WM*. Without this assumption, less designs would be in the differential TR categories. These would appear in the T groups, even though their intended functioning principles are based upon slip.

2.6 Conclusion

In this review, an introduction into commonly used identifiers of *WMs* was given. Then, a new categorization was proposed and put to practice. 141 purely legged *WMs* were categorized, as well as 16 wheeled 'walking machines'. The sample showed a large representation of the T_F, TR_O and TTR_O category *WMs*, with smaller numbers in T_O and TR_F categories and little to none in the others. Afterwards, the results were discussed and possible explanations proposed, together with a reflection and discussion on the applied methods. Summing up, we can say that in terms of walking machines there still is territory to explore. The category of TT machines in general is very scarcely populated and thus provides room for studying. Although one could doubt the relevance of passive machines in the TT, TR and TTR categories, these categories remain untouched and thus also provide pioneering grounds. This also holds for the likely more relevant TR_U, TTR_U and TTR_F categories.
Concluding, we can generally state that despite the large amount of work done on *WMs*, there still is plenty of uncharted territory to explore.

DoFs	Passive	Under-actuated	Fully actuated	Over-actuated
1, T	[132] [96] [26]	[132] [96] [26]	[123, 156, 77] [115, 145, 130] [84, 134, 105] [86, 98, 75] [48, 46, 28] [107, 108, 47] [44, 32, 163] [24, 106, 167] [140, 126, 175] [169, 119, 62] [42]	[23, 17, 160] [16, 65, 94] [63, 114]
2, TT			[91]	[144]
2, TR			[155, 151, 92] [103, 12, 101] [127, 121, 67] [15, 154, 33] [161]	[70, 1, 6] [2, 64, 11] [111, 29, 19] [27, 133, 150] [176, 38, 76] [95, 110, 49] [30, 172, 81] [117, 35, 177] [180, 18, 100] [102, 161, 82] [73, 66, 8] [40, 120, 7] [9, 17, 17] [168]
3, TTR				[164, 41, 153] [170, 171, 39] [10, 25, 136] [147, 13, 52] [148, 178, 20] [50, 85, 141] [45, 173, 31] [58, 135, 174] [79, 57, 166] [149, 157, 56] [179, 22, 55] [118, 53, 143] [51, 159]

Table 2.6: References of the in table 2.3 indicated number of WMs.

Chapter 3

Design of a 2-DOF compliant mechanism for generating closed spatial surfaces, with intended application as leg in omnidirectional walking machines.

3.1 Abstract

This paper presents the design of a 2-DOF compliant mechanism, capable of describing a closed spatial surface. The mechanism is designed with the intended application as leg in an omnidirectional walking machine. Therefore, a conceptual design of a way of coupling a multitude of these mechanisms is also presented. By means of a kinematic analysis it will be shown that the design is able to describe this surface, making it suitable for its intended purpose. Measurements of a physical prototype qualitatively confirm the functioning of the device without external loads, after production by means of additive manufacturing. Furthermore, an analysis of the deviations with respect to the created purely kinematic model is performed, indicating the most prominent improvement directions. This creates a first step towards a compliant walking machine, capable of translating in any direction over its supporting surface.

3.2 Introduction

A considerable amount of research and design has been done on walking machines (WMs). With one of the earlier patents reaching as far back as 1893 [129], the field has since gotten numerous contributions in various directions. One direction comprises machines meant to traverse 'rough' terrain, the Adaptive Suspension Vehicle in the 1980s by Song and Waldron [143], the Dante II project [9] and Big Dog by Boston Dynamics[118] are good examples of this. Another field is that of passive dynamic walkers, with major contributions by McGeer [96] and S. H. Collins, M. Wisse and A. Ruina [26]. But also, there are the statically stable machines as for instance those by Theo Jansen [62], A. Ghassei [42] and ones inspired by the Klann and Chebyshev linkages [69], [72]. A field that has gotten little attention though, is that of machines with the ability to translate in two directions along their supporting surface while only using two actuators. A single report of such a machine is in a 2014 patent by J. Mantzel [91].

Next to walking machines, the field of compliant mechanisms is a currently active field of research. With the advantages of these mechanisms over conventional ones including no backlash, no need of lubrication and low wear, their application in WMs could extend the usage range of these machines. An example of the connection between the two fields has been shown in a compliant WM design by M. Plecnik [113]. With the advances in additive manufacturing, the design of more complex systems and structures becomes more feasible and sensible as monolithic designs are more easily produced. Monolithic design implies the use of compliant mechanisms to replace conventional hinging elements. Provided that WMs are inherently more complex than their wheeled counterparts, these machines seem like an ideal subject for these production techniques. Given the limited work done on fully actuated WMs able to translate in any direction along their supporting surface, as well as that on compliant walking machines in general, this paper presents the design of a mechanism to help fill this gap. Namely a 2-DOF compliant mechanism for generating closed spatial surfaces, with intended application as leg in omnidirectional walking machines.

The design of a compliant WM comes with specific challenges. The inherent limitations of compliant mechanisms, like not allowing for indefinite rotations and the introduction of rotational stiffness create a hurdle. Furthermore, the necessity of such a system to be spatial also poses a challenge to the designer. Lastly, the intended walking machine will have to be stable and maintain an approximately constant height with respect to its supporting surface, in order to be relevant and able to be put to use.

One possible solution for this last point is to make sure the legs of the machine draw a straight line, parallel to the motion direction along the plane, during their support phase. This will introduce limited motion of the center of mass (COM) perpendicular to the supporting plane and thus limited undesired dynamics.

Being able to generate a straight line in a certain direction for more than a single time means a return stroke will have to be present. With the application of a WM in mind, this return stroke will have to ensure the end effector is lifted off the surface it contacts. Examples of this are found in the mechanisms by T. Jansen, A. Ghassei, Chebyshev and Klann [62, 42, 72, 69]. When adding the omni-directionality requirement, this means the end effector should be able to trace a spatial surface with a planar DOF during its stance phase, in short: a rotationally symmetric surface with a flat bottom part.

Following this train of thought, this paper presents the design of a compliant mechanism capable of generating such a surface. Furthermore, it is able to do this only using two inputs/actuators. These on their turn are (de)coupled such that one actuator propels the end effector over a path constructed by a plane intersecting the surface, while the other dictates the rotation of this planar path. This enables the use of such a mechanism in an omni-directional walking machine as it could allow the machine to move in any desired direction, at any point in time or space. Next to the detailed design of a physical and kinematic model of this device, a manner of coupling a multitude of these mechanisms is also proposed. The functioning of the kinematic model is analyzed and the physical model is manufactured. Finally, its kinematics without external loading are experimentally evaluated. First the design method will be briefly touched upon in section 3.4. Then the design will be introduced and explained in section 3.5 and section 3.6. A manner of coupling a multitude of these mechanisms to form the kinematic basis of a walking machine is presented in section 3.7. Subsequently, the dimensioning and fabrication will be dealt with in

section 3.8 and the experimental set-up in section 3.9. This will be followed by the results in section 3.10 and this paper is ended by a discussion and conclusion in section 3.11 and section 3.12 respectively.

3.3 Nomenclature

Notation	Definition
$b_{n,i}$	Bar *n*, version *i*
$\|b_{n,i}\|$	Length of bar *n*, version *i*
$...._{...m}$	Mirrored copy of described element
$\angle kj$	Angle between element *k* and *j*
R_n	Revolute joint *n*
S_n	Spherical joint *n*
P_n	Prismatic joint *n*
A,B,D,E,F,G	Indicative points
$X_k(L)$	Relative position in X direction of element k, dependent on L
$Y_k(L)$	Relative position in Y direction of element k, dependent on L
$Z_k(L)$	Relative position in Z direction of element k, dependent on L

Terms	Definition
α_1	Angle of input motion generator 1.
α_2	Angle of input motion generator 2.
β	Angle of the output plane set by α_2.
X_{rot}	Rotated X-axis.
Y_{rot}	Rotated Y-axis.
Z_{rot}	Rotated Z-axis.
WM	Walking Machine
DOF	Degree Of Freedom
IMG1	Input Motion Generator 1
IMG2	Input Motion Generator 2

3.4 Design Method

To generate the design of the mechanism, firstly the scope for the design of an overall walking machine was set up. Herein, the design objective and two lists of requirements were made, one with strict requirements and one indicating the desired design direction. The mechanism itself was made to fit this scope with its own design objective and choices were made to make the mechanism compatible with the scope of the overall machine design. This project definition was followed by the kinematic design of the mechanism and consecutively its transformation into a compliant version of the design.

3.4.1 Project definition

The design objective of the complete machine is defined as:

"Design of a compliant walking machine, capable of translating in any direction along an (almost) horizontal supporting surface."
The accompanying assumption is that gravity is taken to act towards the supporting surface. In addition, this surface is taken to be hard and stiff enough to assume no deformations take place under the influence of the machine. Furthermore, an appropriate amount of friction is assumed to be present between the supporting surface and the WM in order for no slip to occur.
The definition of a WM is taken to be:

"Devices able to propagate along a(n) (almost) horizontal plane, making use of a single or multiple supporting mechanisms which are intermittently in contact with the supporting surface. The support mechanisms or 'legs' in contact with the surface support the structure under the influence of gravity, while the (center of mass of the) machine is allowed to move parallel with respect to the plane."

Following the design objective, a list of hard and soft requirements further specify the objective. The set requirements are listed in the following enumeration in no specific order.

1. The device shall contain only two actuators.
2. The device shall be statically stable.
3. The device shall be capable of omnidirectional movement.
4. The device shall have a greatly higher stiffness in supporting direction than over the supporting plane.
5. The device shall not be limited in its range of motion.
6. The final design shall allow for monolithic fabrication.

The requirements which are not strict to be met, but indicate a direction for design choices are summed up in the following list, in order of high to low importance.

1. The centre of mass shall remain at a constant height.
2. The input to output ratio shall be constant.
3. The transverse stiffness shall be constant.
4. All dynamic forces shall be balanced.

The focus of this last list is towards producing a system with a high bandwidth. The meeting of these requirements is thus not essential for the functioning of the machine. Taking into account the objective and lists of requirements for the complete walking machine, the objective for a single 'leg' for such a device is defined as:

"Design of a 2-DOF compliant mechanism able to generate a motion capable of intermittently translating its connected body in any direction over a supporting plane."

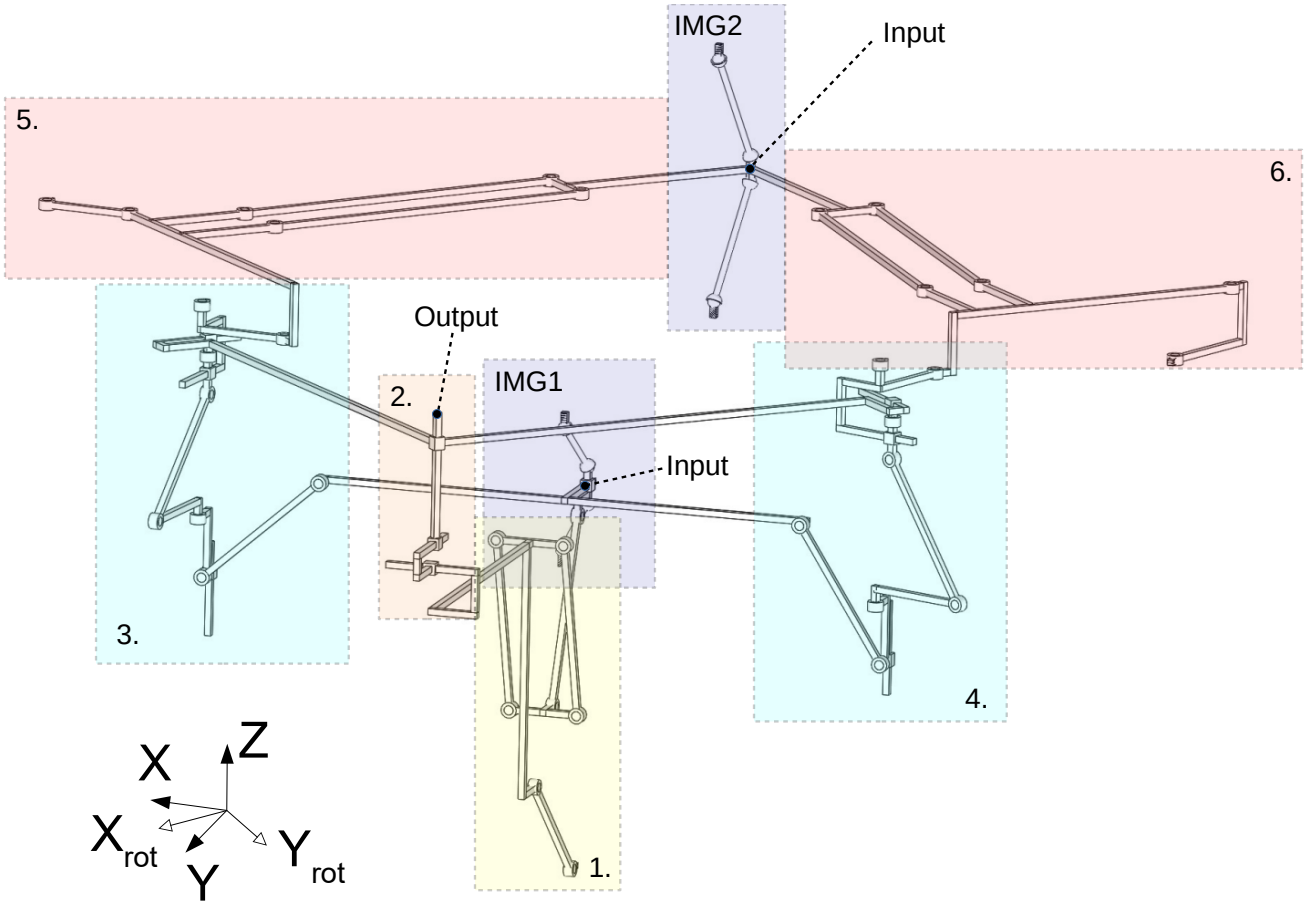

Figure 3.1: Overall kinematic model: (IMG1&IMG2) Input motion generator 1 and 2 resp. (1.) Z transmission, (2.) Motion coupling mechanism, (3.) Y_{rot} transmission, (4.) X_{rot} transmission, (5.&6.) Direction setpoint mechanism.

In order to provide static stability, omnidirectional movement and maintain the distance between the center of mass and the supporting plane, this subsystem is designed to describe a surface with an approximately planar lower part, which is intended to contact the supporting surface. To make sure the device is not limited in its range of motion while allowing for monolithic fabrication, the system is designed such to be able to describe a closed surface. This, instead of for instance one or two open surfaces, which could limit the behaviour of the entire machine.

3.5 Kinematic design

3.5.1 Introduction

To start off with a view on the design, a representation of the kinematic model is shown in fig. 3.1. This shows the locations of its subcomponents with respect to one another. Also, the introduced colours relate to the components of the compliant system as will be elaborated on in section 3.6. An indication of the by the end effector described surface of the kinematic model is shown in fig. 3.2. A step by step explanation of the functioning of the mechanism will be given by consecutively elaborating on the functioning of the various subcomponents. This is done by means of kinematic substitutes and is followed by an explanation of the compliant system. Also, where relevant, each figure will show a single or multiple coordinate systems to be referred to. The *XYZ* coordinate system is constant, irrespective of the orientation of the indicated parts. The rotated coordinate system $X_{rot}Y_{rot}Z_{rot}$ is related to the orientation of the mechanism under examination.

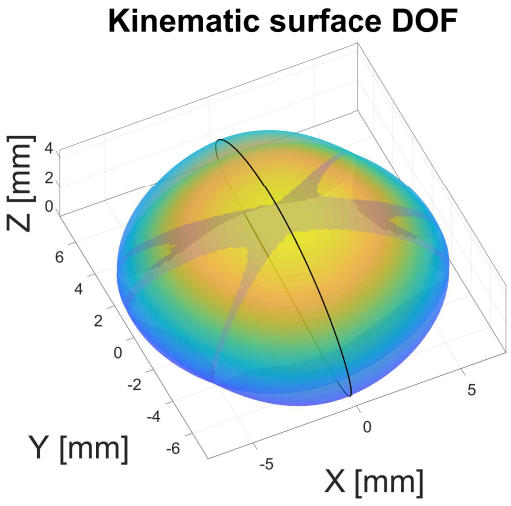

Figure 3.2: Surface generated by the end effector with a line indicating the path for $\alpha_2 = 0$.

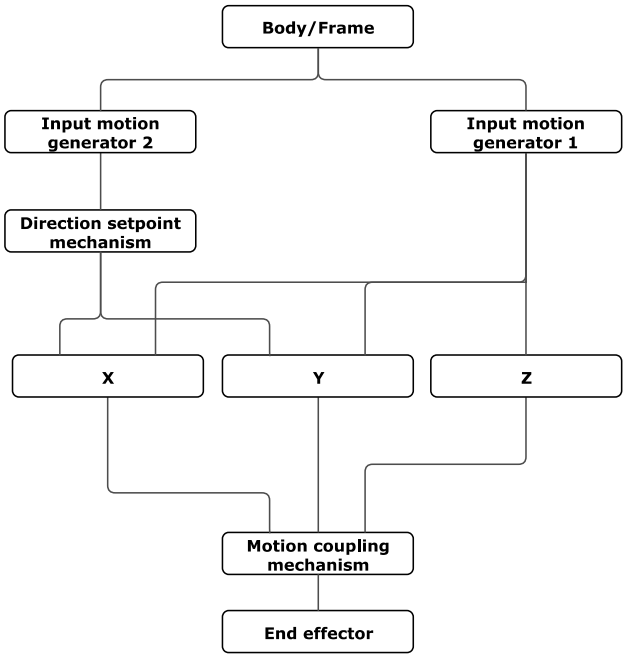

Figure 3.3: Simplified functional breakdown.

To provide an insight in the functioning of the device, an overview of the subcomponents is given in fig. 3.3. Starting from the body or frame of the system, two main mechanisms branch off. One of them, input motion generator 1 (IMG1) generates the motion of the end effector along a plane intersecting the spatial surface which the end effector is constrained to. Input motion generator 2 (IMG2) dictates the rotation of this plane with respect to the axis normal to the intended supporting surface. An indication of this is given in fig. 3.4, where a top view of the generated surface and the output angle of the specified plane, β, are shown. The by IMG1 generated motion is split up into three components, the X, Y and Z position of the end effector. Here, Z is perpendicular to the intended supporting surface and X and Y are parallel, as is shown in fig. 3.2.

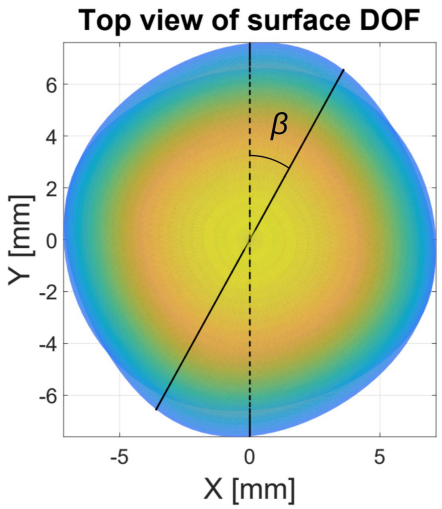

Figure 3.4: Definition of angle β, with the dashed line indicating the line $X = 0$.

The Z position is directly coupled to the input motion of IMG1. The X and Y positions are dependent on the motion of IMG1 and the direction set by IMG2, in combination with the direction setpoint mechanism. At the point where the X, Y and Z position of the end effector are set, the values are merged into a single point by the "motion coupling mechanism". Which position then conducted to the end effector. Thus, by setting a direction and a point in the cycle by respectively IMG2 and IMG1, the position of the end effector is set.

3.5.2 Input motion generator

Going more into depth, we will first look into how the cyclic motion for the propulsion is generated. This is done by making use of a set of spherical joints. One could represent the functioning as in fig. 3.5a. By making sure the length of bars b_1 and b_2 are together longer than the length from point *A* to *B*, the point *D* will trace the circular path with radius r_{input} as indicated in the figure. Here the points *A*, *B* and *D* are defined by the centre point of the spherical joints, the striped elements indicate the fixtures and the lengths $|b_1| = |b_2| = |b|$. The resulting radius r_{input} is then given by:

$$r_{input} = \sqrt{|b|^2 - \left(\frac{1}{2}\,AB\right)^2} \tag{3.1}$$

By adding an additional bar b_3 as depicted in fig. 3.5b, a connection point for the rest of the mechanism is created to provide transmission of the circular movement. As will later be shown, the rest of the mechanism constrains the bar to stay parallel to the Z_{local} axis. In this case the point D is located on the central axis through b_3. Again, the lengths $|b_1| = |b_2| = |b|$ and logically, the radius r_{input} transforms to:

$$r_{input} = \sqrt{|b|^2 - \left(\frac{1}{2}\,(AB - |b_3|)\right)^2} \tag{3.2}$$

What should be noted is that since the final design is compliant, the (internal) rotational degree of freedom around the central axis of bars b_1 and b_2 is taken to be properly constrained by the joint stiffnesses. This axial rotation of b_3 is limited by the rest of the mechanism. Furthermore, as will be referred to later on, the angles α_1 and α_2 of IMG1 and IMG2 respectively are defined by point *D*, the centre of its path and the *Y* axis.

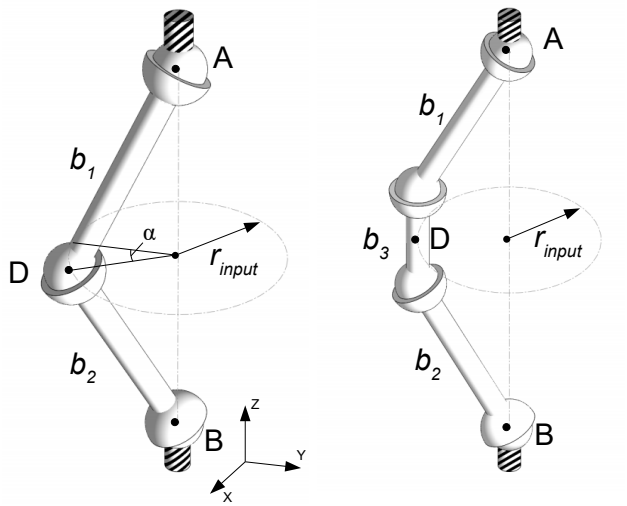

(a) Circular input. *(b) Circular input with additional element.*

Figure 3.5: Kinematic representations of input motion generator.

3.5.3 Z transmission

To generate the Z motion of the end effector from the eccentric (or circular) input motion, a mechanism as schematically represented in fig. 3.6 is used. Bar b_3 is constrained in its rotation around the X-axis by the X/Y transmission mechanisms as will be discussed in section 3.5.4. The circular input motion of b_3 is transformed into a reciprocating motion at point E. Bar b_4 transforms the circular motion in the XY plane into a path of R_2 in Z direction while directly transferring the X-motion of its input. This path is indicated in the figure. Bars b_5 on their turn transform this directly coupled X-motion into a movement in the Z direction as well. Because R_7 describes a circular path with radius $|b_7|$, the previously mentioned bars do not show a perfect Z-motion only but rather a motion which is coupled in the Y-direction as well. This is transmitted due to P_6 and P_7 constraining all rotations. Consequently, b_6 also moves according to this coupled path. With P_7 constrained, the motion in Z-direction is the only remaining motion at point E since P_6 only transfers the Z component. With the correct dimensions and (starting) positions of all bars and fixtures, point E will remain approximately stationary for a part of its cycle. This is over the course $135 \leq \alpha_1 \leq 225$ deg, generating the flattened bottom of the final surface. The dependency of the Z position of point E on α_1 will become clear in section 3.7,fig. 3.19.

3.5.4 X and Y transmission

The *X* and *Y* position are determined by mechanisms which are a mirrored copy of each other so only one will be discussed. This mechanism functions by transforming the input motion of b_3 into a linear motion of point F in the rotated X direction X_{rot}, rotated 45 degrees along the Z axis. See fig. 3.7. This motion in X_{rot} direction is adjustable in amplitude by adjusting the angle θ_1, which determines the rotation of bar b_8 with respect to the Y_{rot} axis.

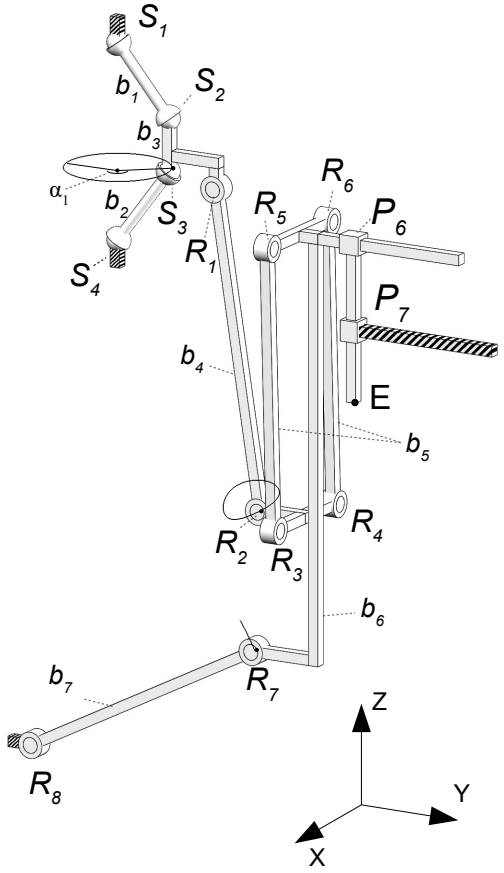

Figure 3.6: Z transmission with the generated paths for distinct points.

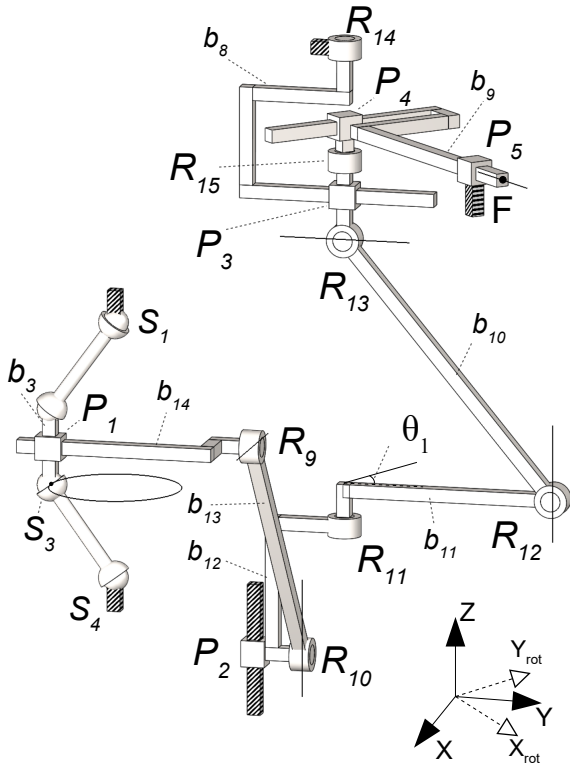

Figure 3.7: X/Y transmission.

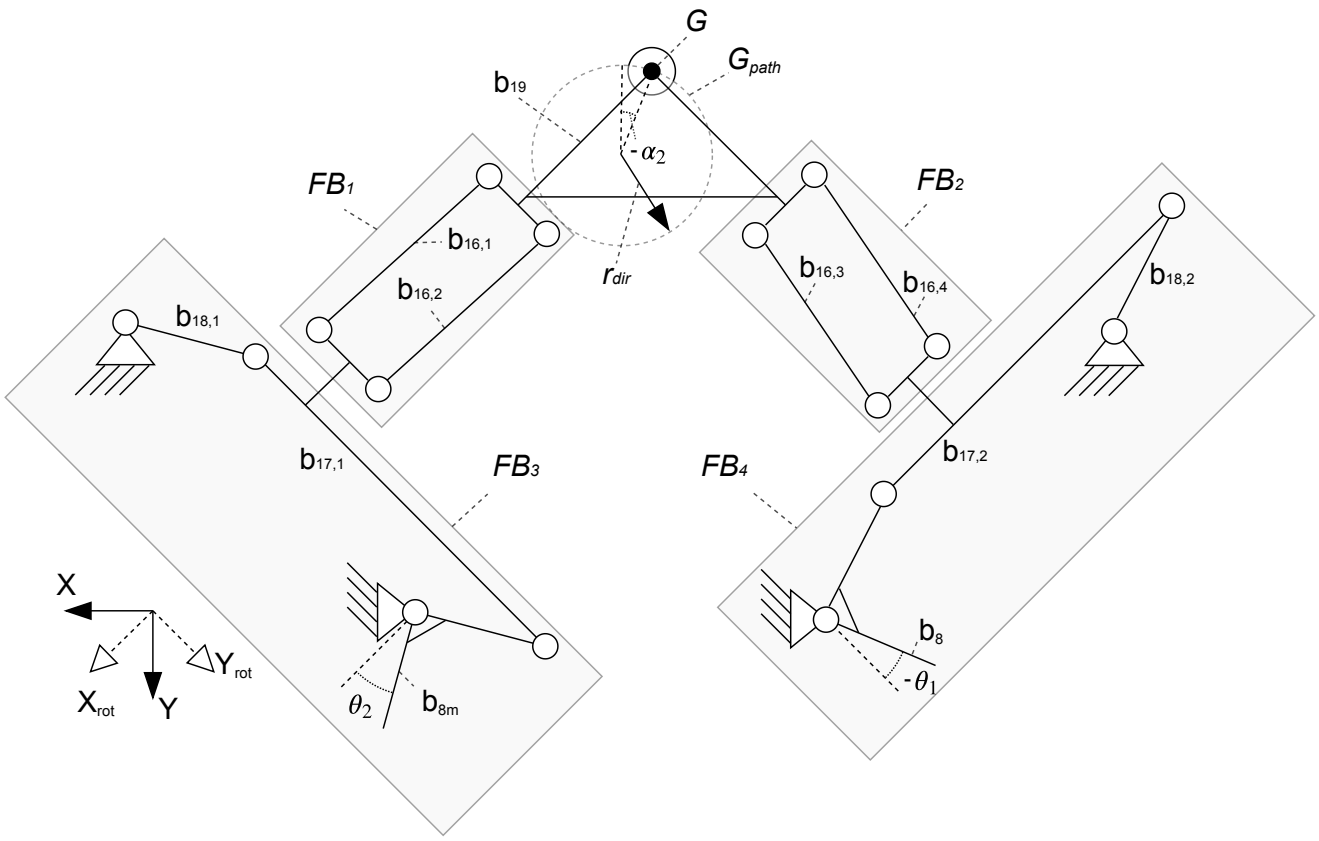

Figure 3.8: Kinematic structure of the direction setpoint mechanism, the mechanism for setting the angles θ_1 and θ_2.

In more detail, from the circular input motion of b_3, a linear motion parallel to X is deducted by the prismatic joint P_1. This is converted into a motion parallel to the Z axis at R_{10} due to the constraints induced by P_2. Then, R_{12} is able to rotate around the axis of R_{11}, which is parallel with Z. With the induced movement in the Z direction, this results into a straight line motion in the XY plane at R_{13}, adjustable in direction around the R_{11} axis.
The rotation is possible because R_{14} and R_{11} are concentric. Next, the translation of R_{13} is guided by b_8 and P_3. Where b_8 has an external input for setting the angle θ_1. This is done by the direction setpoint mechanism as explained in section 3.5.5.
Since b_9 is constrained such that only translation in X_{rot} direction is possible (by P_5), the relative orientation of b_8 and b_9 will determine the amplitude of the movement of point F. This is possible due to R_{15} and P_4 allowing for the respective movements.
As a whole, this is the mechanism determining the position of point F in X_{rot} direction. The same mechanism mirrored over a plane parallel to the ZY plane, coincident with the centre(s) of S_1 (and S_4) determines the position of the mirrored relative of F, F_m. This mirrored version determines the Y_{rot} coordinate of F_m. Figure 3.1 shows the respective positions of these two versions of the mechanism in the final assembled configuration. The mirrored angle of θ_1 is named θ_2 and is defined with respect to X_{rot}. .

3.5.5 Direction setpoint mechanism

The mechanism for setting the direction of the end effector path is symbolically represented in fig. 3.8. Point G is here constraint to move along the circular path (G_{path}) by an equivalent mechanism as shown in fig. 3.5, it is a point on a fixed position on b_{19}.The angle α_2 is defined as the angle of G with respect to the negative Y axis as indicated in fig. 3.8. The direction setpoint mechanism transfers the translation of G in X_{rot} and Y_{rot} direction into the angles θ_2 and θ_1 respectively. This is done by initially decoupling the respective other direction of movement, by making use of a symmetric fourbar linkage FB_1 (and FB_2). With relatively long bars $b_{16,1-4}$ the DOF is perpendicular by approach.
By subsequently coupling these fourbar linkages to another fourbar mechanism (FB_3 and FB_4) of which $b_{17,2}$ and $b_{17,1}$ are the couplers, the translational motion is finally transferred into the two angles θ_1 and θ_2 of bars b_8 and b_{8m} respectively.

3.5.6 Motion coupling mechanism

The motion coupling mechanism transfers and couples the desired X,Y and Z motions, generated by the previously discussed mechanisms, to a single point. This is done for each of the motions, by decoupling the respective other motions. The motion coupling mechanism is symbolically depicted in figure fig. 3.9. Which indicates the Y_{rot} and X_{rot} motion of b_9 and

b_{9m}, as generated by the X and Y transmissions. Furthermore, the input Z motion of bar b_6 is indicated as produced by the Z transmission. The output of this subcomponent is b_{18}, which is the overall end effector.

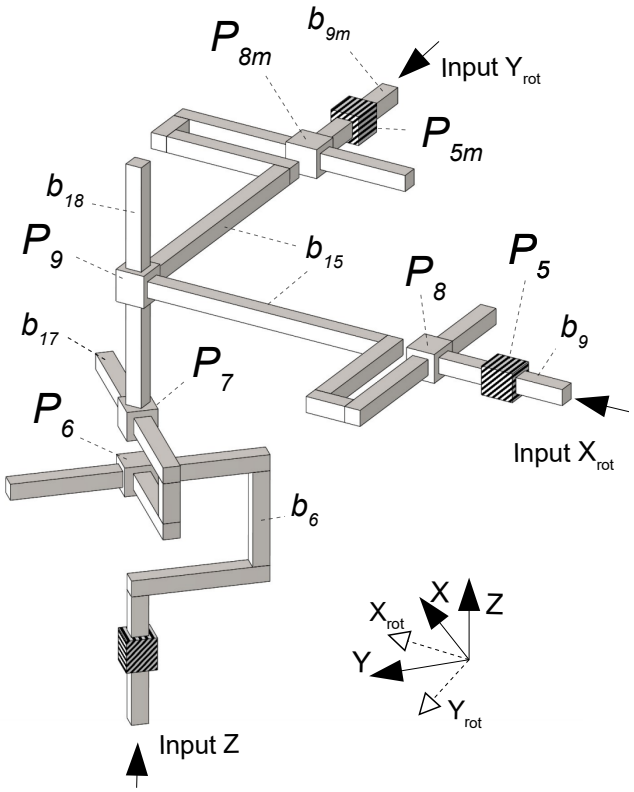

Figure 3.9: Kinematic substitute for the motion coupling mechanism.

To be able to transfer the Z direction input of b_6, the Y and X movements of the end effector are decoupled by P_6 and P_7. For the Y_{rot} input, the Z direction is decoupled by P_9 and the X_{rot} direction by P_{8m}. Since b_9 and b_{9m} remain on the same Z level, the Z level of the X_{rot} input is also decoupled by P_9. Its Y_{rot} direction is decoupled by P_8. This defines the X, Y and Z position of the end effector b_{18}.

3.6 Compliant design

To allow for a monolithic design, the conventional joints displayed in the kinematic diagrams are replaced by their compliant counterparts. Notch flexures replace the revolute joints and compliant spherical joints the conventional spherical joints. To replace the prismatic joints, a compliant version of a Robert's mechanism was used, with again, notch flexures to replace the revolute joints. Figure 3.10 shows the conventional joints and their compliant counterparts graphically.
In the coming subsections, the compliant versions of the components of the system will be discussed in the same order as done in section 3.5. Eventually, this adds up to the 3D drawing of the complete system as given in fig. 3.11.

Joint type	Symbol	Compliant Version
Prismatic	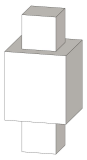	
Revolute		
Spherical		

Figure 3.10: Legend of used joints.

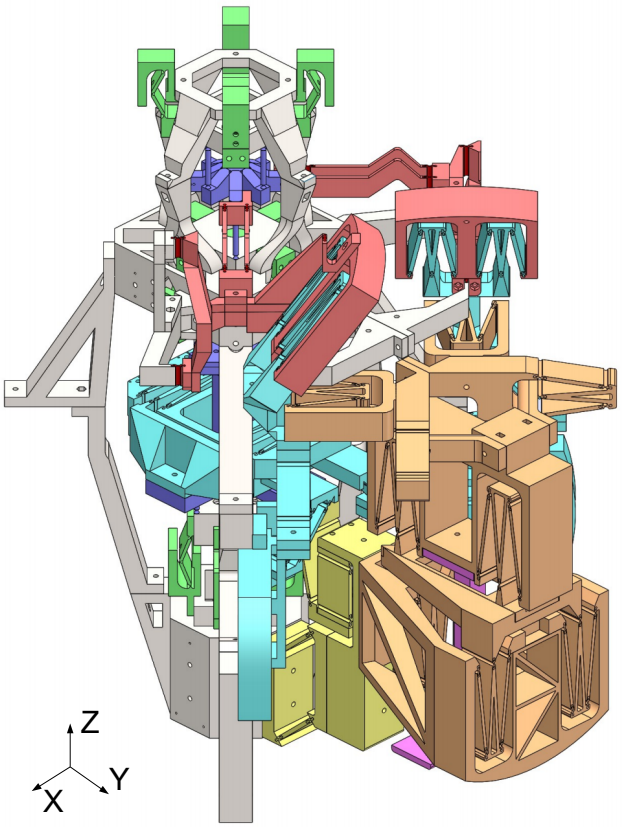

Figure 3.11: 3D view of the assembly of the final compliant design.

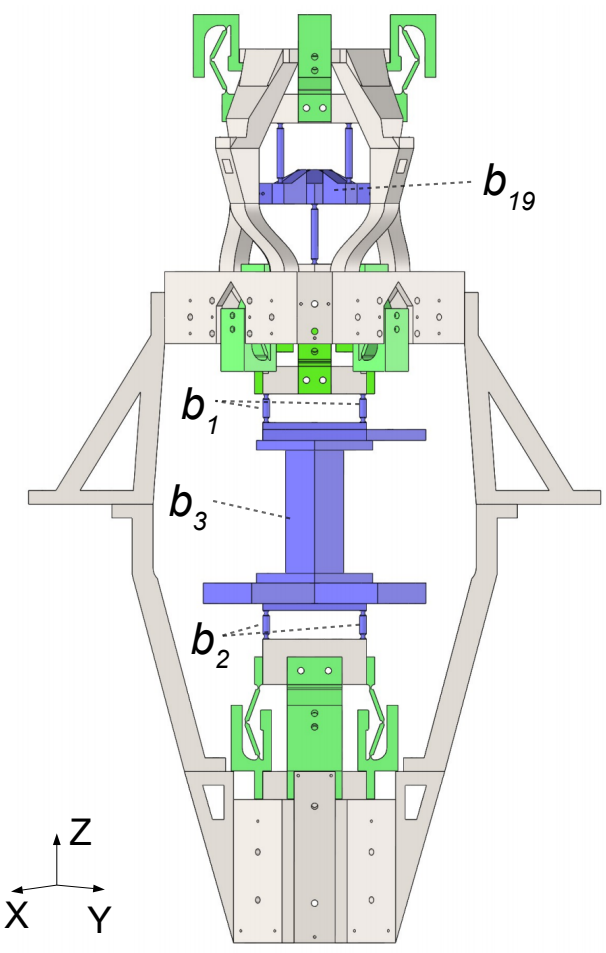

Figure 3.12: The compliant input motion generators (purple) and their Sarrus linkages (green). For the kinematic variant of the input motion generators, see fig. 3.5b.

(a) Half of one of the Sarrus linkages in initial position.

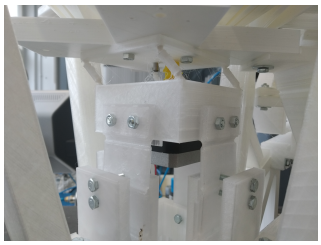

(b) One of the Sarrus linkages under load, also indicating the offset in b_2 generated by the extension of the Sarrus linkage.

Figure 3.13: The Sarrus linkages for compressing the input generator, to realize the offset r_{input} in initial and tensioned stated.

3.6.1 Input motion generator

In fig. 3.12, the two input motion generators are displayed in purple. This drawing shows the input motion generators with $r_{\text{input}} = 0$, which was the manufactured state. By extending the compliant Sarrus linkages shown in green, effectively decreasing the length *AB* (fig. 3.5), the radii r_{input} of both input motion generators were increased to their desired levels. As a reference, see fig. 3.13, showing the manufactured state and the state under tension.
The bars b_1 and b_2 of the bottom input motion generator (IMG1) are present in sets of four to allow for actuation at the centre of b_3 and to add stiffness in the rotation around the *X* and *Y* axes (fig. 3.11). IMG2, with b_{19} replacing b_3 has a similar design, with the exact same reasoning.

3.6.2 Z transmission

The compliant design of the transmission for generating the *Z* position is graphically represented in yellow in fig. 3.14, including bar labels. To increase rotational stiffness of bar b_6 around the *X* axis, bar b_7 is present in twofold, creating a parallelogram. This same holds for b_5 as was already indicated in section 3.5.

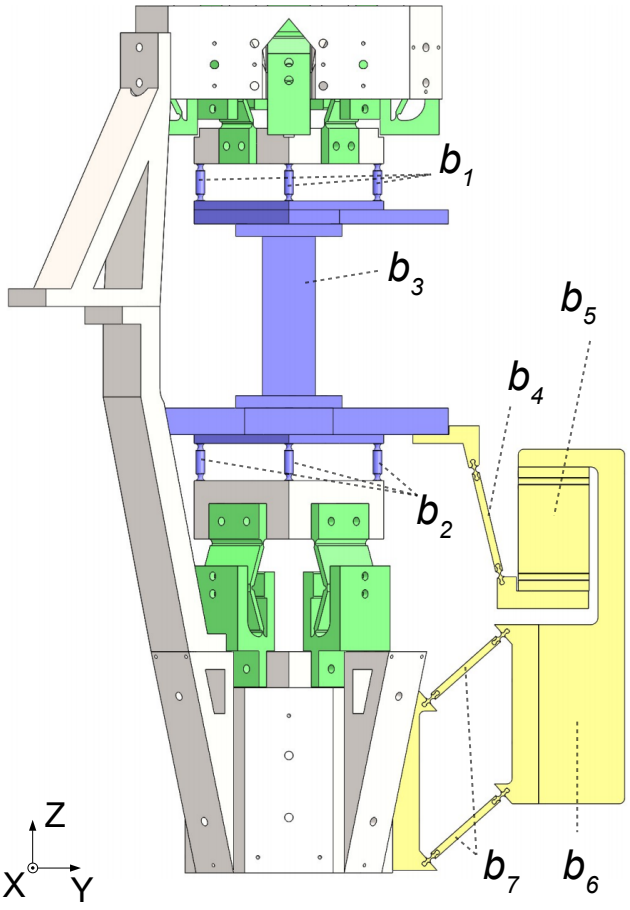

Figure 3.14: IMG1 (purple) connected to the transmission for the Z position (yellow). See fig. 3.6 for its kinematic counterpart.

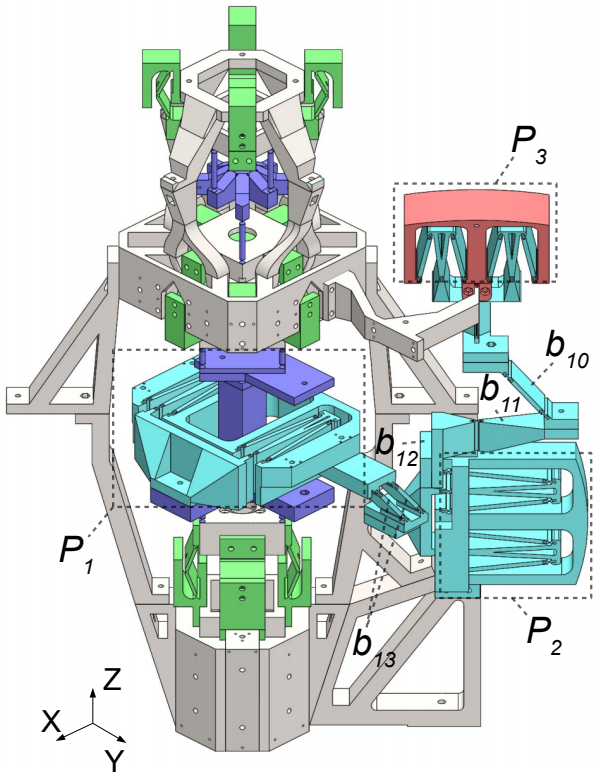

(a) One half of the X/Y transmission in blue. See fig. 3.7 for its kinematic counterpart.

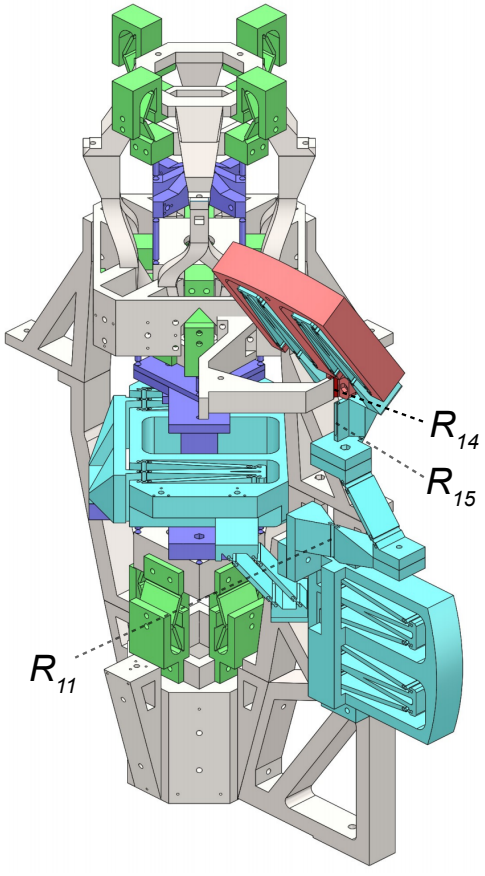

(b) Rotated view of half of the X/Y transmission in blue. See fig. 3.7 for its kinematic counterpart.

Figure 3.15: Half of the X/Y transmission in different view angles.

3.6.3 X and Y transmission

The compliant design of one half of the *X* and *Y* position generator is given in blue in fig. 3.15. As with the explanation of the kinematic model, only the X_{rot} position generator is displayed since the Y_{rot} position generator is a mirrored copy. An example is shown in the compliant 3D CAD drawing in fig. 3.11.
Figure 3.15a shows the double Robert's linkages in the place of the prismatic joints P_1 to P_3. Furthermore, it shows the double version of bar b_{13} to improve the rotational stiffness around the *Y* axis for P_1 and IMG1. Figure 3.15b indicates the locations of relevant revolute joints, where, as indicated in section 3.5, R_{14} is concentric with R_{11}.

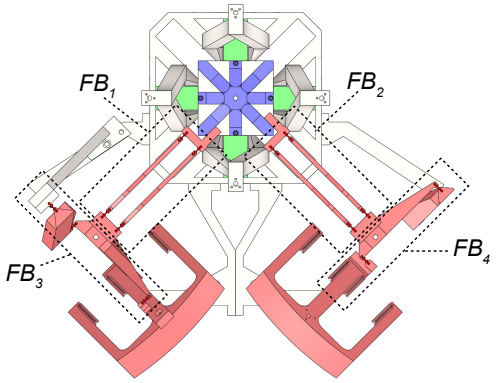

(a) Top view of the compliant direction setpoint mechanism in red. See fig. 3.8 for its kinematic counterpart.

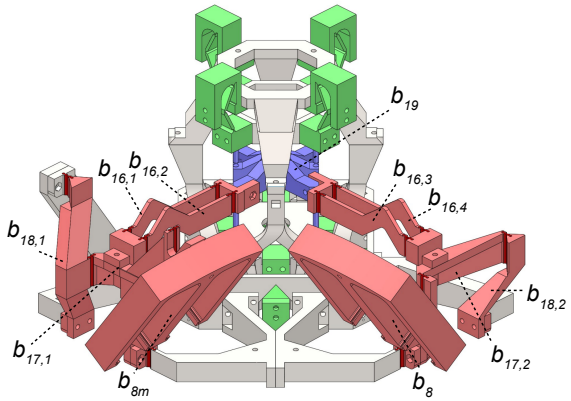

(b) 3D view of the compliant direction setpoint mechanism in red.

Figure 3.16: The compliant direction setpoint mechanism in two views.

3.6.4 Direction setpoint mechanism

The direction setpoint mechanism is shown in fig. 3.16 in red, with its input motion generator in purple. For clarity, the joints are indicated by a darker red colour. Although FB_3 and FB_4 are out of plane, their principal way of functioning complies with the kinematic model in fig. 3.8. As indicated for IMG1 in section 3.6.1, this depicted state also has an $r_{\text{dir}} = 0$. This will increase to the desired value by extending the Sarrus linkages as shown in green.

3.6.5 Motion coupling mechanism

The compliant design of the motion coupling mechanism is given in fig. 3.17 in orange, with the end effector shown in pink. A difference with the shown kinematic version here, is that the single compliant Robert's linkages indicated by P_8 and P_{15} and their mirrored variants labelled P_8m and P_{15m} provide a rotational as well as a translational degree of freedom. This compliant version also varies from its kinematic variant due to P_{8m} providing the *DOFs* P_5 provides in the kinematic model. This relationship also holds for P_8 and P_{5m} and is made possible by the limitation of the rotation around the *Z* axis by P_7, P_6 and the Z transmission. Also, P_7 consists out of three single Robert's linkages to ensure stiffness around the *X* axis of P_6. Broadly speaking, the compliant design combines the *DOFs* of kinematic joints in such a fashion to decrease complexity and improve stiffness where desired.

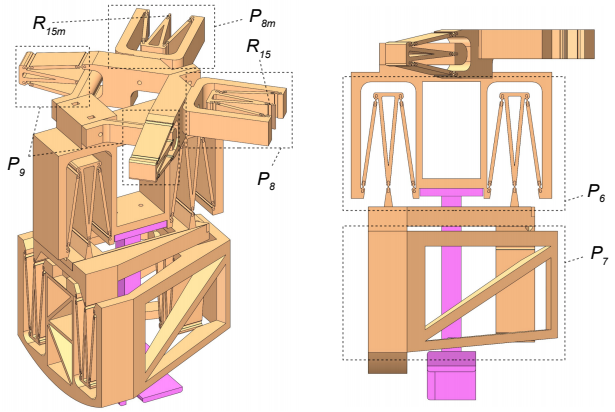

(a) 3D view of the motion coupling mechanism in orange, with the end effector in pink.

(b) Side view of the motion coupling mechanism in orange, with the end effector in pink.

Figure 3.17: Two views of the motion coupling mechanism, including the end effector designed for measuring its displacement. See fig. 3.9 for its kinematic counterpart.

3.7 Machine coupling

With the intention of being used in/as a walking machine, the system is designed such to be able to couple a multitude of these mechanisms or 'legs' in order to synchronize their movement with a phase difference. The presented design consists out of legs with a stance phase of a quarter cycle. This means at least four legs have to be present for the machine to be supported along the entire cycle, provided that each leg can support the entire machine in its stance phase. The intended WM design has the two input generators at the centre, with a leg mechanism in each quarter circle reaching outward. Figure 3.18a indicates this with a top view of the compliant design, together with a schematic diagram of the positions of the legs (L1-L4) in fig. 3.18b. As a reference, the latter also shows the positions and paths of point D and G, the centres of the two input motion generator bars b_3 and b_{19}.

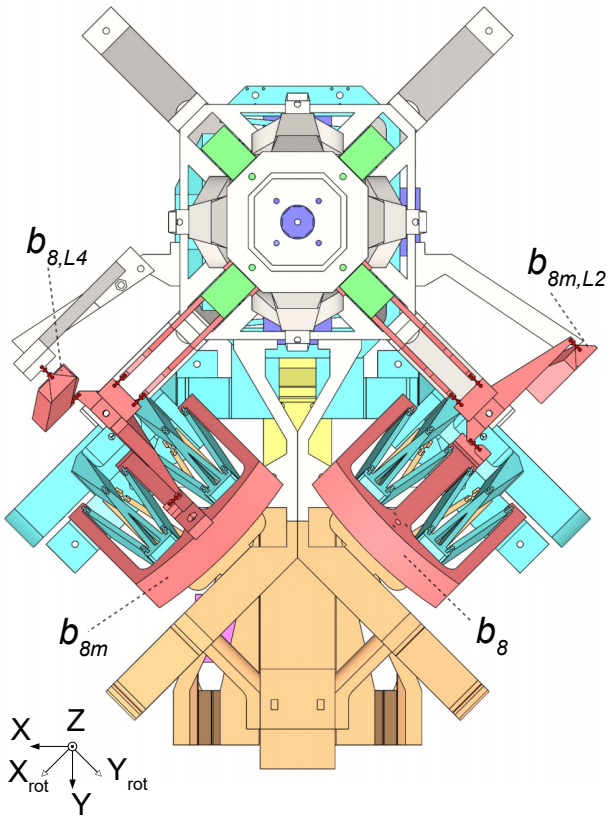

(a) Top view of the design of the compliant design.

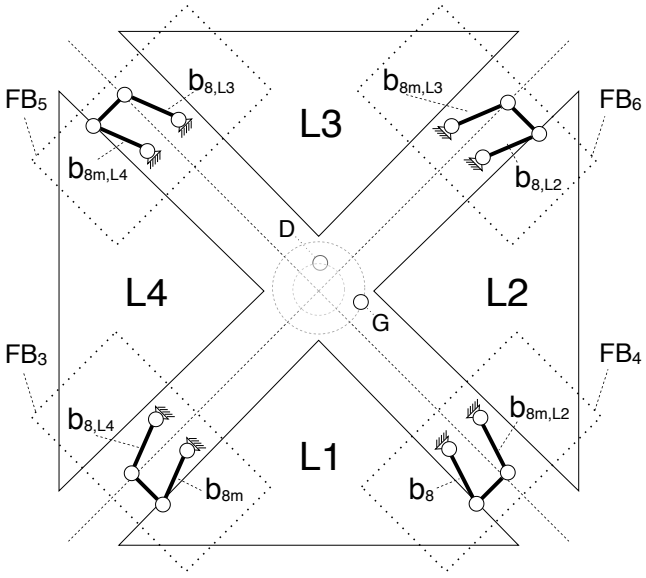

(b) Schematic top view of the integration of the four legs (L1-L4).

Figure 3.18: Two views of the motion coupling mechanism, including the end effector designed for measuring its displacement.

3.7.1 Direction setpoint coupling

In order for all the legs to propel the machine in the same direction, the direction setpoint mechanisms of the separate legs are designed such that they can be coupled among one another. This coupling is realized by means of the fourbar linkages FB_3 to FB_6. As

shown in fig. 3.18b, b_8 of leg 1 (L1) is coupled to the $b_{8m,L2}$ bar of the neighbouring leg (L2) constructing the fourbar mechanism FB_4. With the labelling of the bars, the subscripted L2,L3 and L4 indicate the relative leg it belongs to. As depicted in the drawing, this coupling is made between all four of the legs. For the single compliant design as in this paper presented, $b_{8,L4}$ and $b_{8m,L2}$ were replaced by a less complex substitute. These are indicated in fig. 3.18a.
From the coupling ultimately follows that the angles θ_1 and θ_2 of all the four legs will be related by $\theta_{1,y}$ = -$\theta_{2,x}$, with *x* and *y* indicating the relative neighbouring leg. So for *y* = L1, *x* = L2, for *y* = L2, *x* = L3 and so forth. For clarity, the rotated coordinate system $X_{rot}Y_{rot}Z_{rot}$ of leg L1 is related to the orientation of L1. The other legs are in different orientations thus so are their rotated coordinate systems. With this, the definition of θ_1, y and θ_2, x are always with respect to their respective rotated coordinate systems.

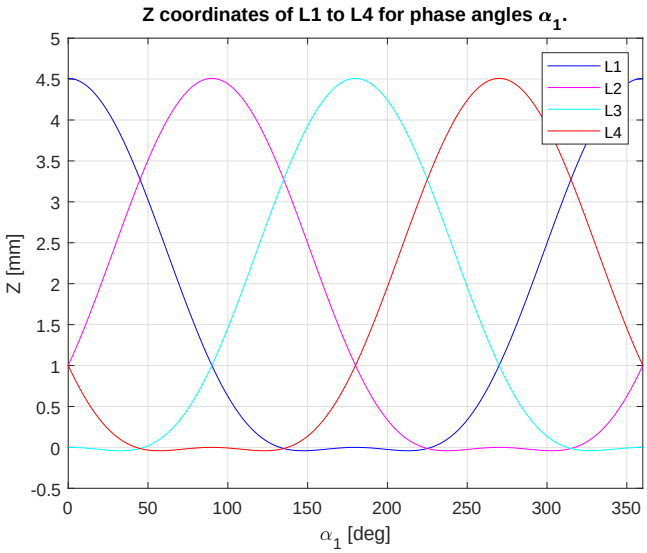

Figure 3.19: Plot of the Z positions of L1 to L4 against α_1.

3.7.2 Output phase coupling

Although the direction coupling as indicated in the previous paragraph reduces the number of links required compared to a system in which each leg has its own direction setpoint mechanism, it introduces undesired behaviour if left unchanged.
A kinematic analysis shows that the direction of set by each of the legs is nearly equal. However, the movement of the end effector along the path of two of the leg mechanisms will be inverted. As an example, figure 3.20 shows the absolute directions of L1 to L4 for the same direction input angle α_2 by means of the projection of the end effector paths for α_1 from 0 to 360 degrees onto the XY plane. This indicates the closely matching movement direction of the four end effectors for similar α_2. The more problematic side is shown by fig. 3.21, where the projections of the paths onto the YZ plane are displayed by the dotted lines. The start of the arrows indicate the point at which α_1 = 0 and the arrows point in the direction of increasing α_1.

Clearly, L2 and L4 oppose the direction of movement of L1 and L3. As indicated by fig. 3.22, inverting the Z position transmission solves this problem. The proposed strategy of physically implementing this is by rotating the Z transmission 180 degrees along the Z-axis, while maintaining the same connection points with the frame and IMG1. Finally, the phase difference between the legs will remain 90 degrees, offering support to the machine over the entire operating range. This is shown in fig. 3.19.

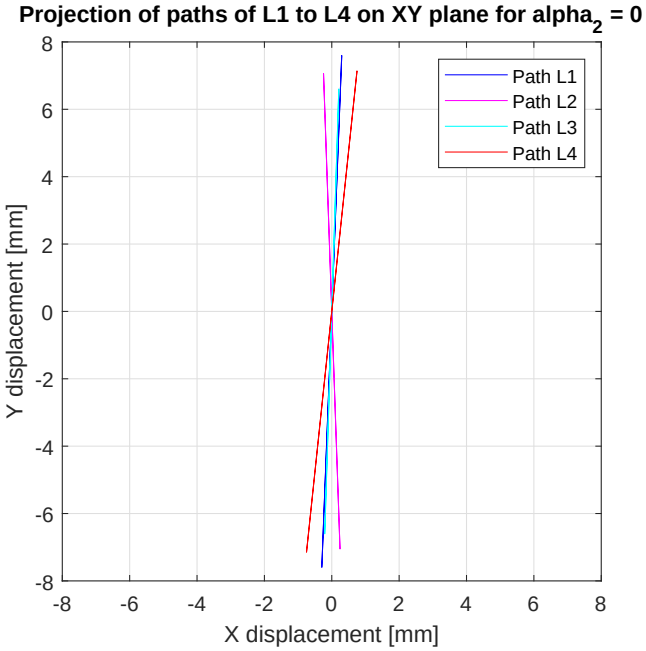

Figure 3.20: Projection of the paths of L1 to L4 onto the XY surface at α_2=0.

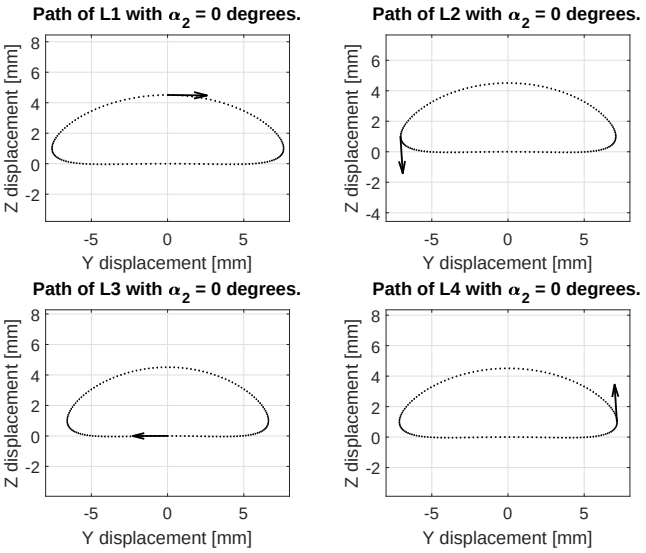

Figure 3.21: Projection of the paths of L1 to L4 onto the YZ surface at α_2=0, without any modifications.

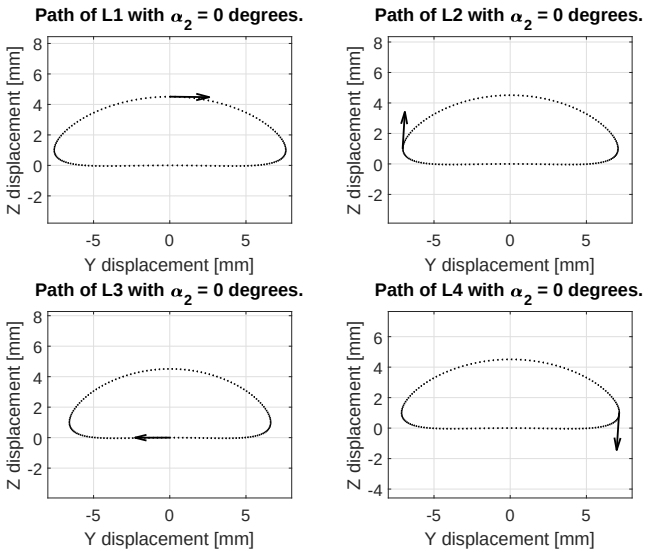

Figure 3.22: Projection of the paths of L1 to L4 onto the YZ surface at α_2=0, with inverted Z transmission.

3.8 Detailed design

3.8.1 Dimensioning and fabrication

Dimensioning and materials

With the construction of the kinematic and physical model comes the dimensioning of the components.The parts were dimensioned to produce a functioning and robust physical model. For the kinematic design this meant a limitation in the angle of rotation of 45 degrees to limit the deflections of the hinges. Furthermore, to limit the overall size of the mechanism, yet produce a properly observable result, r_{input} of IMG1 was set at 10 mm and r_{dir} of IMG2 was set at 20 mm. Taking into account the maximum deflection angle and the input radii, the rest of the kinematic model of the mechanism was dimensioned.

Concerning the physical model, the production process and resulting stiffnesses of the joints were taken into account. The production process of choice was FDM (Fused Deposition Modeling) 3D printing for its possibility of producing multi-material parts at relatively low cost. The Sarrus linkages were printed out of PET (Polyethylene terephthalate)[1] for its toughness, allowing repeated load cycles. Stiff parts were printed out of PLA[2] (polylactic acid) and the compliant hinges out of a TPE[3] (thermoplastic polyester elastomer) with a significantly lower stiffness. This combination was chosen to ensure a low stiffness in motion transmission and a high degree of similarity with respect to the kinematic model as it allowed for the use of notch flexures with relatively small curvatures. The used nozzle diameter was 0.4 mm, with a layer height 0.2 mm. Referring to fig. 3.23, the notch flexures were dimensioned with the minimal thickness (t) the printer could reliably produce (0.8 mm). The curvature (r) and height (h) were consecutively dimensioned such to minimize rotational stiffness with acceptable out of plane and translational stiffnesses.

To ensure a robust printing method and prototype, the physical model was produced in a modular fashion. This allowed for the deposition of the filament in favourable directions as well as easy replacement of subcomponents. The bar lengths of the Robert's linkages providing translational DOFS were maximized up to the constraints of the build volume of the printing process. This lengthened the moment arms and thus minimized the stiffness of the Robert's linkages in the motion direction, while additionally making the Robert's linkages execute their straight-line behaviour more accurately.

Fabrication and assembly

The components were assembled by means of a bolted connection and positioned using steel balls, placed in conical cups (fig. 3.24a) centred around the bolthole. A connection piece is depicted in fig. 3.24b, on which the balls and connection hole for the bolt are shown. To minimize imperfections in the model, the flexible joints were printed simultaneously with the linking elements. To ensure connection between the two materials, a geometrically constraining juncture was used. This is displayed and labelled *c* in fig. 3.23.

3.8.2 Optimization of Z motion

With the objective of tracing a straight line during the stance phase of the leg, or more generally, describing a plane for the lower part of the generated surface, the transmission for the Z position has to ascertain the end effector to remain (approximately) stationary during this part of the cycle. To do so, a dimensional optimization of this mechanism was performed. For this, a kinematic model of this subcomponent was used incorporating rigid links and perfect joints.

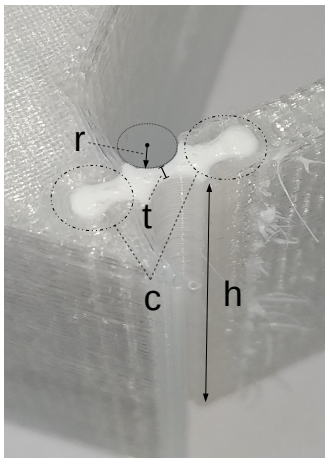

Figure 3.23: Picture showing the connection between flexible and stiff material.

[1] Brand: RS PRO, 1.75 mm
[2] Brand: RS PRO, 2.85 mm
[3] Brand: MTB3D flex 45, 2.85 mm

The optimization problem was defined as follows:

$$\min_{|b_4|,|b_5|,|b_7|,Z_{R_8},Y_{R_8}} \quad \sum_{\alpha_1=\frac{3\pi}{4}}^{\frac{5\pi}{4}} Z_{b_6}(\alpha_1,...) - Z_{b_6}(\frac{3\pi}{4},...) \tag{3.3}$$

$$s.t. \qquad Z_{b_6}(\frac{\pi}{2},...) - Z_{b_6}(\pi,...) + 1 \leq 0 \tag{3.4}$$

$$Z_{b_6}(0,...) - Z_{b_6}(\pi,...) - 8 \leq 0 \tag{3.5}$$

$$\textit{for} \quad \frac{\pi}{2} \leq \alpha_1 \leq \frac{3\pi}{2}\textit{:} \qquad Z_{b_6}(\alpha_1,...) - Z_{b_6}(\frac{\pi}{2},...) \leq 0 \tag{3.6}$$

$$\textit{for} \quad 0 \leq \alpha_1 < \frac{\pi}{2} \quad \wedge \quad \frac{3\pi}{2} \leq \alpha_1 < 2\pi\textit{:} \qquad Z_{b_6}(\alpha_1,...) + Z_{b_6}(\frac{\pi}{2},...) \leq 0 \tag{3.7}$$

$$\angle Yb_7(\alpha_1,...) - \frac{\pi}{2.2} \leq 0 \tag{3.8}$$

$$-\angle Yb_7(\alpha_1,...) - \frac{\pi}{2.2} \leq 0 \tag{3.9}$$

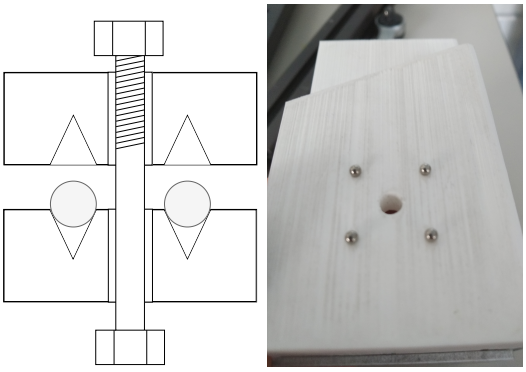

(a) A graphical indication of the used connections, showing a cross section of the two components, bolt, nut and balls.

(b) A connection between the 3D printed components, showing the bolthole and steel balls for centring.

Figure 3.24: Examples of connection between parts.

In words, the path of Z_{b_6} was optimized to stay on its $\alpha_1 = \frac{3\pi}{4}$ level, for $\frac{3\pi}{4} \leq \alpha_1 \leq \frac{5\pi}{4}$. This was done by discretizing, summing up and minimizing the differences of the steps with respect to the $Z_{b_6}(\frac{3\pi}{4})$ position (eq. (3.3)).
The design variables were taken to be $|b_4|, |b_5|, |b_7|, Z_{R_8}, Y_{R_8}$ with $|b_{..}|$ indicating the length of the respective bar and $Z_{...}$ and $Y_{...}$ indicating the Z and Y coordinate of the indicated joint respectively. In eq. (3.3) up to eq. (3.7), these are replaced by ",...".
Constraint eq. (3.4) ascertains the level of the end effector at $\alpha_1 = \frac{\pi}{2}$ is at least a length of 1 (mm) higher than the $Z_{b_6}(\frac{3\pi}{4})$ level. Constraint eq. (3.5) makes sure Z_{b_6} remains below a value of 8 (mm) measured from the midpoint of the desired stationary part. Constraint eq. (3.6) and eq. (3.7) ascertain the path remains respectively below and above the $Z_{b_6}(\frac{\pi}{2})$ value, for according α_1. Eq. 3.8 and eq. (3.9) were implemented by penalizing with a value of 10 in case of violation, this ensured a limited angle between b_7 and the Y-axis for proper load capacity concerning moments around the X-axis.
A Sequential Quadratic Programming method was applied and implemented using the *fmincon()* function in MATLAB. The initial values were set at [40,20,40,-20,-40], with the origin at S_4. The step and function tolerance defining the stopping criterium were set at 1^{-6}.

Bounds of the design variables were 0.1 to 150, except for Y_{R_8} for which the bounds were set at -120 to 130.

3.9 Experimental set-up

The kinematics of the end effector of the physical system was measured by means of three laser triangulation displacement sensors measuring the X, Y and Z position of the end effector, see fig. 3.25. The resolutions of these devices were 4μm, 4μm and .5μm for X,Y and Z respectively. The system was actuated by means of two stepper motors, one actuating IMG1 (α_1) and one actuating IMG2 (α_2). In order to be able to relate the angles (α_1 and α_2) with the position of the end effector, a full rotation of both actuators, discretized into 50 steps was performed and recorded. Furthermore, the starting and final stance of the stepper motors was recorded as respectively a zero and a verification. The resolution of the IMG1 and IMG2 angle measurements were 0.72 and 0.5 degrees respectively. The measurement cycle was performed five times. As shown in fig. 3.25a and fig. 3.25b, flattened aluminium measurement surfaces were glued to the 3D printed end-effector to limit disturbances caused by surface roughness.

(a) Laser triangulation displacement sensors in the setup for measuring the X and Y position, left and right respectively.

(b) Laser triangulation displacement sensor for measuring the Z direction (right) and Y position (left) of the end effector.

Figure 3.25: Close up on the laser triangulation displacement sensors measuring the end effector.

Next to the measuring of the end effector, several time-

lapses were made of the moving system. This provided an indication of the motion of the subcomponents and thus their individual performance.

3.10 Results

In this section the properties of the kinematic and physical model will consecutively be discussed. As a reference, we introduce a system of planes Z_{proj},Y_{proj} and X_{proj}, which indicate the XY plane, ZY plane and the ZX plane respectively, rotated by angle β, as indicated in fig. 3.4. Furthermore, setting α_1 = 0 corresponds with the centre top of the surface, α_1 = 90 and 270 degrees with the extremes in *X* and *Y* direction and α_1 = 180 degrees with the bottom centre, taking the *Z* direction to define the top and bottom. In addition, to provide a meaningful indicator, the dimensions and deviations as measured and calculated will be related to the diameter of IMG1 (20 mm) and/or relevant other dimensions.

3.10.1 Kinematic model

Concerning the kinematic design, the rotation axis of the plane set by IMG2 is located at the centre (of the XY projection) of the spatial surface and is parallel with the Z direction. Also, the surface has a two-fold rotational symmetry for every instance of α_2 comparing $0 < \alpha_1 < 180$ deg with respect to $360 > \alpha_1 > 180$ deg.

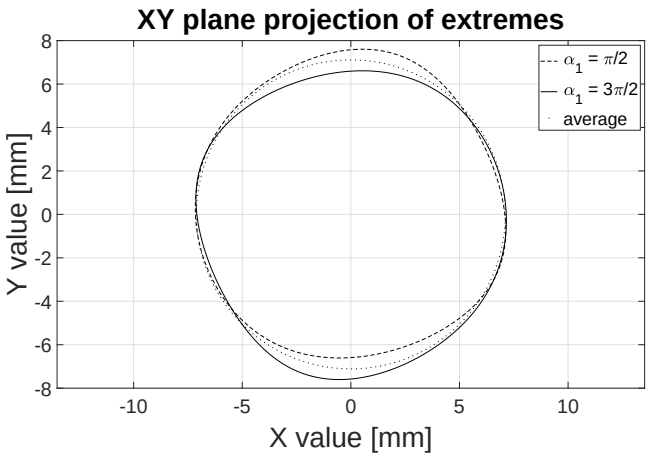

Figure 3.26: Projection of the outer values of the surface described by the kinematic model onto the XY plane.

Quantitatively, the kinematic model shows the following properties. In Z direction, the height of the surface, comparing the extreme values is 4.55 mm. Meaning the transmission ratio from IMG1 to the surface height is .2275. The average diameter of the projection (of 10^3 samples) upon the XY plane of the most outer points is 14.22 mm. This length has maximum of 15.33 mm and a minimum of 13.09 mm. This means that the diameter of IMG1 is transmitted through a mean ratio of 0.711. The lengths and mean diameter of these extreme values are shown in fig. 3.26. Several paths over the surface at rotation angles α_2 around the central axis are shown in fig. 3.27 to provide a view on this length variation and the overall surface shape. For $135 < \alpha_1 < 225$ deg, the surface deviates from the Z coordinates of $\alpha_1 = 135$ deg and $\alpha_1 = 225$ deg by a maximum of -27.48 μm at α_1= 147.07 deg and 212.93 deg with a total difference between the extremes of 41.39 μm. The course of the deviation is shown in fig. 3.28. The mean absolute deviation out of 10^3 instances is 14.80 μm. Taking the maximum deviation as a reference, this results in a ratio with respect to IMG1 of 0.001374.

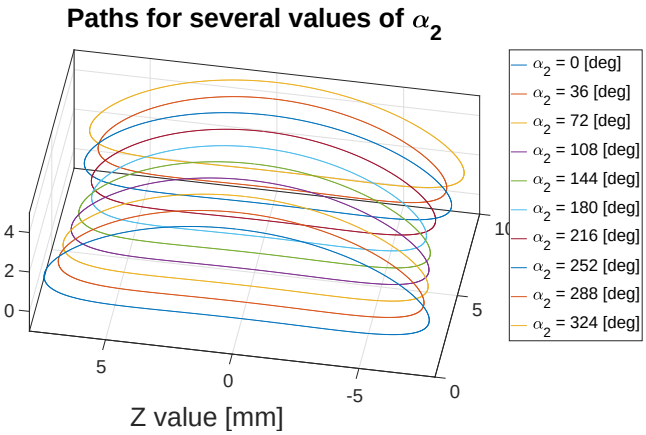

Figure 3.27: Paths along the surface for several values of α_2.

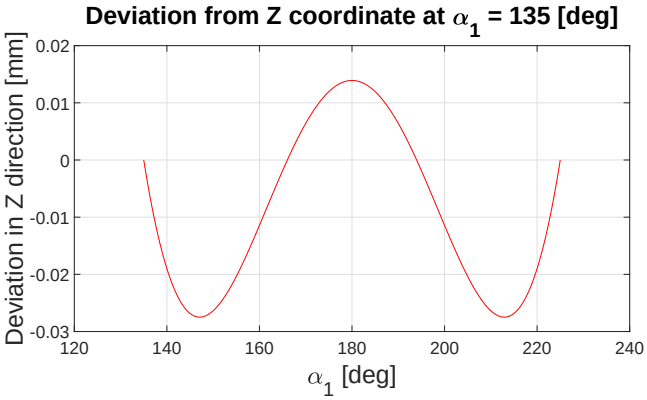

Figure 3.28: Deviation of the Z position of the end effector with respect to $Z(\alpha_1 = 135[deg])$.

3.10.2 Physical model

A comparison of the kinematically determined surface, with respect to the physically measured surface is shown in fig. 3.36. The figures on the right show the surfaces generated by the kinematic model, the figures on the left are created by the measured points of the physical system. Projected side and top views of several paths are shown in figures 3.34 and 3.35 respectively, providing a more detailed view on the path shapes. The deviations with respect to the ideal situation will be presented by means of several indicative values, starting off with the differences in the angles β of the physical system with respect to the theoretical model. The denoted error bars indicate the maximum

possible values as introduced by the measurement uncertainties. In addition, the standard deviation of the five samples is included to indicate influences not accounted for in the error bars, including vibrations of the system. This is denoted by σ.

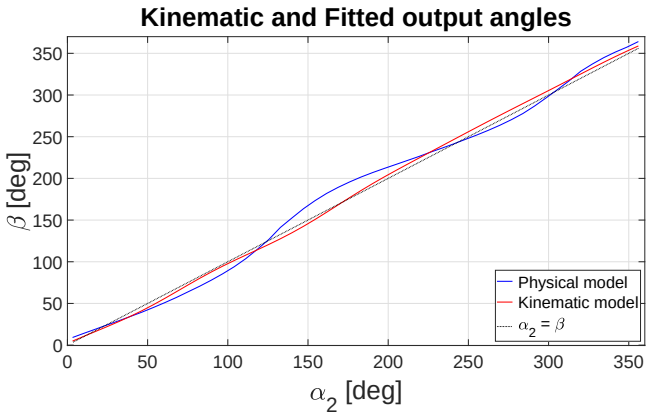

Figure 3.29: Resulting angles β with input angle α_2.

The angles fitted by means of a least squares method onto the measured dataset, as well as the angles generated by the kinematic model and a 1:1 relation between α_2 and β as a reference are shown in fig. 3.29. The deviations are depicted in fig. 3.30, where the subscript Pmodel and Kmodel indicate the physical and the kinematic model respectively. The whiskers indicate the measurement uncertainties, with an incertainty in α_2 of 0.5 deg.

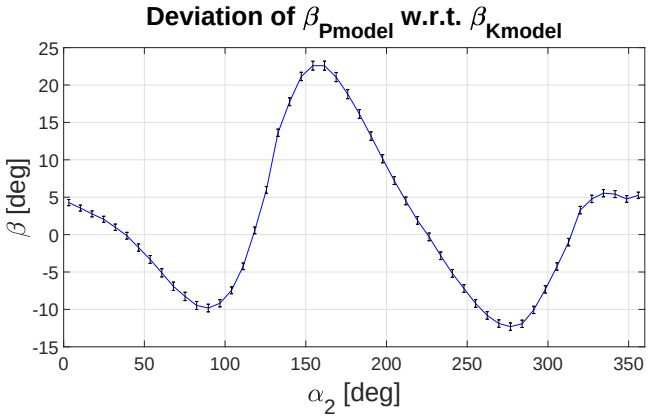

Figure 3.30: Deviation of measured angles with respect to kinematically determined angles.

Other deviations include the variation in the approximately planar part of the surface for $135 < \alpha_1 < 225$ deg. A least squares fit for all the measured angles α_2 shows a varying angle of this part of the surface with respect to the horizontal. The mean of this angle, for each measured α_2, is shown in fig. 3.31. As well as a difference in angle, the vertical variations from a line drawn on Y_{proj} from Z(α_1= 135 deg) to Z(α_1= 225 deg) are indicated in fig. 3.33 for all measured angles α_2. The mean maximum deviation from this line is -0.1$^{+0.01}_{-0.01}$mm, with σ = 0.01 mm. The mean difference over all angles α_2 is -0.05$^{+0.007}_{-0.008}$mm with σ = 0.011mm.

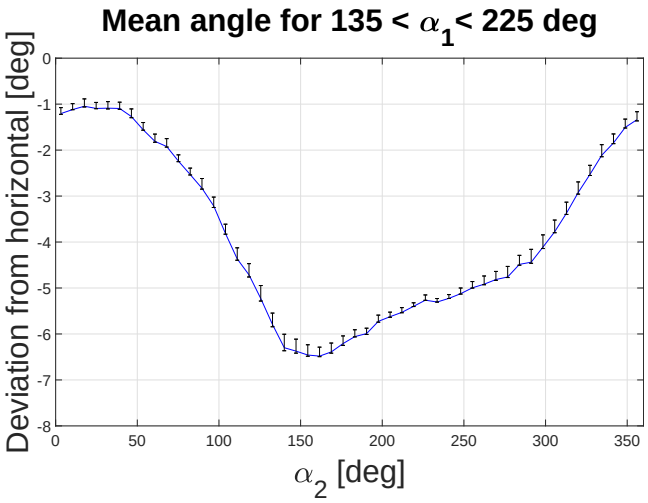

Figure 3.31: Angle of fitted line through the points $135 < \alpha_1 < 225$ deg, w.r.t. horizontal.

The height of the measured model, taken as the difference in Z direction between α_1 = 0 and α_1=180 degrees has a mean of 4.248$^{+0.03}_{-0.03}$ mm and σ = 0.03 mm. This means a ratio of the diameter of IMG1 of 0.212. Observing figs. 3.36a, 3.36c, 3.36e and 3.36g more thoroughly, an eccentricity of the travelled paths becomes clear. To give a measure of the eccentricity of the measured surface, the path-lengths of the XY-plane projection of α_1 = 0 and 180 degrees are taken. A plot is given in fig. 3.32. The mean path-length at α_1 = 180 deg is 7.4$^{+0.3}_{-0.3}$ mm with σ = 0.1mm. The mean path-length at α_1 = 0 is 4.2$^{+0.1}_{-0.1}$ mm with σ 0.1mm.

Concerning the Y_{proj} width, the on Y_{proj} projected length from α_1 = 90 deg to α_1 = 270 deg is taken as indicator. This results in a mean value of 3.9$^{+0.03}_{-0.02}$ with σ = 0.53mm, a ratio of 0.194 times the IMG1 diameter.

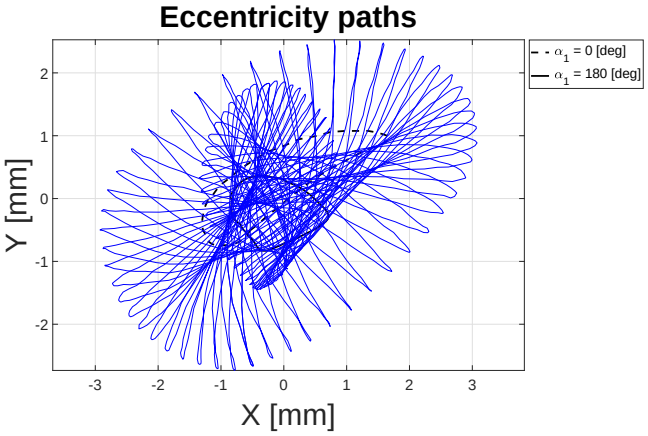

Figure 3.32: Projections of the paths of $\alpha_1 = 0$ and 180 degrees on the XY plane, for all the angles α_2.

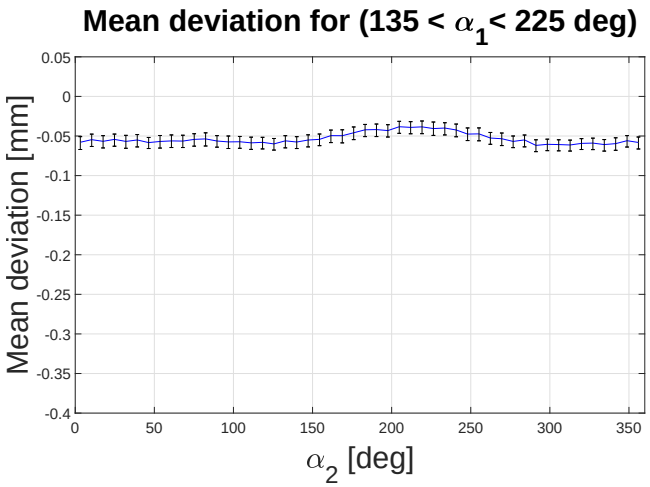

Figure 3.33: Mean absolute deviation of the measured Z position with respect to the line through $Z(\alpha_1 = 135\ deg)$ and $Z(\alpha_1 = 225\ deg)$.

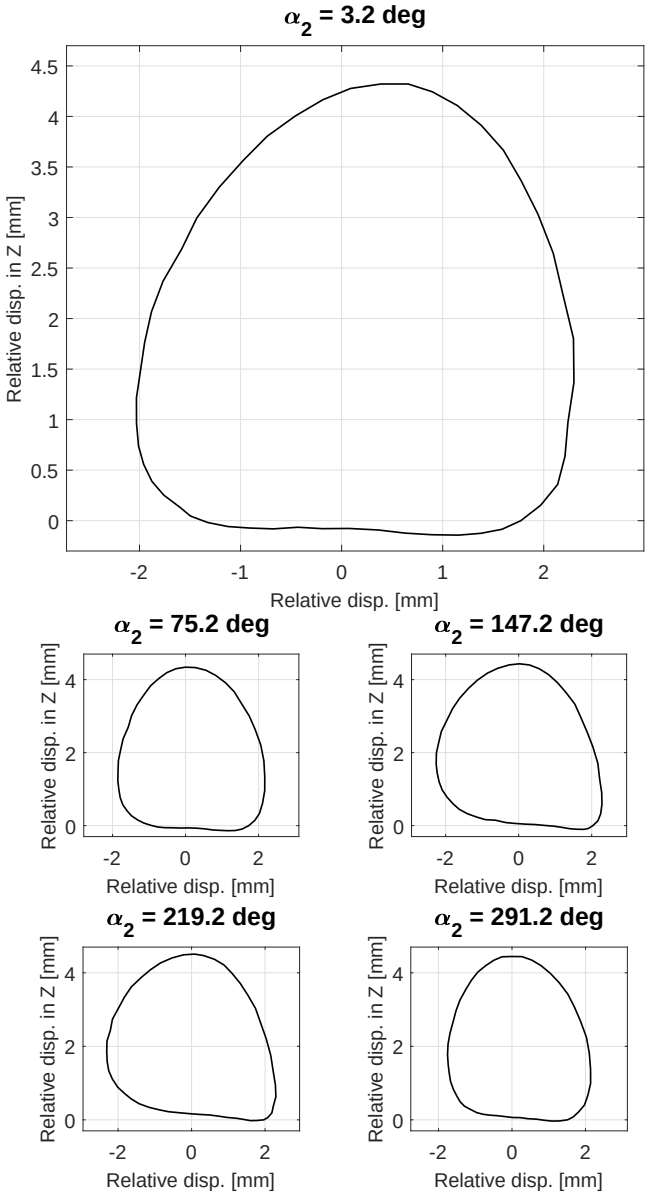

Figure 3.34: Examples of projections of measured paths onto a plane rotated by kinematically determined angle β, at several values of α_2.

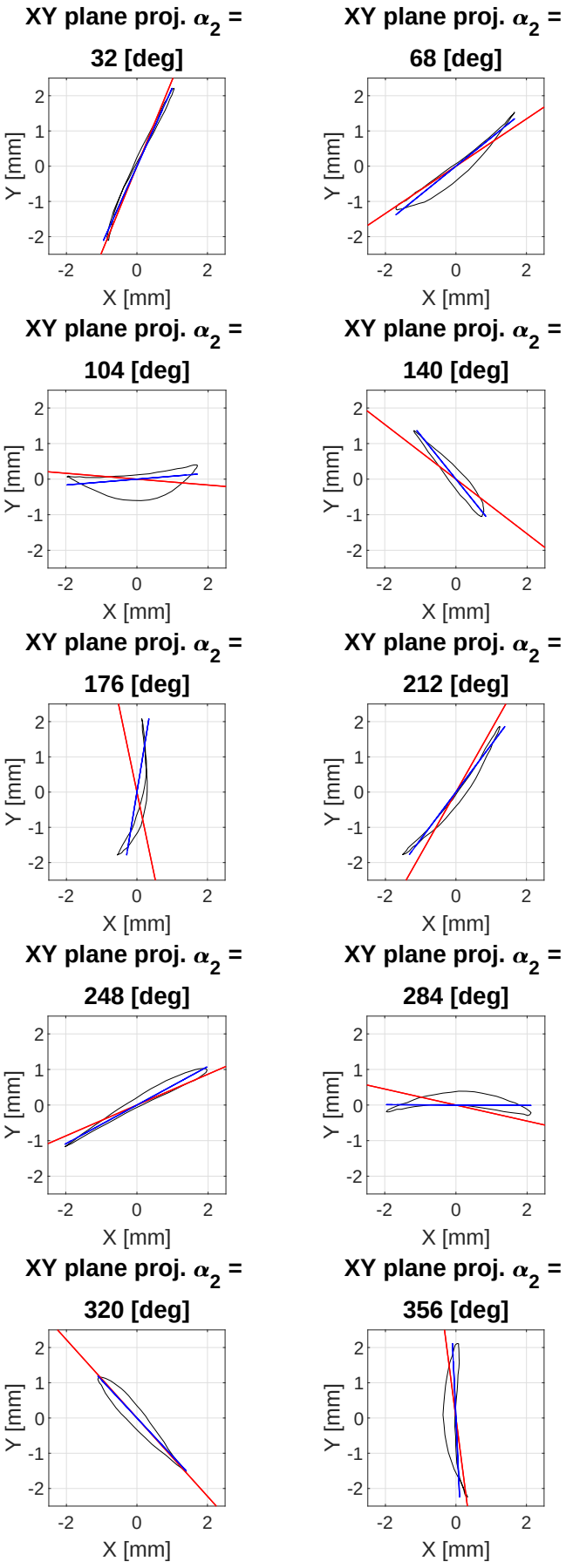

Figure 3.35: Projections of the paths onto the XY plane of several values of α_2. Here, the red lines indicate the kinematically calculated angles and blue the angles fitted on the measured dataset.

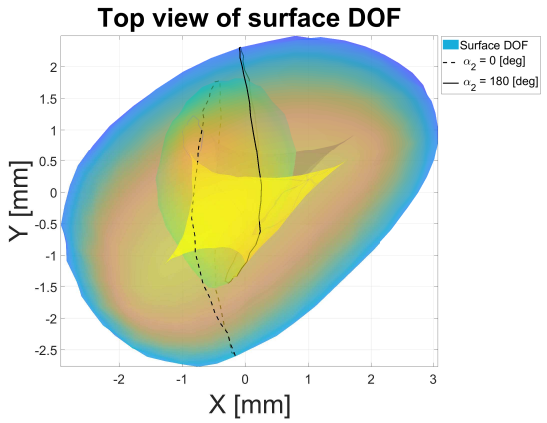

(a) Top view of measured surface.

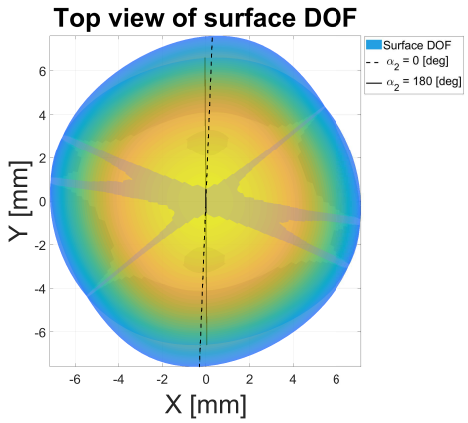

(b) Top view of surface generated by the kinematic model.

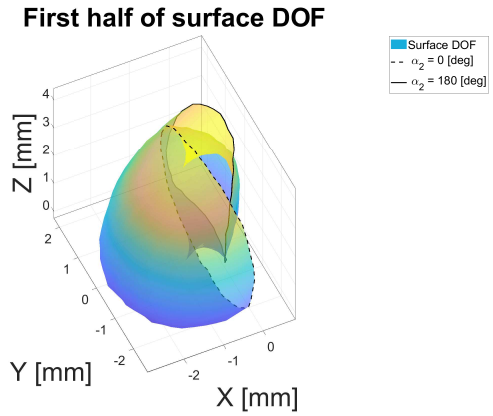

(c) Measured surface for α_2 = 0 to 180 deg.

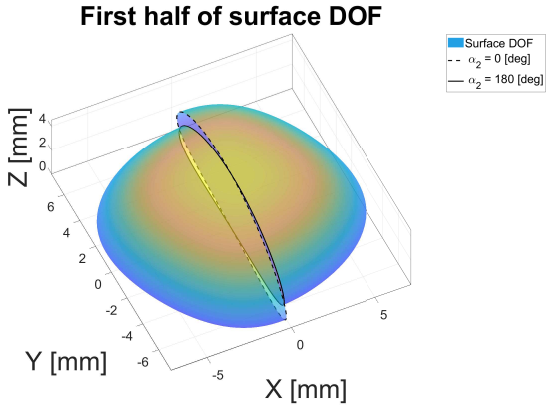

(d) Surface for α_2 = 0 to 180 deg. as generated by the kinematic model.

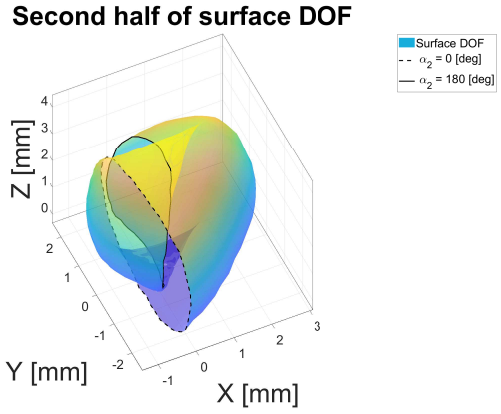

(e) Measured surface for α_2 = 180 to 360 deg.

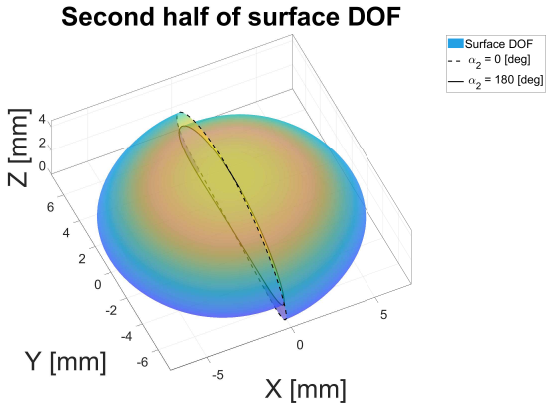

(f) Surface for α_2 = 180 to 360 deg. as generated by the kinematic model.

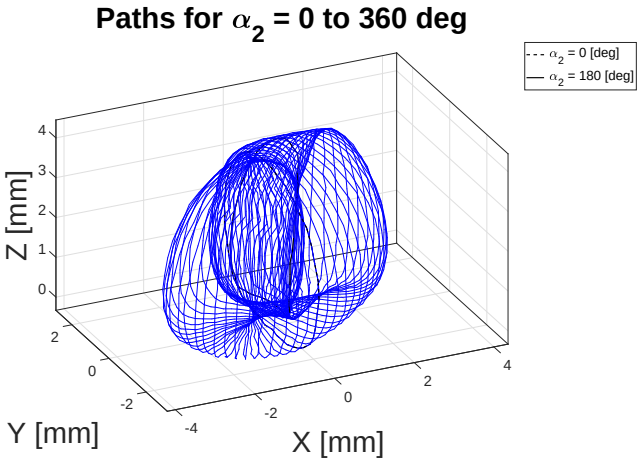

(g) Measured paths.

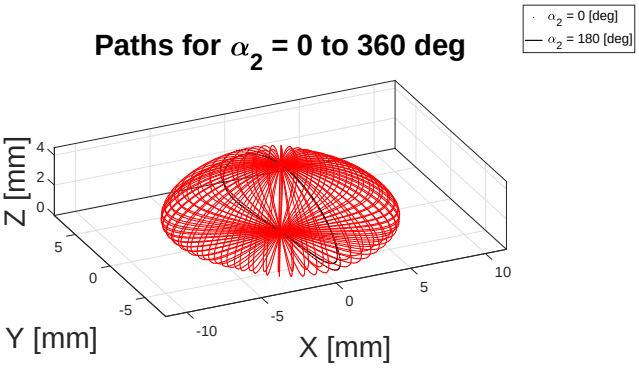

(h) Paths as generated by the kinematic model.

Figure 3.36: Plots of measured points (left)] and by the kinematic model generated points (right).

3.11 Discussion

As the results indicate, the design process has led to a design which enables the overall intended machine to fulfil the objectives stated in section 3.8. The kinematic and physical model both verify this. In addition, both give an indication of the deviations from the assumed ideal situation. We will first discuss the performance of the kinematic model and then continue with the discussion of the results of the physical system.

3.11.1 Kinematic model

Concerning the results of the kinematic model, several remarks can be made. Firstly the average diameter of the outer values of the surface as projected onto the XY plane. The indicated ratio between IMG1 and mean output diameter is 0.711. This ratio stems from the rotations of b_8 and b_{8m}, which are designed to ideally stay within the bounds of a 45 degree rotation, resulting in a reduction of the transmitted displacement. The deviations from this mean are most likely due to the parasitic motions induced by the parallel mechanisms FB_1 and FB_2 in the direction setpoint mechanism. These cause the θ_1 and θ_2 angles to reach values larger (and smaller) than 45 degrees in an asymmetric fashion, where the design intended to set them at 45 degrees. This generates a rotationally asymmetric surface.
Additionally, with the presented design of the direction setpoint mechanism, angle α_2 and β are related in a ratio unequal to 1:1. For the design of a single mechanism this is not a problem. However, when combining four of these (to form the kinematic basis of a walking machine) by the coupling as proposed in section 3.7, these deviations will introduce velocity and directional change in the behaviour of the entire system when applying a constant angular input velocity at IMG1. This is undesirable and a solution strategy for this would be to either implement a control system for the angular velocity of the input motion generators, or modify the direction setpoint mechanism such that these variations are no longer present.
The height of the surface in Z direction is related to the dimensions of the Z transmission mechanism. The optimization has resulted in the presented deviations from the desired level, this is a relatively good result when comparing with respect to the overall height of the surface and the diameter of IMG1. However, a more optimal approach of a straight line might be achieved by modifying the optimization process of the Z transmission. Running the optimization from different starting points has shown different results, indicating local minima. A different optimization algorithm, a more thorough analysis of the problem or a parallel run with a large set of starting values might improve the outcome of the optimization. Concerning the design itself, a main advantage is that the loading of the mechanism is such that the directions of force are predominantly in the tension/compression direction. This is the stiffest direction of the used notch flexures and thus does this introduce a minimal amount of unwanted deflection in case of applied external loads.
Lastly, again referring to the use of the designed mechanism for its proposed purpose as walking machine, the X and Y transmission velocity is directly related to the X velocity of IMG1. This means that over the period 135 deg < α_1 < 225 deg, the velocity is not constant but rather follows the top part of a sinusoid curve. Assuming this period is the stance phase, the overall machine will show minor deviations in velocity with a constant angular velocity on IMG1. This issue could be addressed by modifications in the X and Y transmission.
Finally, these mentioned modifications are all possible because the design of the mechanism is such that the subcomponents responsible for the respective movement can be altered as desired, without requiring a complete design overhaul.

3.11.2 Physical system

In the measured physical system, the largest deviation from the kinematic model is in the projected mean diameter/width of the outer points of the surface onto the XY plane. Correcting for the shown eccentricity, the resulting mean XY-projected diameter of the physical system would be 3.880 mm. Which is a factor of 0.273 times the kinematically perfect situation. Observations of the time-lapses of the machine show that during the rotation of IMG1 for any given setpoint of IMG2, the b_8 and b_8m bars show an oscillation in phase with the position of IMG1. Effectively, this rotational deflection is the most likely cause of this largely reduced diameter/width of the output surface. Possibly, the stiffnesses in the motion coupler mechanism are significant with respect to the stiffness of the direction setpoint mechanism, resulting in these rotational deflections and thus a smaller than desired movement in the XY plane. This might be related to the fact that FB_3 and FB_4 are constructed out of plane, impeding the overall stiffness. Another influencing factor to the direction setpoint mechanism stiffness might be the orientation of b_8 and b_{8m}. Since FB_1 and FB_2 can only transmit force in the tension/compression direction, the stiffness in rotation of bars b_8 and b_{8m} is lower for higher rotations in angles θ_1 and θ_2. This is due to the load vector rotating more towards the unconstrained direction of the FB_1 and FB_2 parallel fourbars. Next to the observed oscillations in b_8 and b_{8m}, the motion of IMG1 showed a variation as well. For $\pm$ 45 < α_1 < $\pm$ 135 degrees, the radius of IMG1 appeared to be smaller than for the rest of the cycle. The time-lapse videos clearly indicate this change in radius. Since the radius of IMG1 determines the displacement over the XY-plane of the end effector, this could partially explain the asymmetry and reduced diameter/width of the described surface.
Another type of deviation of the physical system with respect to the kinematic model is the deviation of a straight line in the projection onto the XY plane. The resulting fitted angle β as indicated in fig. 3.29 is based upon a least squares method. With the curvature of the paths as indicated in fig. 3.35 it is hard to judge if the fitted angle gives a proper indication of the angle of

the path. The cause of this curvature might lie in the angular deflections of b_8 and b_{8m} as well. An undesired rotation of one of these bars respectively increases the influence of the other of the two in the generation of the path and can thus produce the discussed curvature.
Another indication that the deviation of the measured angle β relates to the curvature in the paths is explained by means of fig. 3.30 where three extreme values appear to be around 90, 160 and 275 degrees. Figure 3.35 shows that the fitted angle of the projection onto the XY plane at 104 degrees, 176 and 284 degrees, is influenced by the curvature of the path. With FB_3 and FB_4 extending out of plane and being asymmetrical, the amplitude of the undesired deflection of b_8 and b_{8m} is likely to be different and therefore another possible explanation for the curvature in the XY-plane projection. This then forms a contribution to the deviation in the angles β between the kinematic and physical model.
The physical model shows a deviation of a straight line which is slightly larger than the calculated deviation. The absolute mean deviation is measured to be 3.72 times larger. Putting this into perspective by taking the total calculated height as a reference, the mean absolute deviation of the kinematic model is a ratio of 0.00325, with respect to 0.012 for the physical system. Or a ratio of 0.001374 and 0.005 with respect to the IMG1 diameter for the kinematic and physical model respectively. This deviation is expected to be mainly caused by the stiffnesses of the joints, altering the behaviour of the Z transmission.Other spotted variations for which a clear cause is not readily extracted include the eccentricity and the angle in the lines drawn from α_1=135 to 225 degrees for any given α_2. Factors one could think off possibly contributing to these deviations include all of the above, just as well as other finite stiffnesses of the system and misalignment due to the printing process and assembly. Also, the weight of the motion coupler might have deformed the structure such that the paths of the end effector were influenced. Additionally, due to finite stiffnesses in the system, the point of measurement might have shown a rotation induced displacement. Essentially, this could have made a slight rotation appear as a displacement due to the arm lengths from the centre of rotation to the measured points.

3.12 Conclusion

We have presented a kinematic and physical design of a compliant system capable of describing a closed spatial surface. This two DOF motion can be generated by making use of only two actuated inputs and it is not limited in its motion by the inherent kinematic constraints of the used compliant mechanisms. The kinematic analysis shows that the shape of the created surface is approximately planar for the angles of the input IMG1 between 135 and 225 degrees, with a maximum deviation of 27.48 μm, a ratio with respect to the diameter of IMG1 of 0.001374. The physical model shows that when introducing materials with finite stiffnesses, this deviation increases to 0.1 mm or a ratio of 0.005 with respect to the diameter of IMG1. Although this increase seems significant, the mean absolute deviation calculated over the 50 discrete paths as set by α_2 is only a fraction of 0.012 of the total height of the kinematically calculated surface.
A further analysis of the shape of the paths drawn by the physical system indicates an XY projected mean diameter of 0.273 times the kinematically perfect situation. Also, the physical system seems to show a curvature in the paths projected onto the XY plane. These indicate that significant improvements can be made in future designs. Having combined this with information obtained from time-lapse videos, proposed improvement directions and their possible impact have been suggested. These involve improvements in the directions setpoint mechanism as well as modelling of the stiffnesses in the design.
Also, slightly declined angles for the line from α_1 = 135 to 225 degrees with respect to the horizontal and an eccentricity was observed. The cause of these deviations remains unclear.
The surface of the physical system shows a height which is 5.79% smaller than the calculated height. This is small with respect to the deviations in width/diameter, from which we conclude that the performance of the physical Z transmission is relatively good.
Next to the generation of the surface, a manner of coupling four of the designed mechanisms was presented, providing a basis for the design of an omnidirectional walking machine.
Altogether, the overall design proves capable of describing the desired type of surface by a kinematic model as well as a physical system. The system has clearly defined function boundaries of its subcomponents and is therefore readily modifiable. Going more into depth, an analysis has indicated prominent improvement directions, from which has furthermore followed that improvements in the performance of the physical system can be made by more accurately modelling the stiffnesses of the system and improving its design correspondingly.
With the proven functioning of this system, a step towards the design of an omnidirectional compliant walking machine, utilizing only two actuators is made. This can extend the use-cases of such machines by adding the benefits of compliant mechanisms, which include no backlash, an absent need for lubrication and the possibility of monolithic fabrication. Also, with the presented shape of the surface, the machines utilizing these kind of mechanisms for their propulsion can have an approximately constant height of their centre of mass with respect to the supporting surface. Future work will have to ensure the load bearing capacity of this mechanism to make it readily applicable, as well as combine a multitude of these mechanisms to create a fully functional machine.
The intended purpose of utilization in a walking machine does not limit the possible uses of the system though. In its coupled form, it could find use in the simultaneous bearing and propulsion of planar stages, where the body of the mechanism is fixed with the end

effectors pointing upwards and a movable surface is supported on top. Furthermore, when attaching different tools onto the end effector, the single mechanism could for instance find use in pick and place procedures or specific curvature milling tasks as found in the production of lenses.

Concluding, the first steps towards a compliant, omnidirectional walking machine have been taken in an attempt to fill the indicated gap in literature. This has produced a 2-DOF compliant mechanism capable of describing a closed spatial surface, intended for use as leg in such a system. A kinematic and experimental evaluation have proved the functioning of the device without the application of external loads. Future work will have to further develop the single mechanism into a complete, functioning machine.

Chapter 4

Extended discussion & conclusion

4.1 Extended discussion

The focus of this project was on the design of a compliant omnidirectional walking machine utilizing only two actuators, predominantly exploring the difficulties that come into play in doing so. To accommodate the understanding of the functions of the system, some initial iterations were made of a single leg, this produced design 1,2 and 3 (appendix B). By consecutively producing, analyzing and ordering solution possibilities, design strategies were extracted (appendix C). The differences between design strategies were considered and consecutively a decision between the strategies was made to guide the choices in the physical solution possibilities in the final design. The advantages or disadvantages of certain strategies were however not always so clear, because not all possible solutions for each strategy were/could be explored. The focus on generating solution possibilities was with the lower level functions to limit the overall size of the solution scope. To give an example, one of the fundamental chosen strategies is the kinematic path design (f.1.3. appendix C.1), choosing a different strategy here would probably result in a completely different final design. The choice between these strategies was not based upon a vast set of concepts for each of the strategies, after which the best performing one was chosen, independent of its strategy. Rather, the resulting design process that would follow for each strategy was chosen, independent of the performance criteria/requirements stated in the objective. The influence of this on the overall performance of the result will remain unclear, it however ensured the production and evaluation of a functional physical system within the given period of time. Furthermore, the overall design breakdown structure into functions and strategies could provide a useful framework for future developments.

The production and evaluation of the design, brought to light possible improvements for further design iterations. The direction setpoint mechanism was identified as most limiting the performance of the current prototype. The stiffness of this system is insufficient in the desired directions, due to which the bars b_8 and b_8m tend to perform unwanted deflections, decreasing the range of the XY displacement of the end effector. Furthermore, this system introduces directional change in the velocity of the WM. This is due to the angle β not being related in a 1:1 fashion with α_2, resulting in different angles β for the different legs. Meaning the WM is not propelled in the exact same direction by each of the legs. Next to this, the mechanism also introduces the deviations in the length of the paths projected onto the XY-plane. With this the stride-length will be different for each of the legs and so will be the propulsion velocity, introducing variations in the overall velocity of the WM. Given the current shape of the surface, the direction setpoint mechanism would ideally change the X and Y directions of the paths of the end effector in such a way that a perfect circle is generated by projecting the outer extremes of the surface onto the XY plane. This would enable a similar stride-length and direction for all of the legs. The proposed solution is to couple the X_{rot} and Y_{rot} amplitudes such that the X_{rot} amplitude is defined by $r\cos(\alpha_2)$ and the Y_{rot} amplitude by $r\sin(\alpha_2)$, with r being any desired value. An attempt could be made to achieve this with the current rotational mechanism for changing the amplitude, but a design based upon a translational principal might be just as effective or even more effective. Concrete solutions for this will have to be come up with.

Next to a design change in the direction setpoint mechanism, other design modifications could also further improve the system. Currently, the velocity during the stance phase fluctuates, following a sinusoid curve for a quarter period centered on one of the extremes. A proposed solution is to alter the transmission between IMG1 and R_{15}, (chapter 3, fig. 3.7) to make sure this velocity remains more constant.

With the focus on producing a physical prototype the stiffnesses resulting from the dimensions of the design were only briefly looked into by means of several design iterations of subcomponents. Further modelling of the stiffnesses in the joints and stiffness of the structure can provide a more detailed view on the points of improvement. This will enable the design of a monolithic system, it will provide insight into the required power of the actuators, can contribute to a less voluminous system because the Robert's linkages can be reduced in dimensions and it will enable the design of legs capable of supporting the mechanism itself and possibly additional load. Extending on this, a topology optimization could be a future research direction to increase the stiffness of the frame and reduce the stiffnesses in the hinges. As well as reduce the entire volume of the device.

Considering the actuators, the current design incorporates two stepper motors. These were chosen to accommodate the measurement procedure. Depending on the future use cases, a different choice of actuators might prove beneficial.

Lastly, although additive manufacturing in the form of FDM 3D printing has been under development for quite some years by now, it was experienced that the process is still rather delicate. After several test runs to find the right print settings, enough confidence was obtained that an overall multi-material print out of the intended materials would be a reasonable choice. During the production phase however, various unexpected problems occurred leading to failed prints. This caused a severe delay in the production process. With the dependency on multi-material printers, the solution possibilities were limited. Therefore, the advice for future attempts to fabricate such a system is to make sure that the fabrication process is independent of a specific type of printer. In short, the advice would be to produce a system out of a single material. Specifically, SLS printing could be a favourable method as the device can be monolithically produced without the need of extensive support material and thus its removal.

4.2 Extended conclusion

This report has shown the kinematic and physical design of a compliant 2-DOF mechanism capable of describing a closed spatial surface. Additionally, a manner of coupling this device is presented. This proposes the manner of transforming a multi of these mechanisms into an omnidirectional walking machine using only two actuators. The most promising improvement directions were indicated and it was argued that a more detailed model of the system is a logical next step. Hereby, the preferred direction would be towards the design out of a single material to enable a monolithic production process. The resulting system will then extend the capabilities of walking machines in general with the benefits of compliant mechanisms and a limited number of actuators.

Bibliography

[1] George L Adams. Tiltable deep mining auger machine, April 11 1961. US Patent 2,979,320.

[2] George L Adams. Stepper-type tramming support for mining equipment, December 17 1963. US Patent 3,114,425.

[3] Abhishek Agarwal, Praveen Kumar Gautam, and Shibendu Shekhar Roy. Dynamic modeling and optimal foot force distribution of quadruped walking robot. *Communications in Computer and Information Science*, 103 CCIS:146–153, 2010. ISSN 18650929. doi: $10.1007/978\text{-}3\text{-}642\text{-}15810\text{-}0\_19$.

[4] Paul Alexandre and AndrÉ Preumont. On the gait control of a six-legged walking machine. *International Journal of Systems Science*, 27(8):713–721, 1996. ISSN 14645319. doi: $10.1080/00207729608929271$.

[5] YAO Y AN, MA QIANLI, ZHAO SHUNQING, and WU JIANXU. Manpower-operated leg type walking vehicle, 6 2014. URL `https://nl.espacenet.com/publicationDetails/biblio?adjacent=true&locale=nl_NL&FT=D&date=20140604&CC=CN&NR=103832505A&KC=A`.

[6] Vincent G Anderson. Walking-motion propelling apparatus, September 19 1922. US Patent 1,429,551.

[7] Milan Andre. Modelling and control of walking robots. (August), 2015.

[8] YIN BAOLIN, YAN BINGBING, REN WENBO, YU FENG, CHEN CHAOQI, CHEN CHANGCHUN, WANG LIN, SHENG YINHE, SI YANJIAO, and LIU CHENCONG. Reconstructable multi-legged robot, 6 2015. URL `https://nl.espacenet.com/publicationDetails/biblio?adjacent=true&locale=nl_NL&FT=D&date=20150624&CC=CN&NR=104724202A&KC=A`.

[9] J. E. Bares. Dante II: Technical Description, Results, and Lessons Learned. *The International Journal of Robotics Research*, 18(7):621–649, 1999. ISSN 0278-3649. doi: $10.1177/02783649922066475$.

[10] John E Bares and William Whittaker. Orthogonal legged walking robot, July 7 1992. US Patent 5,127,484.

[11] George B Baron. Walking mechanism and control therefor, May 19 1970. US Patent 3,512,597.

[12] Irwin R Barr. Amphibious walking vehicle, December 29 1959. US Patent 2,918,738.

[13] Stephen J Bartholet. Walking machine, July 9 1985. US Patent 4,527,650.

[14] Anton Becker. Apparatus for walking heavy structures, March 19 1957. US Patent 2,785,761.

[15] JOHN N BISHOP. Walking drag line, 2 1981. URL `https://nl.espacenet.com/publicationDetails/biblio?adjacent=true&locale=nl_NL&FT=D&date=19810224&CC=US&NR=4252204A&KC=A`.

[16] Mavor John Bridie. Apparatus for mining, May 20 1947. US Patent 2,420,755.

[17] M Buehler. RePaC design and control : Cheap and fast autonomous runners. *Universidad mcgill Montreal*, pages 1–7, 2001. URL `http://www.rhex.web.tr/buehler.clawar2001.pdf`.

[18] MARTIN BUEHLER, DANIEL E KODITSCHEK, and ULUC SARANLI. Single actuator per leg robotic hexapod, 12 2001. URL `https://nl.espacenet.com/publicationDetails/biblio?adjacent=true&locale=nl_NL&FT=D&date=20011227&CC=US&NR=2001054518A1&KC=A1`.

[19] Colin Mcleod Cameron. Excavating machine, November 2 1948. US Patent 2,452,632.

[20] HONG CANXIONG. Personification biped walking robot, 9 2017. URL `https://nl.espacenet.com/publicationDetails/biblio?adjacent=true&locale=nl_NL&FT=D&date=20170922&CC=CN&NR=107187512A&KC=A`.

[21] Frank R Cardinal. Figure wheeled toy., November 27 1917. US Patent 1,248,072.

[22] Jos{\'e} Luis Celaya, Enric and Albarral. Implementation of a hierarchical walk controller for the LAURON III hexapod robot. *International Conference on Climbing and Walking Robots*, (January):409–416, 2003.

[23] Henry B Chambers. Apparatus for moving multi-ton objects, April 27 1971. US Patent 3,576,225.

[24] SANG-EUN CHO, KYUNG-IL and BAEK. Micro robot, 3 2002. URL `https://nl.espacenet.com/publicationDetails/biblio?adjacent=true&locale=nl_NL&FT=D&date=20020314&CC=US&NR=2002029915A1&KC=A1`.

[25] Arthur A Collie. Robot devices, June 16 1992. US Patent 5,121,805.

[26] Steven H Collins, Martijn Wisse, and Andy Ruina. A Three-Dimensional Passive-Dynamic Walking Robot with Two Legs and Knees. *The International Journal of Robotics Research*, 20(7):607–615, 2001. doi: 10.1177/02783640122067561.

[27] Paul E Corson. Walking tractor, February 11 1958. US Patent 2,822,878.

[28] John M Danko and Kasarda John. Walking toy animal, May 26 1931. US Patent 1,807,391.

[29] Trevor O Davidson. Supporting propulsion means for draglines and the like, November 24 1953. US Patent 2,660,253.

[30] ZHANG DONG, ZHUANG TINGDA, HU HAIPENG, YANG JINSHUI, and CAI DEZHENG. Single-motor-driven robot walking mechanism, 5 2017. URL https://nl.espacenet.com/publicationDetails/biblio?adjacent=true&locale=nl_NL&FT=D&date=20170510&CC=CN&NR=106625580A&KC=A.

[31] SHI DONGYAN, ZHA SHUAI, ZHANG HONG, HE DONGZE, and YU SHUQIN. Horse-imitating gait planar connection rod type quadruped walking robot, 4 2017. URL https://nl.espacenet.com/publicationDetails/biblio?adjacent=true&locale=nl_NL&FT=D&date=20170426&CC=CN&NR=106585761A&KC=A.

[32] Earl Dunshee. Quadruped-walking mechanism, March 16 1926. US Patent 1,576,956.

[33] ZHENG C E, HANG MINGXIANG, GAO ZIHAN, WANG YU, and ZHANG HENGYU. Bionic multi-legged walking robot and robot leg thereof, 6 2015. URL https://nl.espacenet.com/publicationDetails/biblio?adjacent=true&locale=nl_NL&FT=D&date=20150624&CC=CN&NR=204415556U&KC=U.

[34] Adolf Ehrlich. Vehicle propelled by steppers, November 13 1928. US Patent 1,691,233.

[35] DONG ERBAO, YANG JIE, WANG ZHIRONG, JIN HU, WANG HAO, LU DONGPING, and XU MIN. Multi-foot moving device based on combination driving mechanism, 11 2013. URL https://nl.espacenet.com/publicationDetails/biblio?adjacent=true&locale=nl_NL&FT=D&date=20131120&CC=CN&NR=103395457A&KC=A.

[36] Peter Esser. Walking toy, August 18 1925. US Patent 1,550,309.

[37] Williams et al. Walking wheeled vehicle, October 1974. US Patent 3,842,926.

[38] Todd A Ferrante. Modular robot, November 11 1997. US Patent 5,685,383.

[39] Philippe Garrec. Device for transmitting movement between a solid and a member, in particular for a robot able to be moved on legs, June 15 1993. US Patent 5,219,410.

[40] Tao Geng, Bernd Porr, and Florentin Wörgötter. Fast Biped Walking With A Reflexive Controller And Real-time Policy Searching. *Advances in Neural Information Processing Systems*, pages 427–434, 2006. ISSN 10495258. doi: 10.1177/0278364906063822.

[41] Ricouard Henri Leon Georges. Apparatus for walking heavy equipment, November 24 1959. US Patent 2,914,127.

[42] Amanda Ghassaei, Phil Choi, and Dwight Whitaker. The Design and Optimization of a Crank-Based Leg Mechanism. page 168, 2011. URL www.amandaghassaei.com/files/thesis.pdf.

[43] Amanda Ghassaei, Professors Phil Choi, and Dwight Whitaker. The design and optimization of a crank-based leg mechanism. *Pomona, USA*, 2011.

[44] Vittorio Gobbato. Mechanism for reproducing all the movements of the steps of quadrupeds, August 9 1927. US Patent 1,638,332.

[45] HIROSHI GOMI, KAZUSHI HAMAYA, and TAKASHI MATSUMOTO. Biped mobile robot, 5 2003. URL https://nl.espacenet.com/publicationDetails/biblio?adjacent=true&locale=nl_NL&FT=D&date=20030520&CC=US&NR=6564888B1&KC=B1.

[46] William F. Goodwin. Automatic toy, January 1867. US Patent 61416.

[47] Donald Greenwood, Michael E Ieda, and Stopek Benjamin. Mechanical toy with walking action, April 20 1965. US Patent 3,178,853.

[48] Jr Henry G Grimm. Animated toy, March 25 1958. US Patent 2,827,735.

[49] MA GUANGYING, CHEN YUAN, HAN SHUO, GAO JUN, and ZHAO CHENYAO. Foot-type walking robot, 9 2017. URL https://nl.espacenet.com/publicationDetails/biblio?adjacent=true&locale=nl_NL&FT=D&date=20170926&CC=CN&NR=107200080A&KC=A.

[50] QU HAIBO, YU ZHIYUAN, ZHANG CHUANLIANG, and GUO SHENG. Dual-foot walking robot mechanism with parallel leg structure, 5 2017. URL https://nl.espacenet.com/publicationDetails/biblio?adjacent=true&locale=nl_NL&FT=D&date=20170531&CC=CN&NR=106741287A&KC=A.

[51] A. Halme, K. Hartikainen, and K. Kärkkäinen. Terrain adaptive motion and free gait of a six-legged walking machine. *Control Engineering Practice*, 2(2):273–279, 1994. ISSN 09670661. doi: 10.1016/0967-0661(94)90208-9.

[52] SHI HAOBIN, LIU CHAOCI, SHI YIDONG, LIANG TIAN, and LU HAIYANGBO. Small humanoid robot capable of realizing omni-directional walking and control method thereof, 9 2017. URL https://nl.espacenet.com/publicationDetails/biblio?adjacent=true&locale=nl_NL&FT=D&date=20170926&CC=CN&NR=107203212A&KC=A.

[53] Paul Hebert, Max Bajracharya, Jeremy Ma, Nicolas Hudson, Alper Aydemir, Jason Reid, Charles Bergh, James Borders, Matthew Frost, Michael Hagman, and Others. Mobile Manipulation and Mobility as Manipulation—Design and Algorithms of RoboSimian. *Journal of Field Robotics*, 32(2):255–274, 2015. ISSN 15564959. doi: 10.1002/rob.21566. URL http://www.ece.ucsb.edu/{~}katiebyl/papers/Hebert{_}JFR{_}2014.pdf.

[54] Henry Selby Hele-Shaw. Vehicle., March 3 1908. US Patent 880,526.

[55] K. Hirai, M. Hirose, Y. Haikawa, and T. Takenaka. The development of honda humanoid robot. In *Proceedings. 1998 IEEE International Conference on Robotics and Automation (Cat. No.98CH36146)*, volume 2, pages 1321–1326 vol.2, May 1998. doi: 10.1109/ROBOT.1998.677288.

[56] Shigeo Hirose. A Study of Design and Control of a Quadruped Walking Vehicle. *The International Journal of Robotics Research*, 3(2):113–133, 1984. ISSN 17413176. doi: 10.1177/027836498400300210.

[57] Takashi Horinouchiuchi. Legged robot, 5 2015. URL https://nl.espacenet.com/publicationDetails/biblio?adjacent=true&locale=nl_NL&FT=D&date=20150511&CC=JP&NR=WO2013121469A1&KC=A1.

[58] AHN S HWAN, ROHKYUNGSHIK , YOON S JUNE, and HYUNG S YONG. Walking robot and simultaneous localization and mapping method thereof, 12 2017. URL https://nl.espacenet.com/publicationDetails/biblio?adjacent=true&locale=nl_NL&FT=D&date=20171218&CC=KR&NR=20170138977A&KC=A.

[59] Nb Ignell, N Rasmusson, Johan Matsson, Sven Böttcher, Roland Siegwart, Illah R Nourbakhsh, Aravind Seeni, Bernd Schäfer, and Gerd Hirzinger. Introduction to Autonomous Mobile Robots. *Idt.Mdh.Se*, 23(January):47–82, 2004. ISSN 0263-5747. doi: 10.5772/6930. URL http://www2.cs.siu.edu/{~}hexmoor/classes/CS404-S09/RobotLocomotion.pdf{%}5Cnhttp://www.idt.mdh.se/kurser/ct3340/ht12/MINICONFERENCE/FinalPapers/ircse12{_}submission{_}21.pdf.

[60] Anthony James Ingram. A New Type of Mechanical Walking Machine. (November):158, 2006.

[61] WILLIAMS J, BRADLEY C, and MOTTIN H. Walking wheeled vehicle, 10 1974. URL https://nl.espacenet.com/publicationDetails/biblio?adjacent=true&locale=nl_NL&FT=D&date=19741022&CC=US&NR=3842926A&KC=A.

[62] T. Jansen. *De grote fantast*. Uitgeverij 010, 2007. ISBN 9789064506499.

[63] Joseph F Joy. Coal mining machine, December 1 1936. US Patent 2,062,657.

[64] Joseph F Joy. Automatic stepper type transport device, July 30 1957. US Patent 2,800,968.

[65] Joseph F Joy. Mobile base for mining machines, May 6 1958. US Patent 2,833,531.

[66] SYUJI KAJITA. Method and apparatus for dynamic walking control of robot, 5 1989. URL https://nl.espacenet.com/publicationDetails/biblio?adjacent=true&locale=nl_NL&FT=D&date=19890530&CC=US&NR=4834200A&KC=A.

[67] Keiichi Kazami, Shin-ichi Suda, Masayoshi Sato, and Yuji Sawajiri. Walking apparatus, May 29 2001. US Patent 6,238,264.

[68] Iwaya Keikichi and Kuramochi Shigeaki. Walking toy figure, January 5 1965. US Patent 3,163,960.

[69] JOSEPH C KLANN. Walking device, 4 2002. US Patent, US6364040 (B1).

[70] Karl Klein and Franz-Josef Platte. Excavating machine, May 3 1966. US Patent 3,249,168.

[71] Loek van der Klis. URL http://qeprize.org/createthefuture/wp-content/uploads/2016/03/loek-van-der-Klis-Umerus-Silent-beach.jpg. Visited: 18-06-2018.

[72] T. Koetsier and M Ceccarelli. *Explorations in the History of Machines and Mechanisms*. Springer, 2012. ISBN 9789400741317.

[73] KYOUNG C KONG, JUNG S CHOI, and BYEONG H NA. Multi-leg walking robot, 4 2017. URL https://nl.espacenet.com/publicationDetails/biblio?adjacent=true&locale=nl_NL&FT=D&date=20170428&CC=KR&NR=101731731B1&KC=B1.

[74] Philip Kopf. Mechanical toy, July 11 1950. US Patent 2,514,450.

[75] Lyle L Kramer. Motor operated ambulatory vehicle, July 18 1967. US Patent 3,331,463.

[76] Melvin W Kraschnewski and Learmont Tom. Stepping-type propulsion means for excavators, April 2 1968. US Patent 3,375,892.

[77] Rhinehart V Kuen. Quadrupedal toy, April 2 1929. US Patent 1,707,735.

[78] Josef Kurelic. Mechanical animal, June 7 1938. US Patent 2,120,102.

[79] YOSHIHIRO KUROKI, TATSUZO ISHIDA, and JINICHI YAMAGUCHI. Ambulation control apparatus and ambulation control method of robot, 12 2002. URL https://nl.espacenet.com/publicationDetails/biblio?adjacent=true&locale=nl_NL&FT=D&date=20021205&CC=US&NR=2002183897A1&KC=A1.

[80] Galina Kuteeva, Boris Ershov, and Tatiana Voloshinova. Models of mechanisms by P. L. Chebyshev in St. Petersburg University. *2015 International Conference on Mechanics - Seventh Polyakhov's Reading*, (May):64–67, 2015. doi: 10.1109/POLYAKHOV.2015.7106745.

[81] KEE-MAN [HK] KWOK, ZHIXIN ZENG, and WEIGUANG LI. Electric toy, 5 2004. URL https://nl.espacenet.com/publicationDetails/biblio?adjacent=true&locale=nl_NL&FT=D&date=20040527&CC=US&NR=2004099450A1&KC=A1.

[82] WANG LIANGWEN, XIAO YANQIU, DU WENLIAO, WANG XINJIE, MENG FANNIAN, WANG CAIDONG, SONG KANGKANG, MU YALIN, LI ANSHENG, and YUE LEI. Cam connecting rod combined mechanism driven walking robot, 6 2017. URL https://nl.espacenet.com/publicationDetails/biblio?adjacent=true&locale=nl_NL&FT=D&date=20170609&CC=CN&NR=106809294A&KC=A.

[83] Jing Liu, Min Tan, and Xiaoguang Zhao. Legged robots – an overview. 2(95):185–202, 2007.

[84] H. O. Lund. Mechanical toy, July 1882.

[85] QINGSHENG LUO, QING CHANG, BAOLING HAN, and PENG MA. Leg drive and transmission device for legged mobile platform, 7 2012. URL https://nl.espacenet.com/publicationDetails/biblio?adjacent=true&locale=nl_NL&FT=D&date=20120704&CC=CN&NR=102530122A&KC=A.

[86] William C MacArthur, Michael S Campbell, James C Barnes, and James A Campbell. Robotic toy, November 25 2003. US Patent 6,652,352.

[87] J a Tenreiro Machado and Manuel F Silva. An Overview of Legged Robots. *Proceedings of the MME 2006 International Symposium on Mathematical Methods in Engineering*, 2006.

[88] Davood Farhadi Machekposhti and Just L Herder. A Review on Compliant Joints and Rigid-Body Constant Velocity Universal Joints Toward the Design of Compliant Homokinetic Couplings. (March), 2015. doi: 10.1115/1.4029318.

[89] Frank A Manfredi. Mechanical walking animal, October 5 1948. US Patent 2,450,674.

[90] David J. Manko. *A General Model of Legged Locomotion on Natural Terrain*. Kluwer Academic Publishers, Norwell, MA, USA, 1992. ISBN 0792392477.

[91] Jaimie Hartwig Barrett Mantzel. Walking machine, February 25 2014. US Patent 8,657,042.

[92] Oscar J Martinson. Traction machine, May 10 1927. US Patent 1,627,984.

[93] Nestor Mauger. Motor-tractor with propulsive levers, May 3 1921. US Patent 1,376,717.

[94] Vincent J Mccarthy. Mining machine having independently operable skids, May 3 1960. US Patent 2,935,309.

[95] Robert J Mccracken. Hydraulically actuated load carrying apparatus, September 6 1966. US Patent 3,270,828.

[96] T McGeer. Passive dynamic walking. *Int. J. Robot. Res.*, 9(2):62–82, 1990.

[97] R. B. McGhee and A. A. Frank. On the stability properties of quadruped creeping gaits. *Mathematical Biosciences*, 3(1-2):331–351, 1968. ISSN 00255564. doi: 10.1016/0025-5564(68)90090-4.

[98] Michael T McKittrick Jr and Nicholas DeAnda. Animated toy, December 16 1986. US Patent 4,629,440.

[99] H. B. McMurray. Traction engine, June 1891. US Patent 455,240.

[100] SANJUAN P MONTERO and GUTIERREZ RAMALLO. Crawler robot equipped with a work unit, and governing equipment for such crawler robots, 3 2008. URL https://nl.espacenet.com/publicationDetails/biblio?adjacent=true&locale=nl_NL&FT=D&date=20080327&CC=US&NR=2008077276A1&KC=A1.

[101] Poche John Morris. Dredge or excavator, October 4 1938. US Patent 2,132,184.

[102] NAKAMURA MOTOHIRO. Two-leg walking robot for toy, 9 2017. URL https://nl.espacenet.com/publicationDetails/biblio?adjacent=true&locale=nl_NL&FT=D&date=20170907&CC=JP&NR=2017153896A&KC=A.

[103] Thomas C Mullins. Walking apparatus for excavators, April 30 1946. US Patent 2,399,375.

[104] ZHANG NAN. Walking robot, 4 2017. URL https://nl.espacenet.com/publicationDetails/biblio?adjacent=true&locale=nl_NL&FT=D&date=20170419&CC=CN&NR=206107390U&KC=U.

[105] Yoshio Nishikawa. Walking apparatus, December 3 2002. US Patent 6,488,560.

[106] LEV [IL] NISNEVICH. Method and apparatus for flat surface treatment, 10 2004. URL https://nl.espacenet.com/publicationDetails/biblio?adjacent=true&locale=nl_NL&FT=D&date=20041019&CC=US&NR=6805504B1&KC=B1.

[107] Yoshiro Nomura. Device of walking legs for a toy animal, July 25 1972. US Patent 3,678,617.

[108] Zenkichi Nozaki. Toy having capacitance switch, February 2 1971. US Patent 3,559,336.

[109] ANDERS J OLSEN. Walking-tractor., 12 1918. URL https://nl.espacenet.com/publicationDetails/biblio?adjacent=true&locale=nl_NL&FT=D&date=19181210&CC=US&NR=1287086A&KC=A.

[110] Hoppmann Otto, Karl J Klein, and Platte Franz-Josef. Walking mechanism for excavating machines, June 14 1966. US Patent 3,255,836.

[111] John W Page. Self-propelled apparatus, September 27 1932. US Patent 1,879,446.

[112] F. Pfeiffer, J. Eltze, and H. J. Weidemann. The tum-walking machine. *Intelligent Automation and Soft Computing*, 1(3):307–323, 1995. ISSN 2326005X. doi: 10.1080/10798587.1995.10750637.

[113] Mark Plecnik. Leg mechanisms, 2017. URL https://www.markplecnik.com/leg-mechanisms/. Visited: 11-04-2019.

[114] Je Pratt. Exploiting inherent robustness and natural dynamics in the control of bipedal walking robots. *Electrical Engineering*, (1995):1–157, 2000. ISSN 00189286. doi: 10.1109/TAC.2002.808489. URL http://oai.dtic.mil/oai/oai?verb=getRecord{&}metadataPrefix=html{&}identifier=ADA475455.

[115] Edward Herbert Price. Animated toy, December 11 1928. US Patent 1,695,205.

[116] Pearl Rachel Price. Figured toy, February 14 1939. US Patent 2,147,215.

[117] CHANGXIAN QIU. Obstacle-overcoming wheelchair, 1 2018. URL https://nl.espacenet.com/publicationDetails/biblio?adjacent=true&locale=nl_NL&FT=D&date=20180118&CC=WO&NR=2018010551A1&KC=A1.

[118] Marc Raibert, Kevin Blankespoor, Gabriel Nelson, and Rob Playter. *BigDog , the Rough-Terrain Quadruped Robot*, volume 41. IFAC, 2008. ISBN 9783902661005. doi: 10.3182/20080706-5-KR-1001.01833.

[119] M.H. Raibert. *Legged Robots that Balance*. Artificial Intelligence. MIT Press, 1986. ISBN 9780262181174. URL https://books.google.nl/books?id=EXRiBnQ37RwC.

[120] Alireza Ramezani, Jonathan W. Hurst, Kaveh Akbari Hamed, and Jessy W. Grizzle. Performance Analysis and Feedback Control of ATRIAS, A Three-Dimensional Bipedal Robot. *Journal of Dynamic Systems, Measurement, and Control*, 136(2):021012, 2013. ISSN 0022-0434. doi: 10.1115/1.4025693. URL http://dx.doi.org/10.1115/1.4025693{%}5Cnhttp://dynamicsystems.asmedigitalcollection.asme.org/article.aspx?doi=10.1115/1.4025693.

[121] Mitch Randall. Apparatus and method for producing ambulatory motion, March 15 2005. US Patent 6,866,557.

[122] Peter A Rasmussen. Perambulating tractor, June 28 1921. US Patent 1,382,854.

[123] Venzlaff Richard. Stepper, January 5 1926. US Patent 1,568,109.

[124] W. E. Richardson. Traction engine, June 1883. US Patent 278,822.

[125] Christian Ridderström. Legged locomotion: Balance, control and tools—from equation to action. *Phd Dissertation*, 2003. ISSN 1400-1179. URL http://citeseerx.ist.psu.edu/viewdoc/download?doi=10.1.1.15.299{&}rep=rep1{&}type=pdf.

[126] RUDOLF [DE] ROSENBERGER. Motor powered climber for diagonal transportation of heavy loads over staircase, has seven climbing legs secured on endless chain for climbing staircase, where climbing legs are evenly spaced from each other along chain, 6 2012. URL https://nl.espacenet.com/publicationDetails/biblio?adjacent=true&locale=nl_NL&FT=D&date=20120614&CC=DE&NR=102010054328A1&KC=A1.

[127] Robert E Roy. Tractor, July 8 1924. US Patent 1,500,723.

[128] Robert E Roy. Tractor, November 3 1925. US Patent 1,560,325.

[129] Rygg. Mechanical horse, February 1893. US Patent 491,927.

[130] Haruhiro Saito. Animated mechanical toy, April 1 1952. US Patent 2,591,469.

[131] Y. Sakagami, R. Watanabe, C. Aoyama, S. Matsunaga, N. Higaki, and K. Fujimura. The intelligent ASIMO: system overview and integration. *IEEE/RSJ International Conference on Intelligent Robots and System*, 3(October):2478–2483, 2002. doi: 10.1109/IRDS.2002.1041641. URL http://ieeexplore.ieee.org/document/1041641/.

[132] TAKAO SAWANO, KEIZO OHTA, and MASASHI SHIOMI. Passive walking device and passive walking module, 12 2017. URL https://nl.espacenet.com/publicationDetails/biblio?adjacent=true&locale=nl_NL&FT=D&date=20171214&CC=WO&NR=2017212899A1&KC=A1.

[133] Arthur W Scruggs. Multi-ped vehicle, June 2 1964. US Patent 3,135,345.

[134] John C Shaffer. Mechanical toy horse, May 1 1934. US Patent 1,957,110.

[135] AMIR [IL] SHAPIRO. A quadruped legged robot driven by linear actuators, 7 2008. URL https://nl.espacenet.com/publicationDetails/biblio?adjacent=true&locale=nl_NL&FT=D&date=20080717&CC=WO&NR=2008084480A2&KC=A2.

[136] Eric Sheeter. Stepping vehicle, December 13 1988. US Patent 4,790,400.

[137] W. B. Shieh, L. W. Tsai, and S. Azarm. Design and optimization of a one-degree-of-freedom six-bar leg mechanism for a walking machine. *Journal of Robotic Systems*, 14(12):871–880, 1997. ISSN 07412223. doi: 10.1002/(SICI)1097-4563(199712)14:12<871::AID-ROB4>3.0.CO;2-R.

[138] Joseph E Shigley. THE MECHANICS OF WALKING VEHICLES. 1960.

[139] Eungsoo Shin and Donald A Streit. An Energy Efficient Quadruped with Two-Stage Equilibrator. *Journal of Mechanical Design*, 115(1):156–163, 1993. ISSN 07380666. doi: 10.1115/1.2919313. URL http://link.aip.org/link/?JMD/115/156/1.

[140] NIKOLAY SHKOLNIK. Walking apparatus, 7 1984. URL https://nl.espacenet.com/publicationDetails/biblio?adjacent=true&locale=nl_NL&FT=D&date=19840731&CC=US&NR=4462476A&KC=A.

[141] MA SHUYAO, DUAN XUECHAO, LIU BO, SHAO WENQI, DU JINGLI, and MI JIANWEI. Spherical hexapod robot capable of rolling and walking, 12 2017. URL https://nl.espacenet.com/publicationDetails/biblio?adjacent=true&locale=nl_NL&FT=D&date=20171201&CC=CN&NR=107416063A&KC=A.

[142] Metin Sitti, Arianna Menciassi, Auke Jan Ijspeert, Kin Huat Low, and Sangbae Kim. Survey and Introduction to the Focused Section. 18(2):409–418, 2013.

[143] Shin-Min. Song and Kenneth J. Waldron. *Machines that walk : the adaptive suspension vehicle / Shin-Min Song, Kenneth J. Waldron*. MIT Press Cambridge, Mass, 1989. ISBN 0262192748.

[144] PIAO SONGHAO. Multi-legged walking robot based on 3-rpc parallel mechanism, 5 2017. URL https://nl.espacenet.com/publicationDetails/biblio?adjacent=true&locale=nl_NL&FT=D&date=20170524&CC=CN&NR=106697103A&KC=A.

[145] J. Spelling. Walking animal, May 1925. US Patent 1,538,140.

[146] Joseph Srakula. Walking vehicle, December 29 1925. US Patent 1,567,684.

[147] David ES Stewart. Walking vehicle, May 5 1987. US Patent 4,662,465.

[148] TIANQI SUN. General-purpose six-legged walking robot, and main structure thereof, 10 2017. URL https://nl.espacenet.com/publicationDetails/biblio?adjacent=true&locale=nl_NL&FT=D&date=20171026&CC=WO&NR=2017181975A1&KC=A1.

[149] TORU TAKENAKA. Gait pattern generating device for legged mobile robot, 3 2004. URL https://nl.espacenet.com/publicationDetails/biblio?adjacent=true&locale=nl_NL&FT=D&date=20040304&CC=US&NR=2004044440A1&KC=A1.

[150] Hiroki Takeuchi. Multi-legged walking apparatus, December 1 1998. US Patent 5,842,533.

[151] Meredith W Thring. Walking machine, August 4 1970. US Patent 3,522,859.

[152] Tibbits. Tractor, December 1919. URL https://worldwide.espacenet.com/publicationDetails/biblio?CC=US&NR=1326805A&KC=A&FT=D#.

[153] Adolf Tomas. Load moving striding device, May 27 1969. US Patent 3,446,301.

[154] TAKAHASHI TOMOTAKA. Bipedal walking type robot, 8 2002. URL https://nl.espacenet.com/publicationDetails/biblio?adjacent=true&locale=nl_NL&FT=D&date=20020806&CC=JP&NR=2002219673A&KC=A.

[155] Joe R Urschel. Walking tractor, December 13 1949. US Patent 2,491,064.

[156] Charles Van Antwerp. Walking-ditcher., October 5 1915. US Patent 1,155,975.

[157] ROBERT J VIOLA. Frame walker predicated on a parallel mechanism, 5 2010. URL https://nl.espacenet.com/publicationDetails/biblio?adjacent=true&locale=nl_NL&FT=D&date=20100506&CC=US&NR=2010107795A1&KC=A1.

[158] Kenneth J Waldron and Robert B Mcghee. The Mechanics of Mobile Robots. 1986.

[159] Zhiying Wang, Xilun Ding, Alberto Rovetta, and Alessandro Giusti. Mobility analysis of the typical gait of a radial symmetrical six-legged robot. *Mechatronics*, 21(7):1133–1146, 2011. ISSN 09574158. doi: 10.1016/j.mechatronics.2011.05.009. URL http://dx.doi.org/10.1016/j.mechatronics.2011.05.009.

[160] CHENG WEI, ZHANG LONG, ZHANG WEN, WANG YUNFENG, LI GUANGYONG, and TENG DAXIANG. Multifunctional work platform based on walking, 3 2016. URL https://nl.espacenet.com/publicationDetails/biblio?adjacent=true&locale=nl_NL&FT=D&date=20160302&CC=CN&NR=205059783U&KC=U.

[161] YAN WEISHENG, XU HUI, CUI RONGXIN, GAO JIAN, ZHANG FUBIN, and ZHANG LICHUAN. Swimming and walking combined underwater operation robot and control method thereof, 8 2017. URL https://nl.espacenet.com/publicationDetails/biblio?adjacent=true&locale=nl_NL&FT=D&date=20170829&CC=CN&NR=107097238A&KC=A.

[162] E.R. Westervelt, J.W. Grizzle, C. Chevallereau, J.H. Choi, and B. Morris. *Feedback Control of Dynamic Bipedal Robot Locomotion*. Automation and Control Engineering. CRC Press, 2007. ISBN 9781420053739. URL https://books.google.nl/books?id=nYfLBQAAQBAJ.

[163] ROY WILCOX. Hobby horse, 4 1987. URL https://nl.espacenet.com/publicationDetails/biblio?adjacent=true&locale=nl_NL&FT=D&date=19870414&CC=US&NR=4657098A&KC=A.

[164] Kraus Hans Wilhelm. Load transportation means, June 28 1960. US Patent 2,942,676.

[165] CARL F WILSON. Walking-machine., 5 1918. URL https://nl.espacenet.com/publicationDetails/biblio?adjacent=true&locale=nl_NL&FT=D&date=19180521&CC=US&NR=1267033A&KC=A.

[166] DING XILUN, ZHENG YI, and XU KUN. Six-freedom-degree walking robot single-leg structure capable of carrying out leg-arm fusion operation, 8 2017. URL https://nl.espacenet.com/publicationDetails/biblio?adjacent=true&locale=nl_NL&FT=D&date=20170804&CC=CN&NR=107010136A&KC=A.

[167] DENG XINGQIAO, ZHANG PAN, JIANG YUANYUAN, FENG ZHIPENG, and LI SHUANGCEN. Robot walking mechanism, 5 2017. URL https://nl.espacenet.com/publicationDetails/biblio?adjacent=true&locale=nl_NL&FT=D&date=20170531&CC=CN&NR=106737596A&KC=A.

[168] RUAN XUEYUN, GUO YONGCUN, WU JIYING, CAO JUN, and ZHOU YUBAO. Full-pneumatic stepping-type traveling mechanism and pneumatic control system thereof, 6 2016. URL https://nl.espacenet.com/publicationDetails/biblio?adjacent=true&locale=nl_NL&FT=D&date=20160601&CC=CN&NR=105620584A&KC=A.

[169] TOSHIO YAMASAKI. Walking toy vehicle with ramp, 9 1986. URL https://nl.espacenet.com/publicationDetails/biblio?adjacent=true&locale=nl_NL&FT=D&date=19860930&CC=US&NR=4614504A&KC=A.

[170] Ken Yanagisawa. Walking robot, October 4 1994. US Patent 5,351,773.

[171] Ken Yanagisawa. Walking robot, October 4 1994. US Patent 5,351,626.

[172] YAO YAN'AN, WU JIANXU, and WANG MENGJUN. Multi-leg walking transport platform, 3 2017. URL https://nl.espacenet.com/publicationDetails/biblio?adjacent=true&locale=nl_NL&FT=D&date=20170308&CC=CN&NR=106476927A&KC=A.

[173] SOO S YANG, YEON T OH, and YOUN B LEE. Walking robot, 12 2009. URL https://nl.espacenet.com/publicationDetails/biblio?adjacent=true&locale=nl_NL&FT=D&date=20091210&CC=US&NR=2009301798A1&KC=A1.

[174] ZHIWEI YU, ZHENDONG DAI, CE GUO, HAO ZHANG, HONGKAI LI, and HAO YU. Hydraulically-driven four-foot robot, 4 2011. URL https://nl.espacenet.com/publicationDetails/biblio?adjacent=true&locale=nl_NL&FT=D&date=20110406&CC=CN&NR=102001371A&KC=A.

[175] WANG YUELIN. Elliptic gear drive walking robot and manufacturing method thereof, 8 2014. URL https://nl.espacenet.com/publicationDetails/biblio?adjacent=true&locale=nl_NL&FT=D&date=20140806&CC=CN&NR=103963869A&KC=A.

[176] Giancarlo Zamagni. Machine for arthropod locomotion on a surface, June 9 1998. US Patent 5,762,153.

[177] HUA ZHANG. Walking apparatus of bionic mechanical horse, 11 2006. URL https://nl.espacenet.com/publicationDetails/biblio?adjacent=true&locale=nl_NL&FT=D&date=20061101&CC=CN&NR=2832624Y&KC=Y.

[178] LI ZHENGXI. Multi -functional doubly -linked robot of walking, 10 2017. URL https://nl.espacenet.com/publicationDetails/biblio?adjacent=true&locale=nl_NL&FT=D&date=20171020&CC=CN&NR=206568170U&KC=U.

[179] Teresa Zielinska and John Heng. Development of a walking machine : mechanical design and control problems. 12:737–754, 2002.

[180] MA ZONGLI, ZHANG PEIQIANG, LIU YONGCHAO, LI QINGYANG, FENG SHUANG, and WANG JIANMING. Dog-like quadruped robot, 12 2015. URL https://nl.espacenet.com/publicationDetails/biblio?adjacent=true&locale=nl_NL&FT=D&date=20151202&CC=CN&NR=105109575A&KC=A.

Appendix A

Detailed design method

A.1 Design approach

The design process is layed out in fig. A.1. This flowchart is used as guideline in the elaboration of the methodology in the coming section.

After the project definition, a simplified design objective was set: "Design of a mechanism for the generation of a spherical surface, while taking into account the constraints imposed by compliant hinges." Several iterations were performed to generate a practical understanding of the subject matter. The phases during each iteration can roughly be summarized by the steps indicated in the cycle in fig. A.1. The first step in this cycle comprised the invention of an idea for a mechanism, after which this idea was created by means of 3D modelling or physical prototyping in the creation phase. After this, the resulting behaviour was verified in matching with the intended behaviour and finally the possible reasons for the corresponding or differing results were extracted in the extraction phase. This last step then led to new insights for the invention of the following idea. This process was repeated a number of times until a system capable of tracing a spherical surface was designed.

Following up on this, the functions of the designed system were extracted, leading to an understanding of the needed components of the mechanism. After this subdivision, more solution possibilities were generated. This time only inventing new ideas for the functions alone. Then, similarities between the invented solutions were looked for, leading to a categorization of the solutions into strategies. Where each strategy represented a pool of solutions with the same approach for fulfilling the stated functions.

The analysis and design of this simplified mechanism provided an understanding of the subject matter and thus a good basis for the final kinematic design. We will continue to the right side of the diagram in fig. A.1. The first steps in the final design were made by constructing the set of functions, solutions and strategies for meeting the design specifications of the desired WM. The analysis of the simplified system formed a basis in the construction of these sets of properties.

Guided by the project definition, the most appropriate strategies and their underlying solutions were chosen. From this followed the generation of the final design by the construction of a kinematic model and its verification. Then, suitable compliant replacements for the conventional joints were found and chosen. This ultimately led to the design, construction and verification of a physical model of the final design.

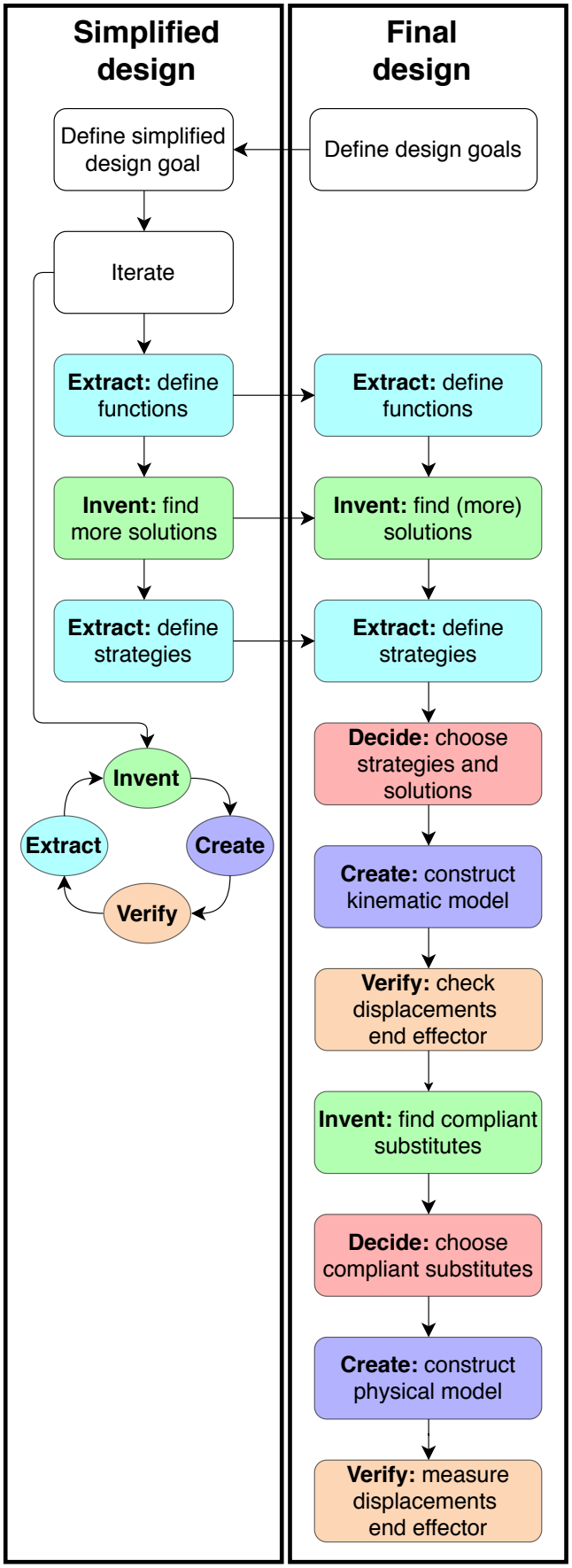

Figure A.1: Overview of the design method.

A.2 List of hard requirements

The set of requirements for the walking machine are summarized in the following list, including a small elaboration.

1. The device shall be fully actuated.

   Referring to the view as implemented in the literature survey in chapter 2, the device shall be fully actuated. Thus, contain only two actuators with its two degrees of freedom.

2. The device shall be statically stable.

   To ensure stable operation with a single actuator per DOF, the device is required to be statically stable.

3. The device shall be capable of omnidirectional movement.

   The device shall be able perform a translational motion in all directions parallel with the supporting surface, at any point in time.

4. The device shall have a greatly higher stiffness in supporting direction than over the transverse plane.

   Given that compliant mechanisms inherently introduce stiffness in the motion direction, it is important for this stiffness to be low with respect to the stiffness in supporting direction.

5. The device shall not be limited in its range of motion.

   The inherent limitation in the range of motion of compliant mechanisms should not influence the operation of the machine.

6. The final design shall allow for monolithic fabrication.

   This allows for additive manufacturing.

A.3 List of soft requirements

The requirements which are not strict to be met, but indicate a direction for design choices are indicated in the following list. Again, with a small elaboration.

1. The centre of mass shall remain at a constant height.

   To make sure the device is dynamically stable, the centre off mass shall remain at the same distance from the supporting surface over the entire range of operation. This limits vibrations.

2. The input to output ratio shall be constant.

   To provide easy control of the machine, the input motion shall be linked to the output motion such to not introduce a varying speed or direction with constant input velocity.

3. The transverse stiffness shall be constant.

   Ideally, the stiffness the machine has in movement direction is constant over the entire range of motion to not induce vibrations due to stiffness.

4. All dynamic forces shall be balanced.

   Again, in order to limit vibrations the device should be designed such that dynamic forces are balanced.

Appendix B

Kinematic design of leg with simplified trajectory

Here an image is created of the several iterations and the major conclusions drawn from the analysis of the designs.

B.1 Design 1

A view on the first attempt to describe a spherical surface is given in fig. B.1

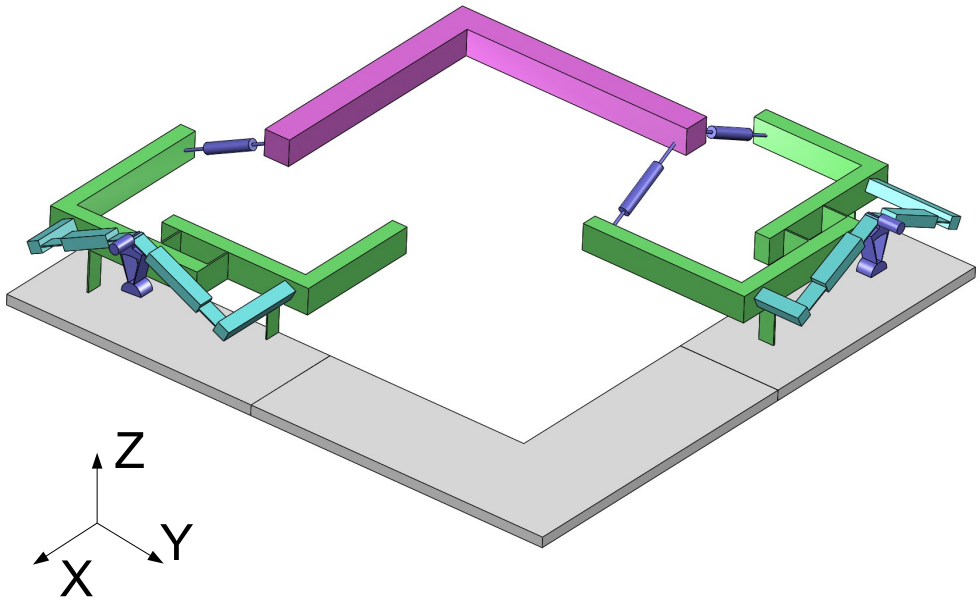

Figure B.1: The first design in the attempt of generating a spherical surface.

As with the final design, the pink colour is used for the end effector. This L shaped beam is constraint in rotation by external constraints not shown here. The smaller sections indicate the location of joints. The purple rods connected to the end effector show similarity with the input motion generators of the final design in their way of functioning. Both the two on the right and one on the left side of the figure produce an eccentric motion. The radius of this motion is altered by changing the distance between the green L shaped beams to which the purple rods are connected. The combination of the blue beams and connected red element determines the distance between the L shaped green beams. This is done by rotating the central red element around the centre of its bottom half cylinder, which was constrained in any direction but its rotation around this axis. Taking the right most setup as example, this rotation causes both of the blue beams align, while simultaneously moving in the indicated Z direction. In the process, the green beams are moved apart and in this Z direction as well, with this changing the radius prescribed by the purple rods and moving the end effector in Z direction as well. The idea behind this is that, as with a sphere, the radius of the circle making up the intersection of the spherical surface and a plane parallel to the XY plane firstly increases with decreasing Z position, until it has reached the centre of the sphere, after which it decreases again. The idea was that by combining this behaviour in the X and Z directions, a sphere could be created. After trying out several modifications it became clear that the problem of this design was in the parallel coupling of the two directions posing to many constraints.

B.2 Design 2

A following step produced the design as given in fig. B.2.

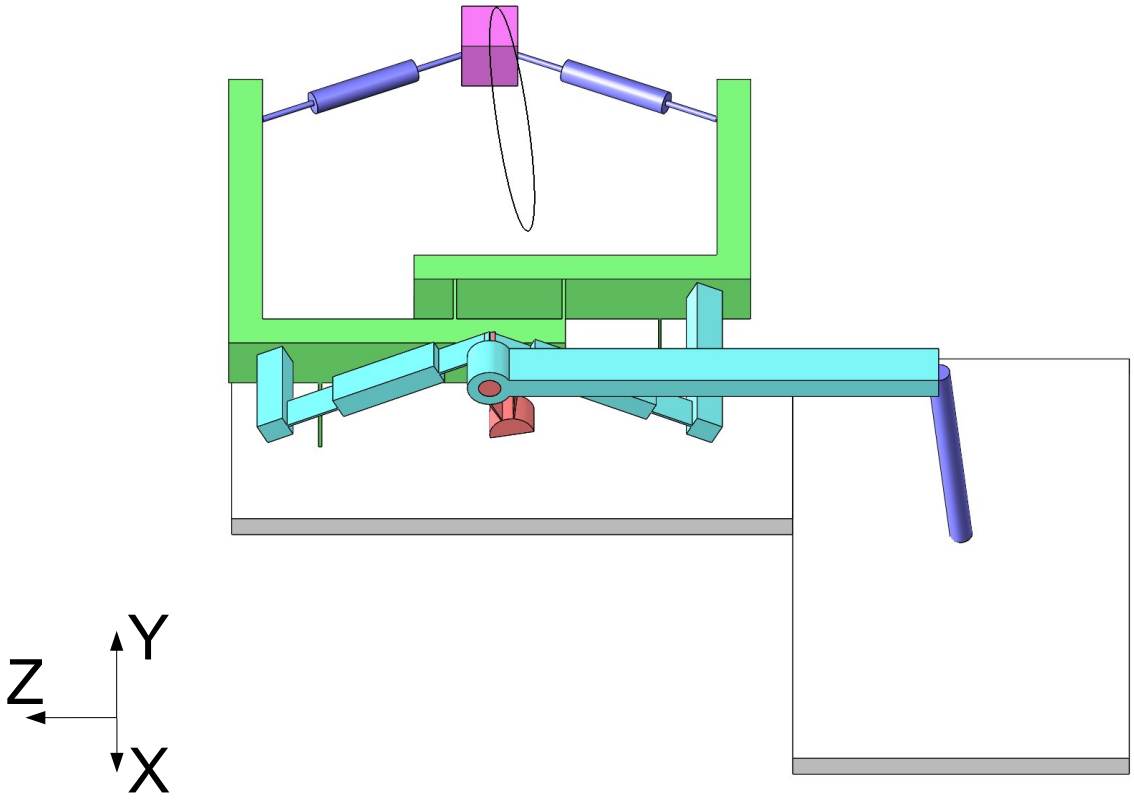

Figure B.2: The second design in the attempt of generating a spherical surface.

With this design the extracted problem of directly coupling the both directions was addressed by linking two motions in series. The input motions are again produced by the purple rods. On the bottom right, the top part of this rod is constrained to moving over a circular path externally, this is not shown. Setting a constant rotational input on the resulting motion of the connected blue beam is in a sinusoidal fashion in the indicated Z direction. This motion is then transferred to the same red element as in design 1, from which the same procedure of links follows. Now, since we actuate both the bottom right and top left input rods with a constant angular velocity, the resulting path is rather circular, with a slight angle with respect to the indicated X axis. This path is shown in fig. B.2. With this second design we moved from a non-functioning towards a seemingly functioning design. By exploring the boundaries of this design and judging its feasibility, the following conclusions were extracted.
As soon as the radius of the circle of the bottom right input rod is increased towards a value at which the angle of the output path with the X axis converges to 90 degrees, the output path starts to show major deviations from its approximately planar state as currently depicted. Of influence here are the dimensioning of the entire transmission and the constant input velocities. Extending this even further, in order to describe a circle on a plane parallel to ZY, the system would need to generate a motion along this path with the rotation of the top left inputs not being able to contribute. Essentially, this means the machine is under-actuated in this mode.
Further analyzing the manner of altering the radius of the purple rods, we notice that to make a full rotation of the circular output path around the indicated Y axis, the system has to go through various singularity positions. These are the positions for which the radius of one of the eccentric input motions is equal to 0. Four of these singularity positions are present at an angle of 90 degrees apart, alternating between the bottom right and top left inputs. At these singularity points, in order to make sure the same rotational direction of the output path is maintained, either a 180 degree phase shift or a directional inversion of the input motion will have to be executed. This insight indicates the difficulties of using this type of mechanism for the generation of circular paths. Therefore, for the next design iteration, an attempt was made to come up with more solutions/strategies for generating the sinusoidal functions and modifying their radius. Another viable solution for this is presented in design 3.

B.3 Design 3

Given the second design and its implications, a third design was made as shown in fig. B.4.
With this design a first attempt at splitting up the motions in the different directions and later merging them together again was made. In this design, the prismatic joints are indicated by a symbolic parallel flexure as indicated in fig. B.3b, where the DOF is parallel to the top and bottom surface and the front facing part side of the indicated representation. Furthermore, components are free to move through one another, collision was not yet taken into account. The colour scheme is again similar to the colour scheme of the presented final design. Starting off with the input motions again, these are displayed in purple. The same principle of these input motion generators was used in the sense that a rod is made to move in an eccentric fashion. The difference here however is that instead of changing the physical radius described by the rod, the entire mechanism is rotated. This changes the amplitude of the extracted output motion. The blue bars, determining the X and Y position of the end effector, are connected to these input motion generators such to extract this output motion. This is a similar construction as in the final design, where bars b_8 and b_{8m} rotate to alter the amplitude of the X or Y outputs. These X and Y transmissions are consecutively connected to the end effector in a similar fashion as in the final design, where the orange elements representing the motion coupling mechanism, conduct the intended displacements while being decoupled from the other respective motions. As with the final design, the yellow elements indicate the Z transmission, being on one side connected to the input motion generators and on the other to the motion coupling mechanism. Lastly, in red is shown the direction setpoint mechanism which directs the orientation of the input motion generators.
This design incorporates four coupled input motion generators, the initial intention of this was to make sure the opposing input motion generators are able to work together to make a change in the direction of the angular motion unnecessary. After critical reflection, it was realized that using a total of two input motion generators of this type was sufficient for the intended purpose. This design, in contrast with the two previous designs is able to describe a closed spatial surface. The surface is not spherical though, due to the 1:1 transmission ratio of the Z component of the end effector with the Z level of the input motion generator a smaller ratio for X and Y, the surface is larger in Z direction than in X and Y. An indication of this is given in fig. B.3a This is due to the rotations of the input motion generators around the Z- axis not reaching 90 degrees, for which the amplitude of the transmitted motion would be equal to the input radius. This was avoided as it is yet another singularity position.

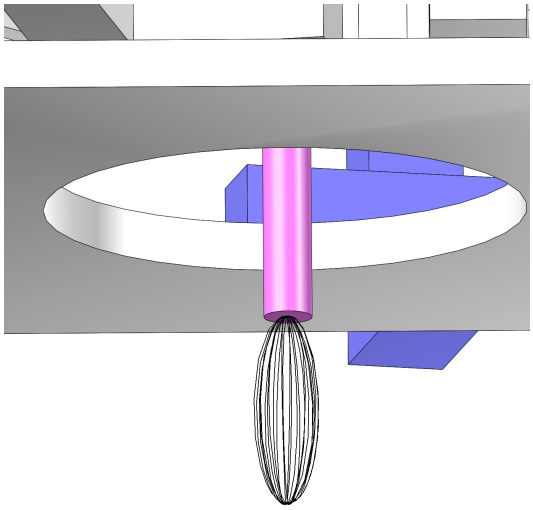

(a) Indication of the surface generated by the third design.

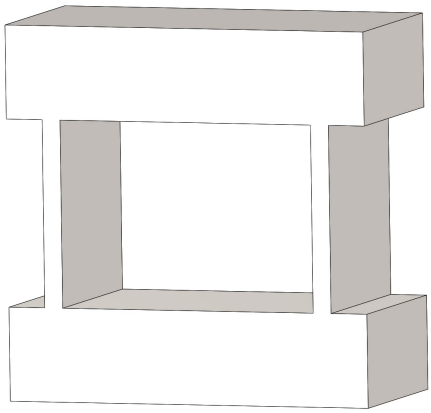

(b) Symbol of prismatic joint, derived from the compliant parallel flexure

Figure B.3: The path described by the design and an indication of the prismatic joint used.

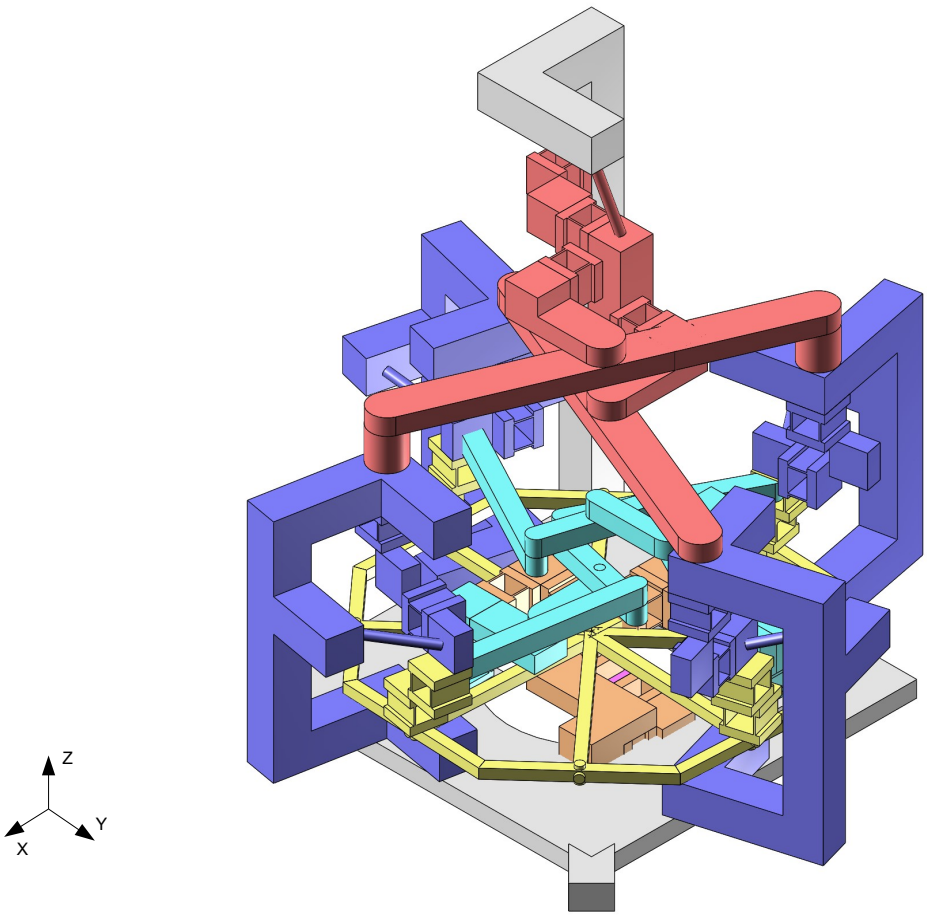

(a) complete view on the third design.

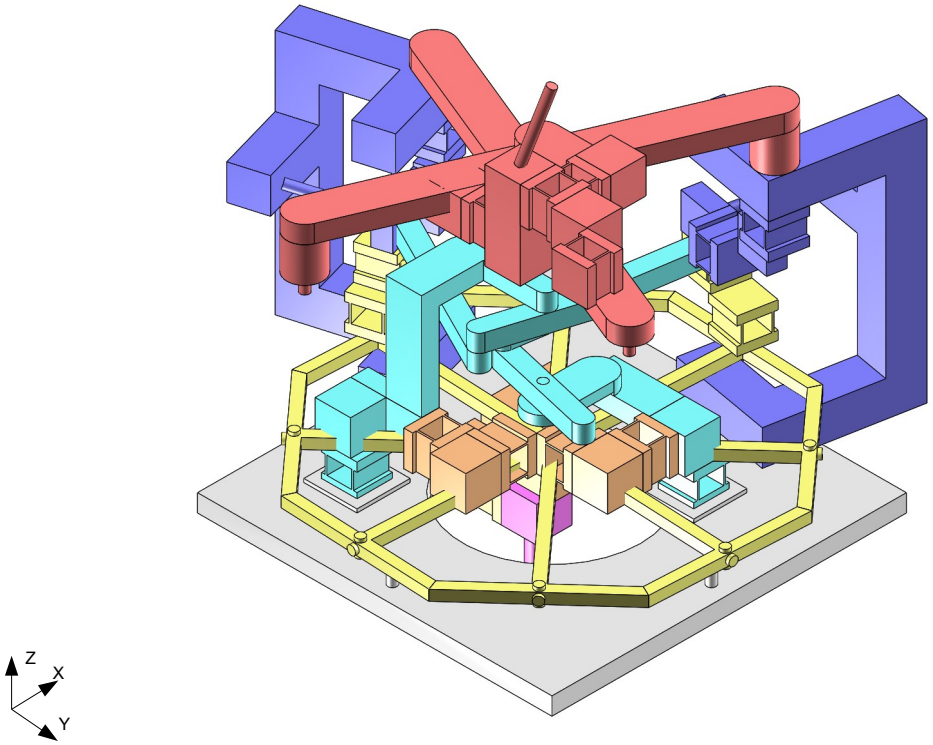

(b) Inside look into the third design.

Figure B.4: The third design in the attempt of generating a spherical surface.

Appendix C

Abstraction

C.1 Design breakdown

After having gotten an insight into the relevant aspects in the design of the mechanism, an abstraction phase followed. Looking at the design of an overall WM more abstractly, one can differentiate several sub-functions of the machine. Furthermore, one can define several solution strategies for these sub-functions, which group underlying solutions to the indicated functions. The breakdown of the functions and strategies of a WM is indicated in appendix C.1. Applying this type of breakdown to one of the legs, the scheme as in fig. C.9 was produced. The coming sections elaborate on the indicated design breakdowns step by step, combining the previously obtained insights and building forth upon these.

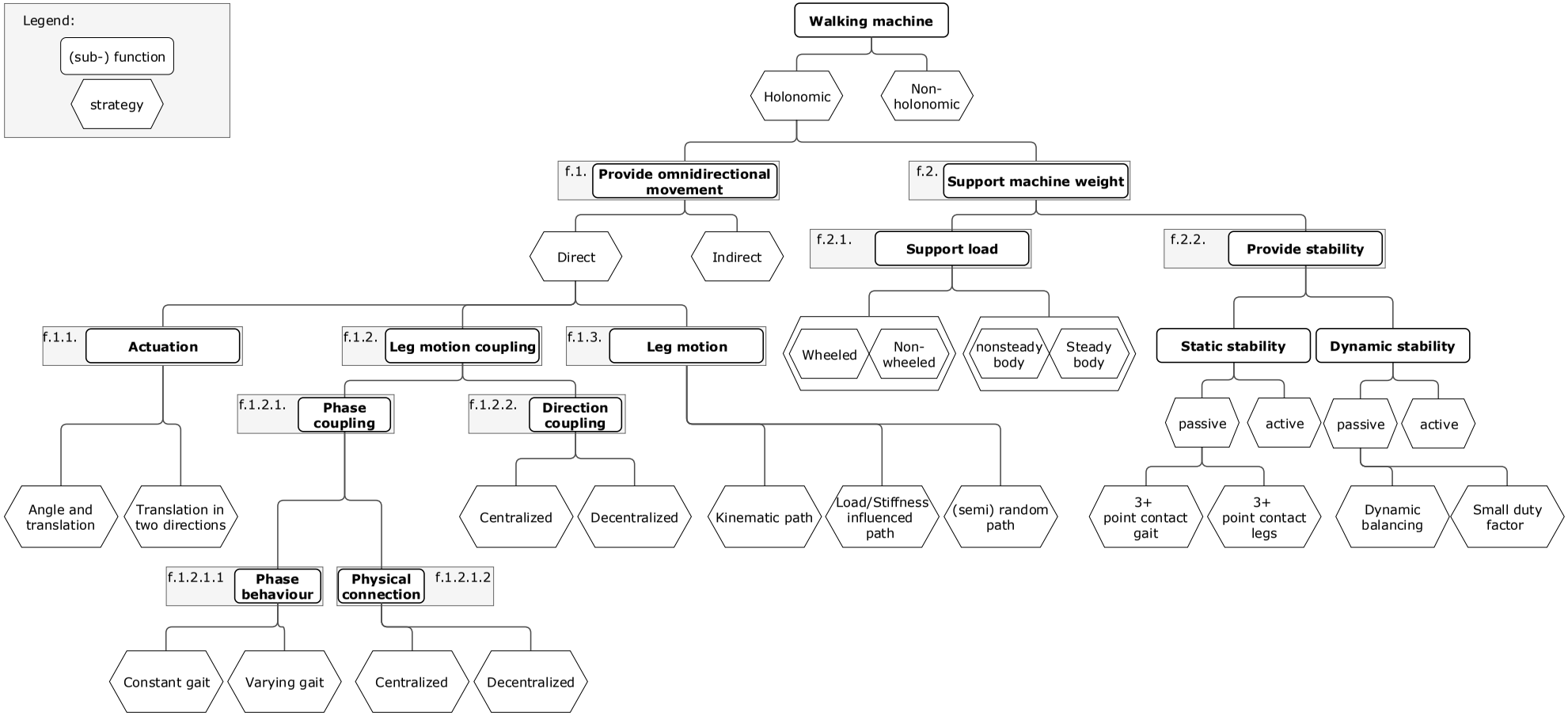

Figure C.1: Functional breakdown of complete walking machine.

At the top of the tree is the walking machine itself with the initial choice between the strategies of a holonomic or non-holonomic design, see fig. C.2. A non-holonomic walking machine is here taken to have a state dependent on its taken path. Say, the rotation of the machine after having moved to the desired point is determined by its path. The states of holonomic systems do not depend on the taken path. Here, the holonomicity is taken to refer to the external state of the system only. Internal path dependencies are not taken into consideration. Taking into account the objective to design a purely translational machine, this automatically means the machine should be holonomic. Any form of rotation should not be induced and the state of the machine is therefore not dependent on the path taken.

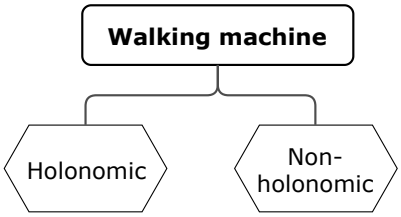

Figure C.2: Top of the design breakdown tree.

(f.1.) Provide omnidirectional movement.
For the device to position itself at another location, a movement will have to be provided. As it is required for the device to position itself at a location over the entire planar DOF, movement will have to be able in any direction on this plane.
(f.2.) Support machine weight.
The device should not collapse under its own weight.

(f.1.) Provide omnidirectional movement

For the provision of omnidirectional movement, two strategies are considered. One is such that the device is able to move in any direction from any position directly. The other is that by smart combination of the length travelled in two different directions, any point in the plane can be reached from a random, respective other. These strategies are indicated in fig. C.3 and are called a direct and indirect strategy respectively.

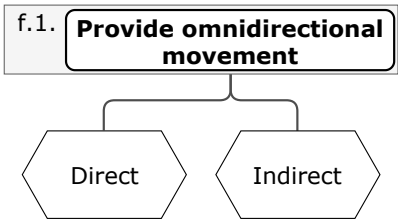

Figure C.3: Function 1, providing omnidirectional movement and its strategies

The direct strategy allows for the shortest path to be taken, which is a straight line per definition, taking into account that the supporting surface is a perfect plane. Since this strategy does not introduce the dynamic effects accompanied with an indirect strategy, this is the strategy of choice.

As this strategy still is rather rudimentary, another subdivision in functions is made. To provide omnidirectional movement in a direct fashion, three more functions can be defined:

(f.1.1.) Actuation.
The device will need actuation in order to operate.
(f.1.2.) Leg motion.
The legs have to perform a motion to make the entire machine move with respect to the supporting plane.
(f.1.3.) Leg motion coupling.
The different legs will have to be coupled for the machine to be able to operate.

(f.1.1.) Actuation

For the device to function, actuation will have to be present. The amount of actuators is chosen to be equal to the desired degrees of freedom of the system, two. As seen in chapter 2, the present amount of fully actuated TT walking machine designs is relatively small. Furthermore, fully actuated systems require relatively simple control schemes. Thus, a WM with these properties contributes scientifically and allows for simple control.

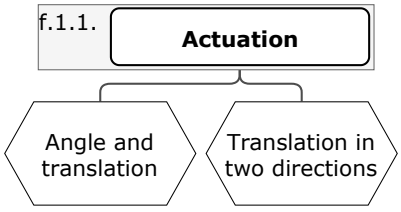

Figure C.4: Function 1.1, actuation and its two strategies.

Two actuation strategies can be thought off as seen in fig. C.4. The first is controlling the direction and propulsion of the machine. The other is placing the actuators such that each propel the machine in a different direction. These movements will then have to be added for a specific direction to be generated.

The chosen strategy is to determine the propulsion and direction of the machine. This is regarded to be the simpler version of the two, because the functions of the two actuators are separate. This means that the system does not have to combine the motion of two actuators into a certain direction of movement, but rather one actuator sets the direction of motion of the other actuator to propel the system into.

(f.1.3.) Leg motion

For the entire WM to be able to move itself, a certain leg motion is needed. This motion itself can be split up in three phases (leg-phases), a translational phase along the supporting plane, a lifting and placement phase, and a return phase. In literature these phases are respectively called support or stance or stride, transition or "retract/reswing and protract" or lift, swing or return [112, 139, 4, 138]. In this document the terminology support phase, transition phase and return phase is used. In the support phase the legs support the WM by being in contact with the supporting surface. In the return phase the leg moves such that it can start its following support phase and the transition phase is the phase between these phases.

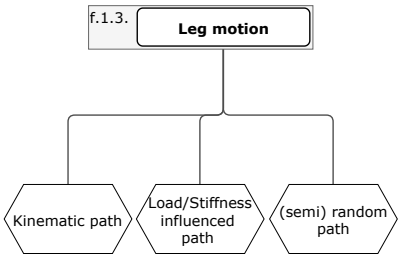

Figure C.5: Function 1.3, leg motion and its three strategies

To provide the motion of the machine in two translational degrees of freedom, various strategies are proposed as indicated in fig. C.5. The first strategy is to design a path kinematically, assuming rigid body links and perfect joints. This results in a fixed freedom space of the end effector. The second strategy is to take into account the influence of loads and/or a stiffness change within the motion of the leg. This might result in a simple leg design, but a low reliability in path shape due to for instance varying dynamic loads. The last proposed strategy is to not necessarily predefine the path of the end effector. Instead, make sure the leg structure is such that under the influence of the actuators, the legs will behave in a(n irregular) manner which propels the device. This could result in a very rudimentary leg design.

The kinematic path design was chosen. Although a (semi) random path generation has the potential of resulting in a very simplistic system design, a mechanism with a well defined kinematic path was judged more interesting and simpler in the design process since the stiffnesses of the system could be left out of the design scope. Knowing that any of the choices would be a contribution to the systems described in literature, this was found to be a good enough foundation.

(f.1.2.) Leg motion coupling

Next to a certain leg motion, the legs also have to work together to make sure the machine is able to operate reliably. As mentioned in the previous section, the leg motion can be split in different phases, leg-phases. Within each leg-phase the leg fulfils a different purpose. To make sure the legs actually fulfil the purpose of the leg-phase, a phase difference has to be present. Enough legs have to be in support phase in order for others to execute the return/transition phases. Next to a phase difference, the leg motions (in support phase) have to propel the vehicle in the same direction. To accommodate the cooperation between the different legs, a coupling has to be present, in short they are named the following, and are indicated in fig. C.6.

(f.1.2.1.) Phase coupling.
(f.1.2.2.) Direction coupling.

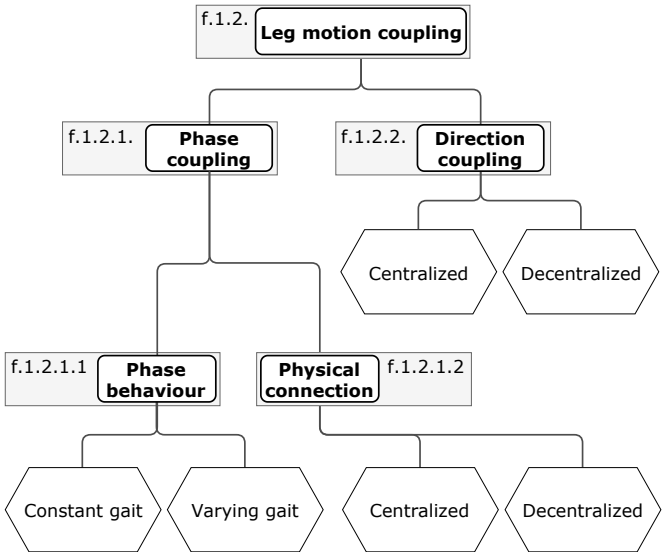

Figure C.6: Function 1.2, leg motion coupling and its subfunctions and strategies.

(f.1.2.1.) Phase coupling

Concerning the phase coupling, two other functions can be defined. One is concerning the behaviour, and one concerning the physical implementation of the coupling.

(f.1.2.1.1) Phase behaviour

The phase behaviour results in the gait of the system. In other words, the position (and its derivatives) of the different end effectors with respect to one another at each point in time, determine the gait of the system. Now,

one could aim for a design which has the possibility of varying its gait during operation. This would mean the phase difference between the legs will have to be able to be adjusted during operation. For the sake of simplicity, the gait is kept constant and thus is the phase difference.

(f.1.2.1.2) Physical connection

The physical connections between the legs which couple the phases can be arranged in two ways. Either the phase of each leg is determined by a single mechanism to which all legs are linked, or the legs can be interconnected with each other by separate links in series. In the first case, the central mechanism contains and determines the phase (information) of each leg and directly communicates this with each leg. In the last case, each leg has information about for instance its neighbouring leg and from that it determines its own phase. In short one could say the first strategy is a centralized approach and the second strategy is a decentralized approach.

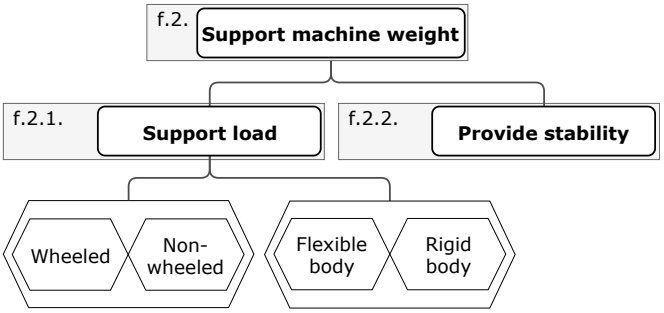

Figure C.7: Function 2, Support of the machine weight, split up in its subfunctions, including the strategies for supporting the load.

The centralized strategy is expected to be more accurate since links are direct and are thus less sensitive to disturbances, including deformations. Furthermore, this strategy is expected to deliver a simple total system as only one mechanism couples all phases.

(f.1.2.2.) Direction coupling

As with the phase coupling, the direction can also be determined by a central mechanism, or by connecting the legs with separate links. As with the phase coupling, these are also respectively called a centralized and decentralized approach. Also for the same reasoning, the centralized approach is expected to deliver better results: an accurate, simple and robust system.

(f.2) Support machine weight.

As indicated in fig. C.7 this support can be split up in two sub-functions:

(f.2.1.) Support load.
(f.2.2.) Provide stability.

(f.2.1.) Support load.

The mechanical connection between the supporting surface and the COM of the machine shall be able to support the load of the machine. Still two strategies can be chosen to give shape to this connection. Wheels could be incorporated in the design, to supplement the behaviour of the machine or not. Several examples of this are found in chapter 2. Furthermore, a specific, easily identifiable steady body can be incorporated, or a choice can be made to not necessarily define a body to which the components are connected.

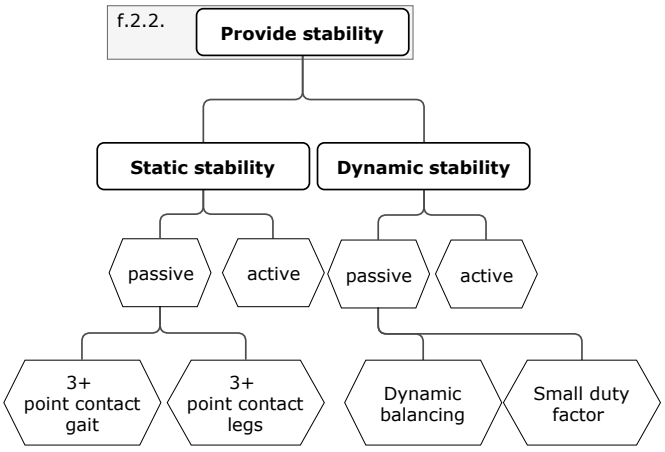

Figure C.8: Function 2.2, provide stability and its subfunctions and strategies.

Concerning the support of the load, a strategy making use of wheels is undesired as it demands the use of infinitely rotating joints. These have the side effect of being less ideal decision within vacuum environments and are therefore not the chosen strategy.

For the ease of the design process, a strategy incorporating a clearly defined frame or body of the machine is chosen.

(f.2.2.) Provide stability.

For the system to be able to robustly operate, stability has to be provided. Two sub-functions are considered, static and dynamic stability. The subdivision is shown in fig. C.8. With two actuators, simultaneously actuating the system and providing dynamic stability is a practically challenging task and will result in a coupling between the actuation of the mechanism and the maintaining of stability. Static stability has the advantage of not needing any actuation, but might result in unwanted behaviour at higher operating velocities/bandwidths. Since the use of only two actuators is desired, static stability is the chosen strategy.
Still, static stability can be accomplished in different ways. One proposed strategy is the use of a gait which makes sure at least three legs are in support phase at every single point in time and keeps the centre of mass within the polygon spanned by the supporting points. A second strategy is to make sure each leg has at least three contact points with the supporting surface, with the centre of mass always in between the polygon spanned by those points.

The second strategy is judged to be superior to the first, as less leg mechanisms are needed. Which in turn decreases the complexity of the system.

Functions and strategies leg design

In this section the considered design strategies for the different functions and sub-functions of the legs of the walking machine will be elaborated on. An overview of the discussed functions and strategies is given in fig. C.9.

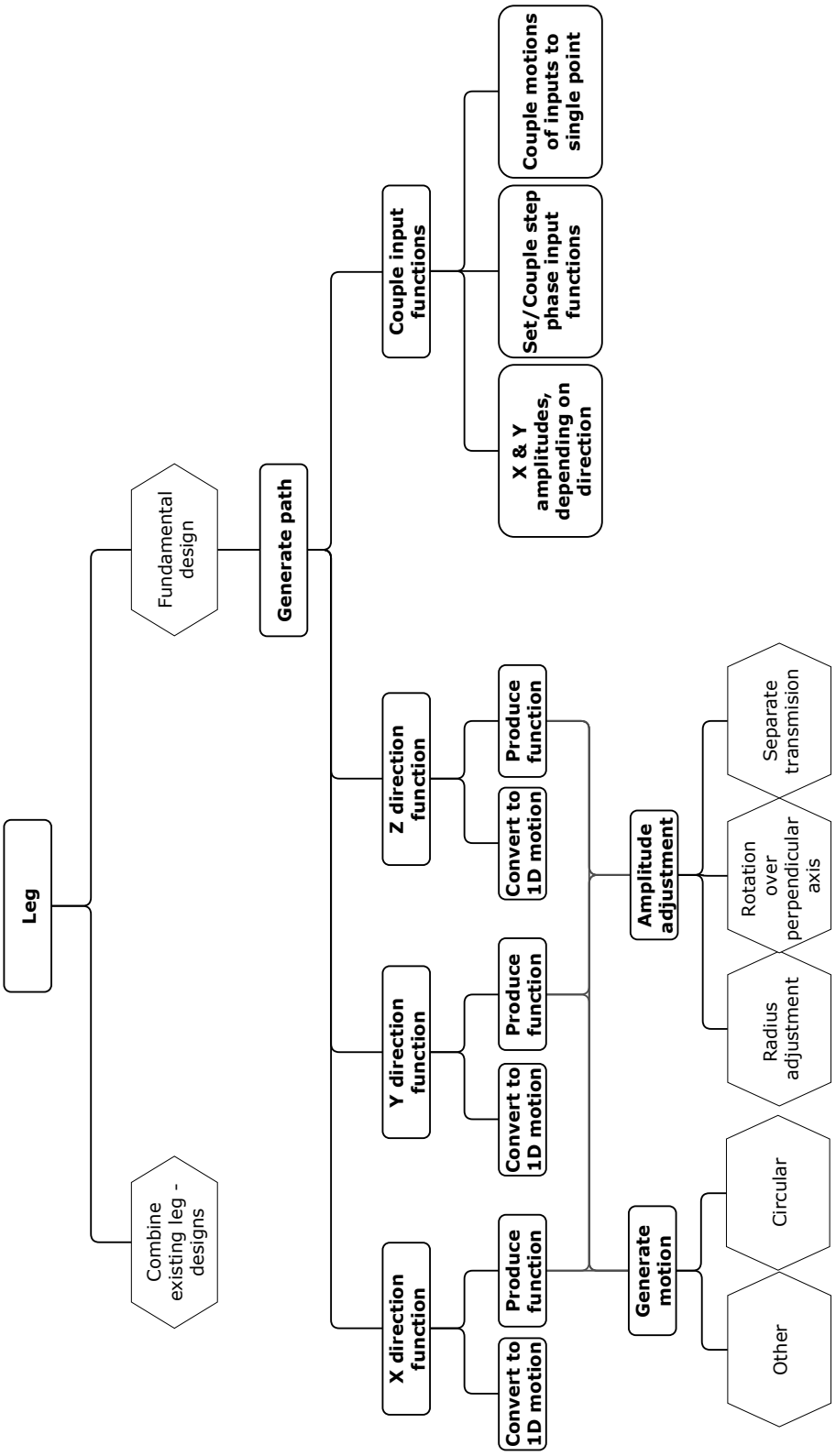

Figure C.9: Functional breakdown of a single leg.

For the design of a leg mechanism, different approaches to the way of designing are taken into account. One strategy would be to combine two existing legs with a single degree of freedom to create a 2-DOF design. Another strategy would be to design more fundamentally, by splitting up the leg in different sub-functions and choosing the best and/or most coherent solution to the different functions. This is graphically represented in fig. C.10.

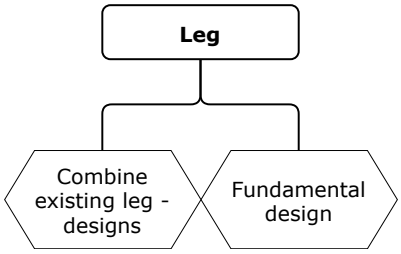

Figure C.10: The leg and its two main strategies of design.

The more fundamental strategy is chosen as it gives more insight in the motions and functioning of the device and gives more design freedom. With this strategy, it is predicted to be easier to more accurately create the desired path shape as no limitations are imposed by the existing leg designs.

Two main functions can be defined for the legs of the WM. At the two points of actuation the direction and propulsion are generated as chosen earlier. These motions are transmitted to the legs from within the machine. The legs on their turn have transform these inputs into the desired path shape. Since this path is within a three dimensional space, the path can be defined by three separate functions, basically the projections of the path onto three surfaces. To avoid dependencies across the functions, these surfaces are set to be perpendicular and can thus be described by a cartesian coordinate system. Separating these functions helps in the design of the physical system. However, since the final path shape of each leg is a combination of all three functions, these will also have to be coupled again. In short, the generation of the leg path (Lf.1.) as indicated in fig. C.11 can be split up in four subfunctions:

(Lf.1.1) Generate X direction function
(Lf.1.2) Generate Y direction function
(Lf.1.3) Generate Z direction function
(Lf.1.4) Couple input functions

In this list, X and Y directions are perpendicular to each other, parallel with the supporting plane. The Z direction is the direction perpendicular to the supporting plane.

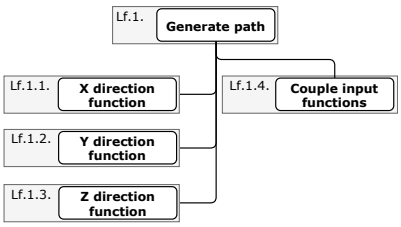

Figure C.11: The main function of the leg and its subfunctions.

(Lf.1.1-3) Generation of X,Y,Z functions

Figure C.12 shows the (mathematical) X, Y and Z functions and their subdivisions. To generate the functions, a basic motion is needed (Lf.1.1-3.2), also this motion has to be transformed into the desired (mathematical) function (Lf.1.1-3.1) and depending on the direction, the amplitudes of the function need to be able to be adjusted (Lf.1.1-3.3). To transform the generated motion into the desired function, a transmission will have have to be present transforming the input function into an output function. Also, in case this input function is not a 1 dimensional function, it has to be transformed into one, as the output functions are motions in either X, Y or Z direction.

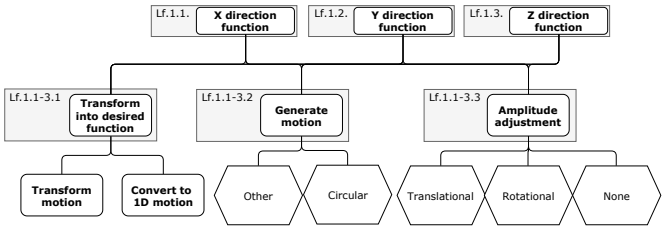

Figure C.12: The three input functions and their subdivisions.

The decision of making use of compliant hinges limits the freedom of movement of the joints. When for instance making use of a planar compliant joint, continuous (circular) movement is always limited by either the maximum deflection of the joint, or links touching each other. This forces the design to move into the three dimensional domain. Within the three dimensional domain, there are various possibilities of creating a continuous motion using compliant joints. In order for the system to remain simple, the focus is set on producing circular movements as a basis.
With a change in the direction of the WM, the amplitudes of the X and Y motions vary. For this reason, the function generated for X and Y also has to be able to vary in amplitude. Two strategies for this function are considered. One makes use of a translation and one of a rotation. Design 1 and 2 are good examples of a system making use of a translation to alter the output function. Design 3 and the final design makes use of rotational amplitude adjustment for the generation of the X and Y

functions.
Since the Z direction does not need a variable amplitude with respect to the direction of the machine, the amplitude adjustment strategy of this function is to have no. For the X and Y direction a choice was made for a rotational amplitude adjustment because a combination solution was found which supported the production of a perfectly sinusoidal function. This was deemed preferable but in this sense does not proof translational amplitude adjustment inferior .

(Lf.1.4.) Couple input functions

Although the motion of the end effector of the leg can be separated in X, Y and Z direction, the motions are not independent. For this reason a coupling has to be present which links the three, the subfunctions of the coupling are given in fig. C.13. First of all, due to the the choice of a direct strategy of the WM, it has to be able to travel in any direction at any point in time or space. For the legs, this means the path of the end effector should be able to rotate around a central axis parallel with the Z-axis. This means the X and Y amplitudes have to be coupled such to make sure a rotation around this axis is produced (Lf.1.4.1). Furthermore, the phase of the functions has to be coupled to produce the desired shape(Lf.1.4.2) and the resulting motions have to be added to a single point (Lf.1.4.3).

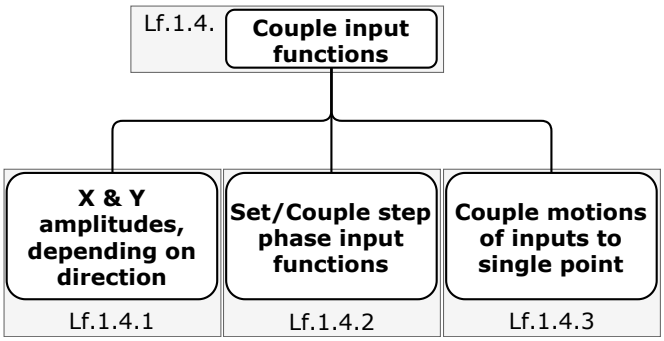

Figure C.13: Leg function 1.4, and its sub-functions.

Appendix D

Final kinematic design

D.1 Design 4

From the understanding that emerged from the previous designs and the analysis thereof, a step towards the final design was made. This was done with a focus on the coupling of the mechanism with multiple others and on simplifying the entire set of links. The mechanism indicated in fig. D.1 was designed from there. This is a partial design to verify and analyse the behaviour of the system.
Again, as with design 3, the symbolic parallel flexures indicate the prismatic joints and components are free to move through one another. Also, the same colour scheme holds. In purple here is the input motion generator represented by an L beam able to rotate around the Z axis, connected to the frame at the center of the top cylinder. Rotating the L beam makes the rectangular purple element move in a circle parallel with the XY plane. The connected yellow bar transmits the motion in X direction and Z direction in a similar fashion as b_4 in the final (Z transmission) design and is thus named b_4. This bar is consecutively decoupled in X direction and connected to the yellow, large U shaped beam, which is constrained to only move in Z direction. In this manner, the large U shape beam dictates the Z position of the end effector. Going back to the b_4 bar, as in the final design, this transmits the X position of the input motion generator directly to the following X and Y transmission. The difference with the final design is that the X and Y transmission are serially connected to the large yellow U shaped beam, which moves in Z direction. Therefore the indicated blue components also move in the Z direction as a whole. Since the design of this X and Y transmission is similar to the final design, the bars indicated with their respective names. The only difference with the final design is that bars the bars b_{13} and b_{10} (as well as their mirrored variants b_{13m} and b_{10m}) are connected in a fashion mirrored over their central plane parallel to the XY plane.
As indicated, this design only has one input motion generator. From the abstraction was concluded that the circular motion did not necessarily have to be transformed into a reciprocating 1D motion near the end effector as in design 3, but rather this could be done in an earlier stage. This simplifies the system since only the reciprocating 1D motions have to be transmitted. Furthermore, the central input motion generator can form the basis for the phase coupling of multiple legs, as well as being their input motion generator.
As indicated, this design does have the X and Y transmission on a moving basis in Z direction. This could benefit the simplicity in the motion coupling mechanism, as the Z motion does not have to be decoupled from the X and Y displacements anymore. However, in the overall direction coupling, this introduces these Z motions as well since the X and Y direction are the two that need coupling. For a single leg system the influence of the Z motions in the direction coupling can be easily dealt with, possibly in a simpler sense that in the manner as presented in the final design, as the entire direction coupler can be made planar and should thus not be influenced by movement in Z direction. However, when attaching and coupling multiple legs which operate out of phase, this direction coupling will have to allow for these Z motions in all phases. Effectively, this

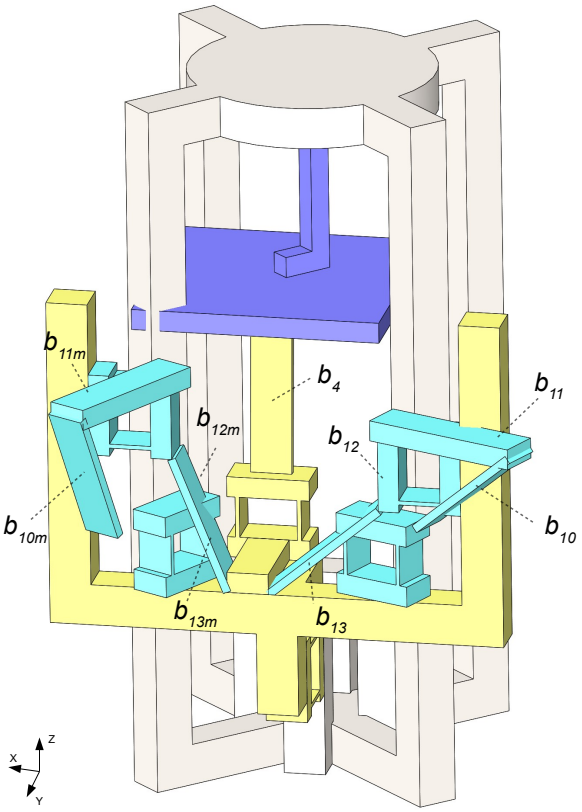

(a) Part of the fourth design.

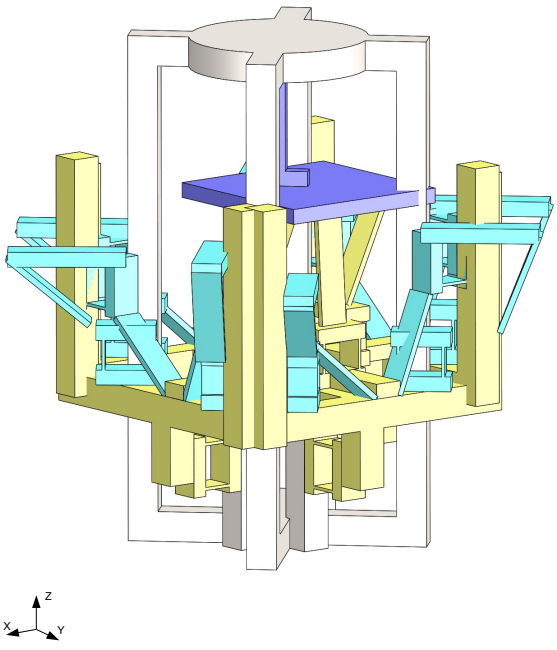

(b) Part of the fourth design, showing multiple leg systems.

Figure D.1: Part of design 4.

would mean that in order to provide a perfect direction coupling, all of these different Z positions would have to be decoupled. To provide a simple connection of the direction coupling mechanism, for the final design this Z decoupling was chosen to be done in a central mechanism: The motion coupling mechanism, which is located at the endpoints of the transmissions. This produces a clear distinction between the functions of the overall machine by separate mechanisms. The advantage of this is that it allows for easy modification of the path shape of the end effector by selectively changing the subcomponents of the system. This is preferable as it allows for the design to be simply altered for specific use cases.
The coupling of several of the partial leg mechanisms in design 4 is shown in fig. D.1b. This coupled kinematic design has provided a verification of the intended kinematic operation of the overall machine. Combining this with the insights gained from the analysis of this design, the following steps in the design process were taken.

D.2 Final kinematic design

D.2.1 Input motion generator

The final design of the input motion generator followed from a comparison of several solutions. The proposed design solutions are schematically represented in fig. D.2. The output points of the mechanisms are shown in green. The solution possibility on the left makes use of three spherical joints to create the circular degree of freedom as desired. As discussed earlier, by making sure the distance between the outer most joints is shorter than the sum of the bar lengths in between these joints, the output point is made to move in a circular fashion. For the solution possibility in the center of fig. D.2, this distance is constrained by means of two prismatic joints serially connected such that a planar DOF is created. The solution possibility on the right side of the figure also creates this planar DOF, but does this by means of a serial chain of a revolute joint as indicated in the bottom right of the schematic and a single prismatic joint.

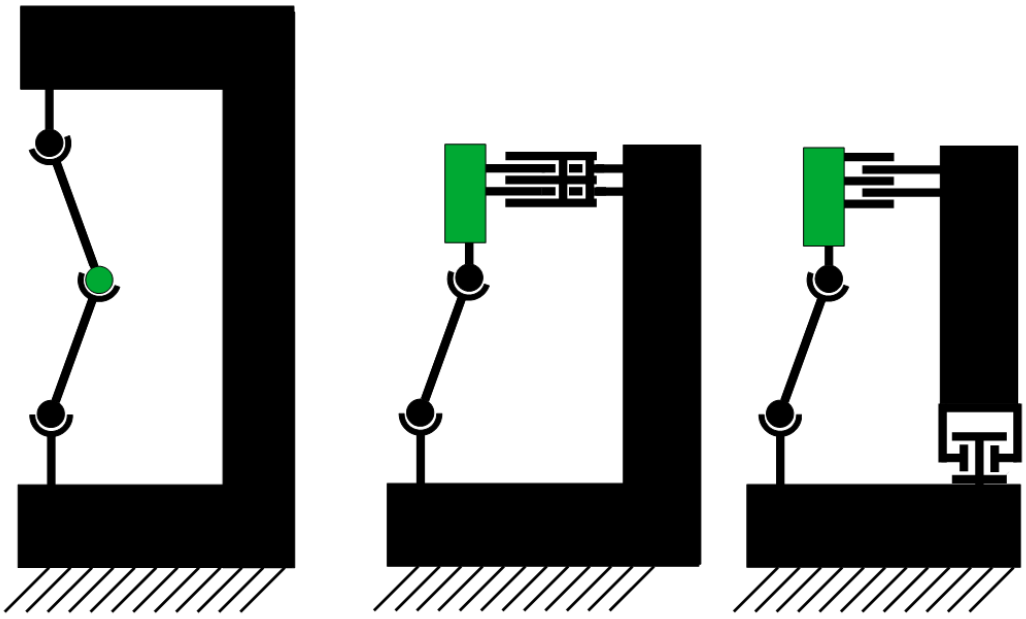

Figure D.2: The proposed input motion generator designs with the outputs shown in green.

The chosen solution is the design utilizing the three spherical joints as indicated on the left of the figure. This is because in this way, the (ultimately compliant) linkage is loaded in its stiffest direction, which makes sure the desired radius is generated. Also, this solution allows for easy connection of the rest of the mechanism to its output point, as only a frame has to connect the bottom and top, which leaves space for the other components on all of its sides.

D.2.2 Z transmission

For the design of the Z transmission several designs were considered as well. Four options were considered, fig. D.3 shows the final decision as presented earlier. One other variation was a design where the bars b_5 functioned as a parallel fourbar in the XY plane instead of the shown XZ plane. This could enable the generation of a perfect straight line when b_5 is of equal length as the radius r_{input}. This will however introduce a singularity point at α_1 = 90 and 270 degrees. Also, with the same dimensions, the stiffness in Z direction would be less than the presented design. For these reasons this design was not chosen, but it might be a promising option in case one is able to deal with the singularity points and accurately models the stiffnesses in the design. The third proposed variation incorporated spherical hinges replacing joints R_1 and R_2. Also, bars b_5 were omitted here, directly connecting R_2 with b_6. After several optimization attempts using the same algorithm as for the final design, it did not appear to be capable of delivering the desired results for generating a straight line during the stance phase. For this reason it was omitted. Another option was to not incorporate the parallel fourbar linkage constructed by b_5, but instead incorporate a prismatic joint. This option would result in a more complex physical design with the prismatic joints being replaced by Robert's linkages, as well as a lesser approximation of a straight line during stance.

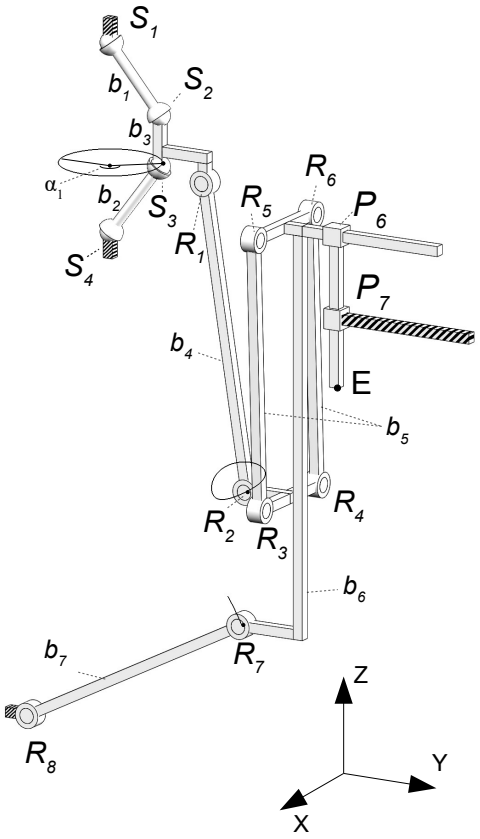

Figure D.3: The final Z transmission.

As stated earlier, the dimensions of the Z transmission were consecutively optimized. This was explained in chapter 3. In more detail, first a kinematic model was made of the Z transmission. This was done based on the concept of loop closure, stating that the sum of the vectors should be equal to zero, representing each bar by a vector. After applying this, together with the constraints of each bar, use was made of the Matlab symbolic toolbox to calculate the remaining unknowns. More specifically, a function was made which calculated the angles between b_5 and the X axis and between b_7 and the Y axis for each input angle of α_1. The variables $|b_4|, |b_5|, |b_7|, Z_{R_8}, Y_{R_8}$ were consecutively optimized such that b_6 would remain stationary over the course 135 < α_1 < 225 deg. This was done by discretizing a full rotation of α_1 into 41 steps and optimizing towards the earlier stated objective by making use of the *fmincon()* function in Matlab, implementing an SQP algorithm, the bounds and the constraints. After having reached a local minimum, the discretization of α_1 was increased to 201 steps to further improve the result. This finally delivered the values given in table D.1, with S_4 being taken as the origin.

	Length
$\|b_4\|$	60.54
$\|b_5\|$	54.05
$\|b_7\|$	52.70
Z_{R_8}	-(25.27 + $\|b_6\|$)
Y_{R_8}	-22.77

Table D.1: Final dimensions of the Z transmission.

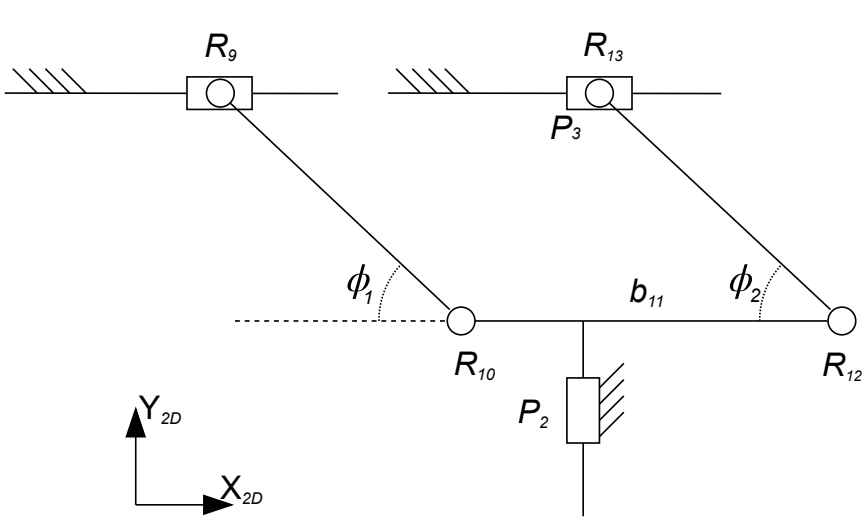

(a) Simplified drawing of part of X/Y transmission.

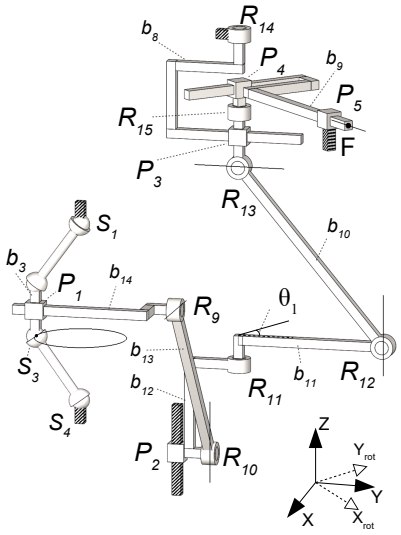

(b) Final X and Y transmission.

Figure D.4: X and Y transmission including a simplified 2D drawing.

D.2.3 X and Y transmission

For the X and Y transmission a single solution was proposed. This is the solution incorporated in the final design, as elaborated on earlier. This design directly transmits the X component of the IMG1 behaviour as will be shown with the help of fig. D.4a. Figure D.4b is added as a reference.

Effectively, when ignoring the rotational DOF of R_{11} and R_{14}, the system can be modelled as indicated in fig. D.4a. In the final design, the initial angles ϕ_1 and ϕ_2 were designed to be equal in the assembly position and $|b_{10}| = |b_{13}|$. This results in a direct coupling of the input motion at R_9 to R_{13}, resulting in a sinusoid curve at R_{13}, dependent on α_1 and r_{input}. In case one would like to modify the output paths in X and Y direction, one can modify this system.

D.2.4 Direction setpoint mechanism

Two designs for the direction setpoint mechanism were come up with. These are indicated in fig. D.5. Figure D.5a shows a version which makes use of prismatic as well as revolute joints. The green square here indicates the output point of the input motion generator, constraint in rotation. By rotating the input motion generator over its circular path, the revolute joints connected to the X and Y transmissions are moved to create the angle θ, as indicated. The connected prismatic joints decouple the undesired motions to leave a single dimensional reciprocating motion at the X and Y transmissions. In the design proposed in fig. D.5b, the motions are transferred by means of single beams, connected by revolute joints. This does not require the rotational constraint at the connection point with the input motion generator, but parasitic motions are introduced in the transmission of the input function to the X and Y transmissions. In the final design this last system was chosen for its simplicity.
Finally, this concept was transformed into the design of the direction setpoint mechanism as presented in fig. D.6. Here FB_4 and FB_3 link the X and Y transmissions of the different legs to reduce the complexity of the overall machine. FB_1 and FB_2 limit the rotation of b_{19} to make sure the position of G is properly transmitted.

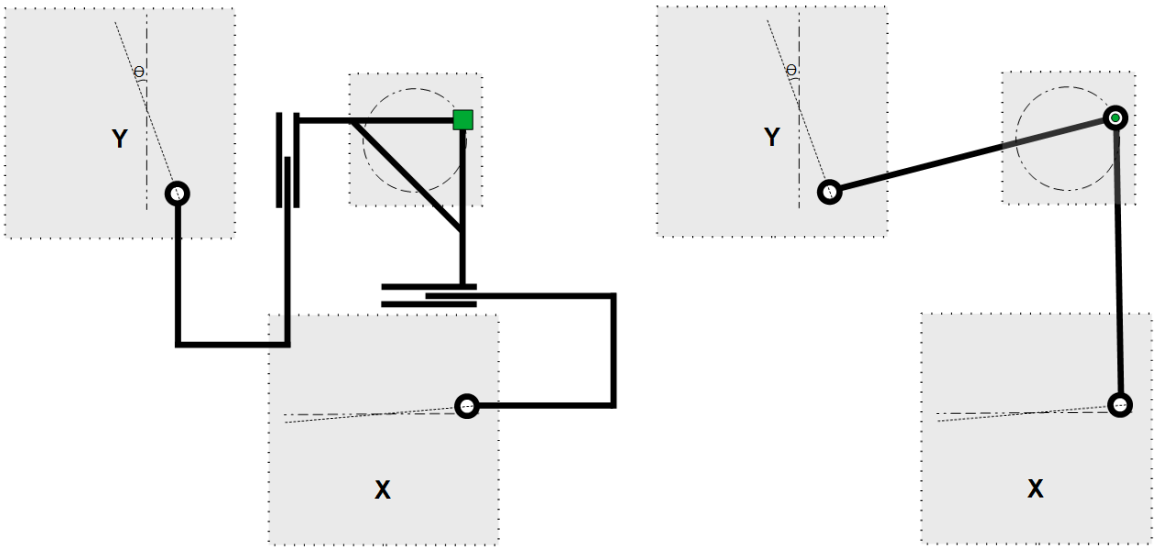

(a) Direction setpoint mechanism utilizing prismatic joints.

(b) Direction setpoint mechanism utilizing only revolute joints.

Figure D.5: The considered solutions for the direction setpoint mechanism.

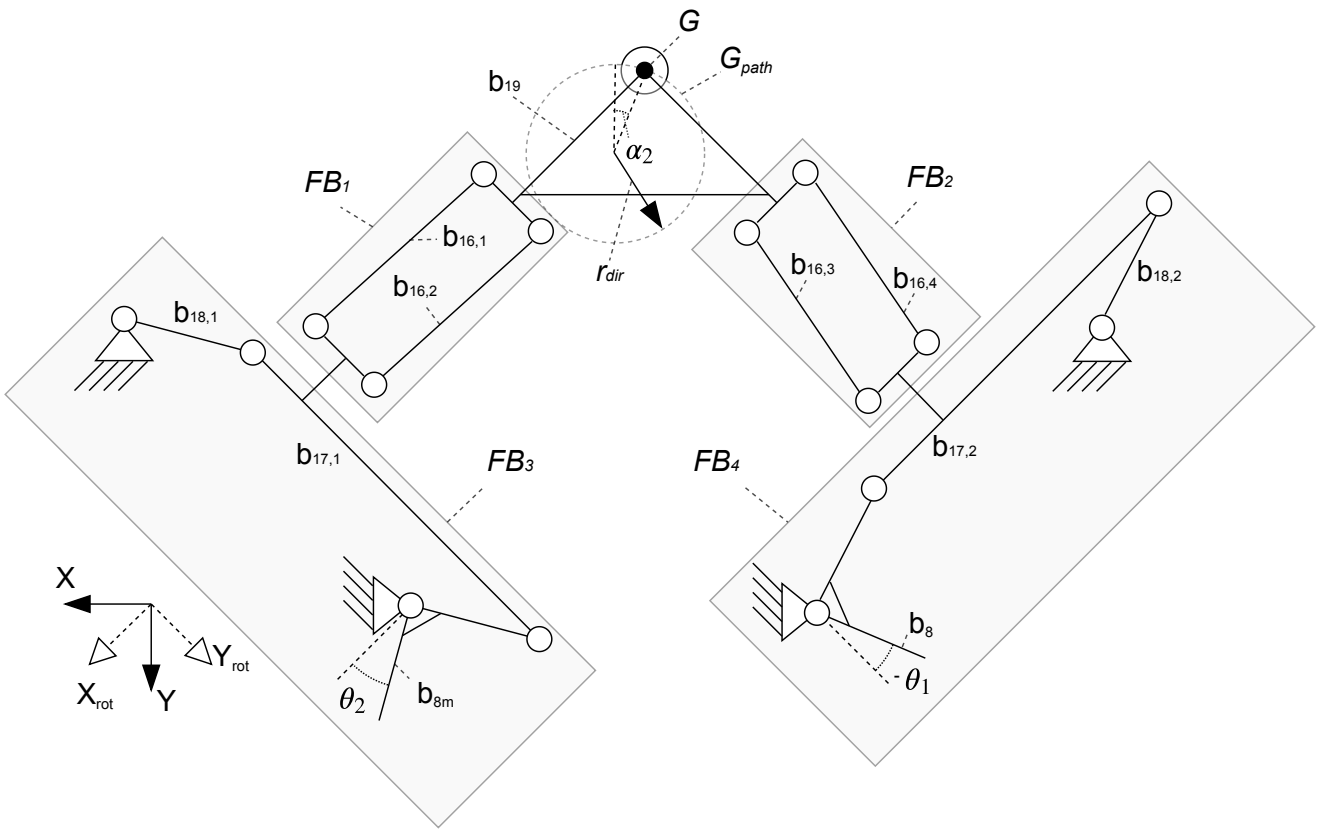

Figure D.6: Final direction setpoint mechanism.

D.2.5 Final kinematic design

Combining the previously gathered knowledge and choices into a single kinematic design finally delivered the result indicated in fig. D.7. For multiple views, see appendix G.1. Next to the 3D CAD model as indicated in this report, a mathematical design was also made and incorporated in the software package MATLAB. As with the Z transmission, this was also based upon loop closure of vectors with each vector representing a bar. A model of the direction setpoint mechanism was made, determining the angles θ_1 and θ_2. Knowing that the X and Y transmission directly transmit the X position of b_3 of IMG1, these were given as inputs to R_{13}, from which the X_{rot} and Y_{rot} coordinates of the end effector were directly calculated. The Z coordinate of the end effector was calculated by means of the earlier made model of the Z transmission. This produced the results as were presented in chapter 3.

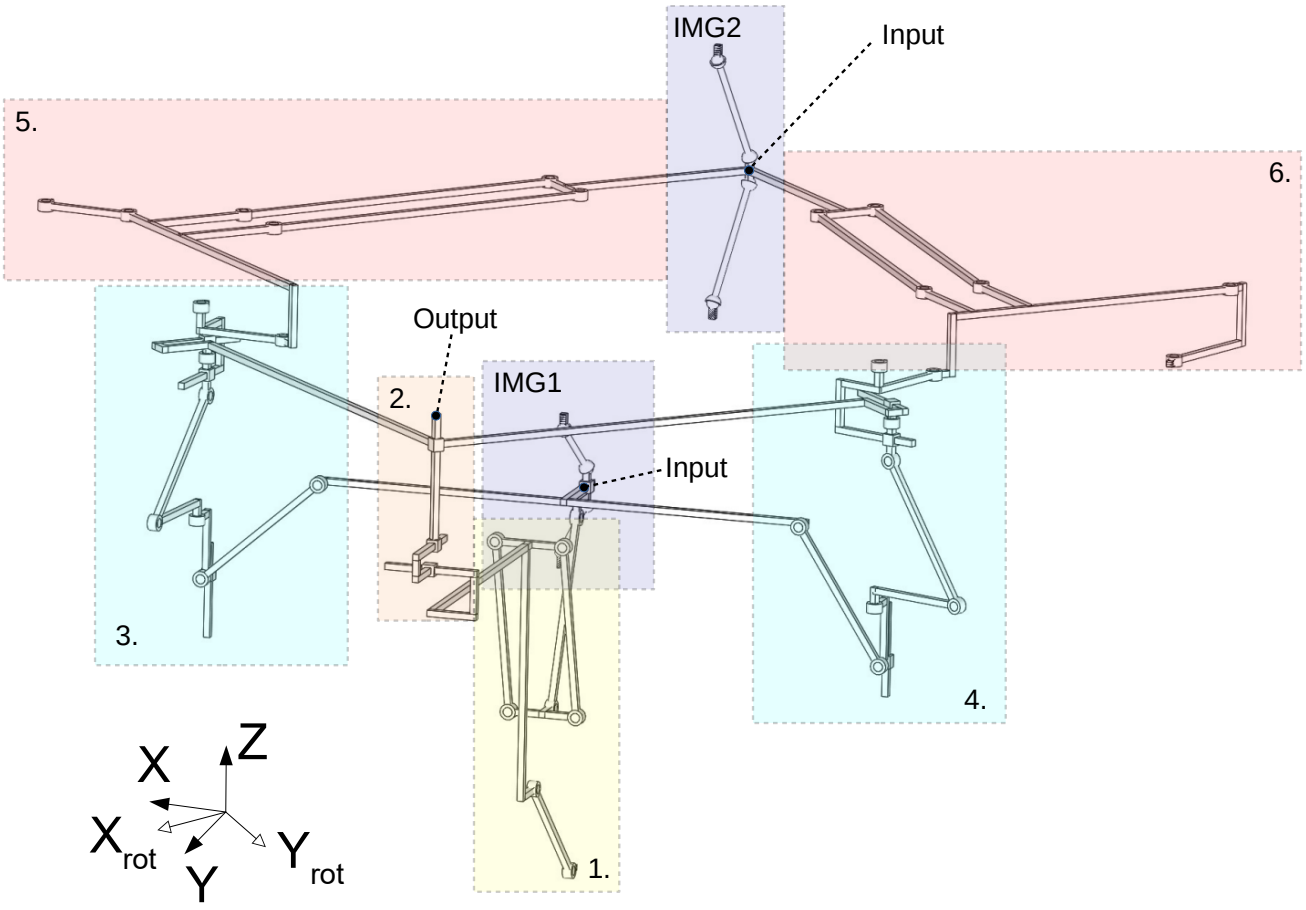

Figure D.7: View on the kinematic 3D CAD model.

Appendix E

physical design and production

E.1 Compliant transformation

The transformation of the kinematic design into a compliant design involved several aspects. The compliant joint types had to be chosen, as well as the materials and manufacturing process. Also, for the physical design to perform according to its kinematic model, the device had to be dimensioned properly. These aspects are discussed in the following appendix. Close-ups of the resulting 3D model are added in appendix G.2 as a reference.

E.1.1 Joint types

To go from a kinematic design to a compliant design, several choices had to be made. The first of which was considered to be the type of compliant joints used. In comparing distributed compliance hinges with their concentrated counterpart, the concentrated compliance was chosen. This provided closely comparable performance with the purely kinematic versions of the joints, therefore little analysis in the performance of the compliant hinges would be needed. The three main joints making up the system, spherical, revolute and prismatic joints each had to have a compliant version. The compliant hinges indicated in [88] were considered and for the revolute joints a circular notch flexure was chosen for its simplicity and low contribution to stress concentrations. For the spherical hinges, a three axis flexure joint was chosen for its simplicity as well. For the prismatic joints, none of the indicated translational joints was chosen, instead it was chosen to convert a conventional Roberts linkage straight line mechanism into a compliant version. This choice was based upon the following criteria, and was between the mechanisms indicated in table E.1, where each single mechanism is graded.

- **Links**

  The amount of links of the system, as an indicator of complexity. The more links, the more complex the system.

- **Mobility**

  The degree of mobility as calculated by the Chebychev–Grübler–Kutzbach criterion.

$$M = 6(N - 1 - J) + \sum_{i=1}^{J} F_i \tag{E.1}$$

  Here, M is the mobility, N the number of links, J the number of joints and F the DOFs allowed by the joints.

- **Straight line**

  To what extend a straight line is produced. A '-' for mechanisms which do not follow a straight line, a '+-' for mechanisms which approximate a straight line. and a '+'sign for mechanisms producing a perfect straight line.

- **Accessibility**

  How well the mechanism can be connected to other parts in the system. Here, '-' indicates a mechanism which limits connectivity in more than one quadrant around its generated line. A '+' indicates accessibility from the three quadrants around the described line.

- **Planar**

  If the mechanism can be made in a planar sense. A '-' is given to systems which need out of plane components. A '+' is given to systems which can be fabricated in a planar fashion.

- **Rotational constraint**

  If the mechanism introduces a rotational constraint. A '-' for systems which do not, a '+' for systems which do. This indicates if an extra mechanism would be needed to constrain this rotation, making the system more complex.

	Links	Mobility	Straight line	Accessibility	Planar	Rotational constraint
Four-bar-notch block [88]	4	1	-	+	+	+
Double notch block [88]	7	2	+	+	+	+
Symmetrical double notch block[88]	12	1	+	-	+	+
Sarrus's	6	1 (0)	+	-	-	+
Peaucellier-Lipkin's (1) [72]	8	1	+	+	+	-
Peaucellier-Lipkin's (2)	8	1	+	+	+	-
Chebyshev's [72]	4	1	+-	+	-	-
Robert's [72]	4	1	+-	+	+	-
Watt's [72]	4	1	+-	-	+	-
Chebyshev's lambda [72]	4	1	+-	+	+	-
Kempe's (quadruplanar inversor)	6	1	+	+	-	-
Hart's inversor (1)	6	1	+	+	-	-
Hart's inversor (2)	6	1	+	+	+	-

Table E.1: Overview of the options for replacing conventional joints and their grading.

The (0) behind the Sarrus's linkage indicates the by the Grübler calculated mobility, but since this is a special case, the real mobility of the linkage is 1. The (1) and (2) behind the Peaucellier-Lipkin's and Hart's inversor indicate the two variants of the systems. From this table the Robert's and Chebyshev's lambda mechanism come forward as preferable mechanisms. The Robert's linkage was finally chosen for its symmetry and high stiffness perpendicular to the described straight line. For constraining the rotational DOF, two of the Robert's linkages were coupled with their paths positioned in a co-linear fashion.

E.2 Materials and manufacturing

To create the physical prototype of the design, choices had to be made concerning the materials and production processes. As indicated in appendix A, the design is meant to be produced in a monolithic fashion. The decision was made to produce the first physical model in a modular fashion nevertheless, because this supports easy replacement of parts in case of failure. Also, in this way the prototype could be produced by means of a FDM (Fused Deposition Modeling) 3D printer process, which is relatively inexpensive, was readily available and supports multi material printing. To limit the extent of analysis needed concerning the dimensioning of the joints and their induced stiffnesses, two materials with a significantly different stiffness were utilized. The lower stiffness material was used for the joints and the higher stiffness material for the links. This ensured a low stiffness in the transmission, without extensive dimensional analysis. The used materials were PLA (polylactic Acid) and a thermoelastic polymer with a significantly lower stiffness.

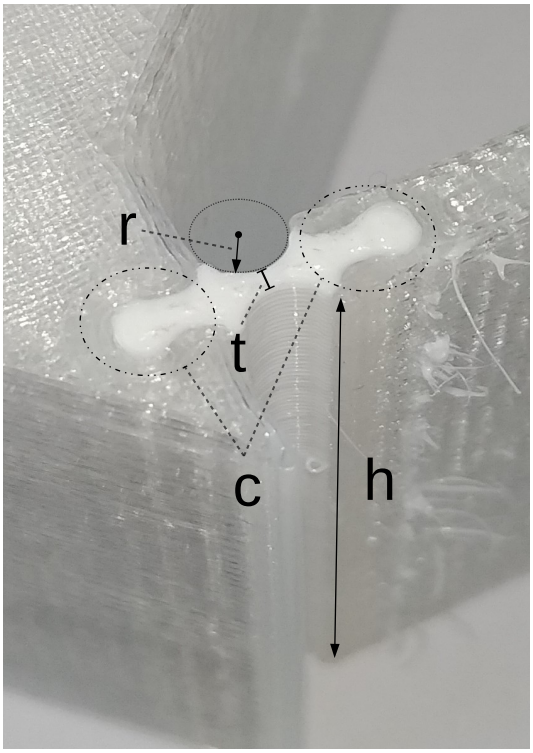

Figure E.1: Picture showing the connection between flexible and stiff material.

Knowing that the deposition of the material in this specific printing process has a directional influence on the strength of the parts, all components were printed with the axes of the revolute joints out of plane with respect to the build plate. Figure E.1 indicates this, one can clearly distinguish the printed layers. Furthermore, several iterations showed that a geometric connection between the two materials was needed to prevent the materials from separating. The designed connections are indicated with at c in the figure.

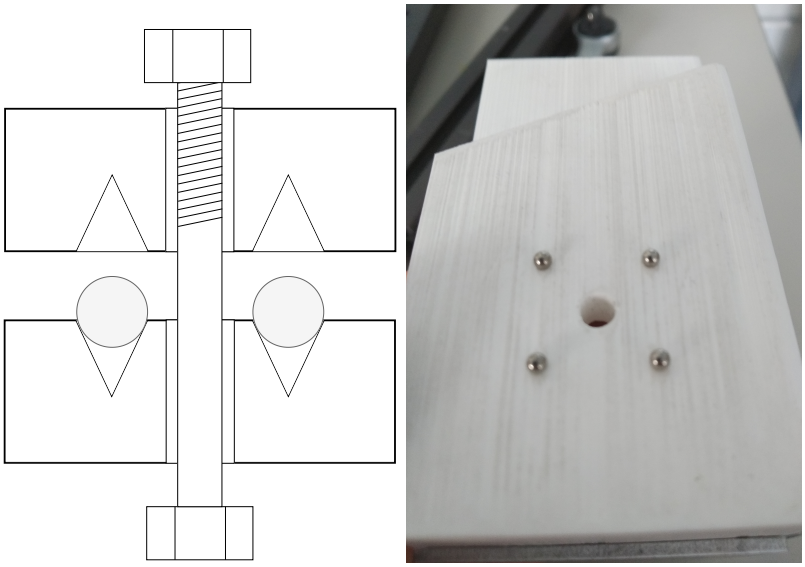

(a) A graphical indication of the used connections, showing a cross section of the two components, bolt, nut and balls.

(b) A connection between the 3D printed components, showing the bolthole and steel balls for centring.

Figure E.2: Examples of connection between parts.

To make sure the parts were connected in a dismountable fashion, a bolt and nut combination was used to connect the components. By making use of steel balls placed in printed conical cups centered around the bolthole, the printed components were ensured to be in the correct position with respect to one another. Figures E.2a and E.2b give a schematic representation of these connections and a picture of one of the components including the steel balls in the cups. Since the resulting dimensions of the printed cups tended to vary depending on the orientation of the connections with respect to the build plate of the printer, different diameter balls were used. These were chosen such to be slightly oversized compared to the cups to ensure contact within the cups, while simultaneously being small enough to ensure connection between the 3D printed parts after tensioning of the bolt. In general, three balls were used in the connections, for the end effector shown in fig. E.2b four balls were used.

E.3 Dimensioning

The printing process introduced dimensional constraints. After a couple of test runs, it was determined that the minimal thickness (t) of the hinges should be set at 0.8 mm for a reliable printing process, see fig. E.1. For the radius (r), a dimension of 1.75 mm was set. This ensured a large enough radius for the two links not to contact during operation as well as not being merged during the printing process. Furthermore, it was deemed small enough to provide enough stiffness in the desired directions. Concerning the overall dimensioning of the model, the input radius of IMG1 and IMG2 were set at 10 and 20 mm respectively. This was chosen such to provide large enough displacements of the end effector to be enable proper measurements. Furthermore, as this amount of displacement is properly visible with the naked eye, it provides visual feedback on the functioning of the system profitable for the analysis of its behaviour. The radii were chosen not to be much larger to limit the overall size of the system. From this basis, the dimensions of the rest of the components were determined. Concerning the dimensioning of the Robert's linkages this meant that the allowed displacement would be large enough for the links not to collide. Also, to reduce the stiffness in the transmission of the displacements, the lengths of the links of the Robert's linkages were increased until the full component reached the maximum dimensions of the build plate of the printer (197x215 mm). Effectively, this increases the moment arms of the Robert's linkages and thus reduces the stiffness in transmission direction. An added benefit is that it improves the performance of the linkage in the approximation of a straight line.
Depending on the loads on the subcomponents, their heights (h) were dimensioned accordingly. Since the design of the overall walking machine is such that each leg is meant to be able to support the entire machine, the heights of the components in the motion coupling mechanism were the largest with a maximum of 55mm. Since the steering mechanism was designed to be under the least amount of load, a height of 20 mm was deemed appropriate.

E.4 Assembly

Several images at different points in time during the assembly process are displayed in table E.2 to give a view on the process.

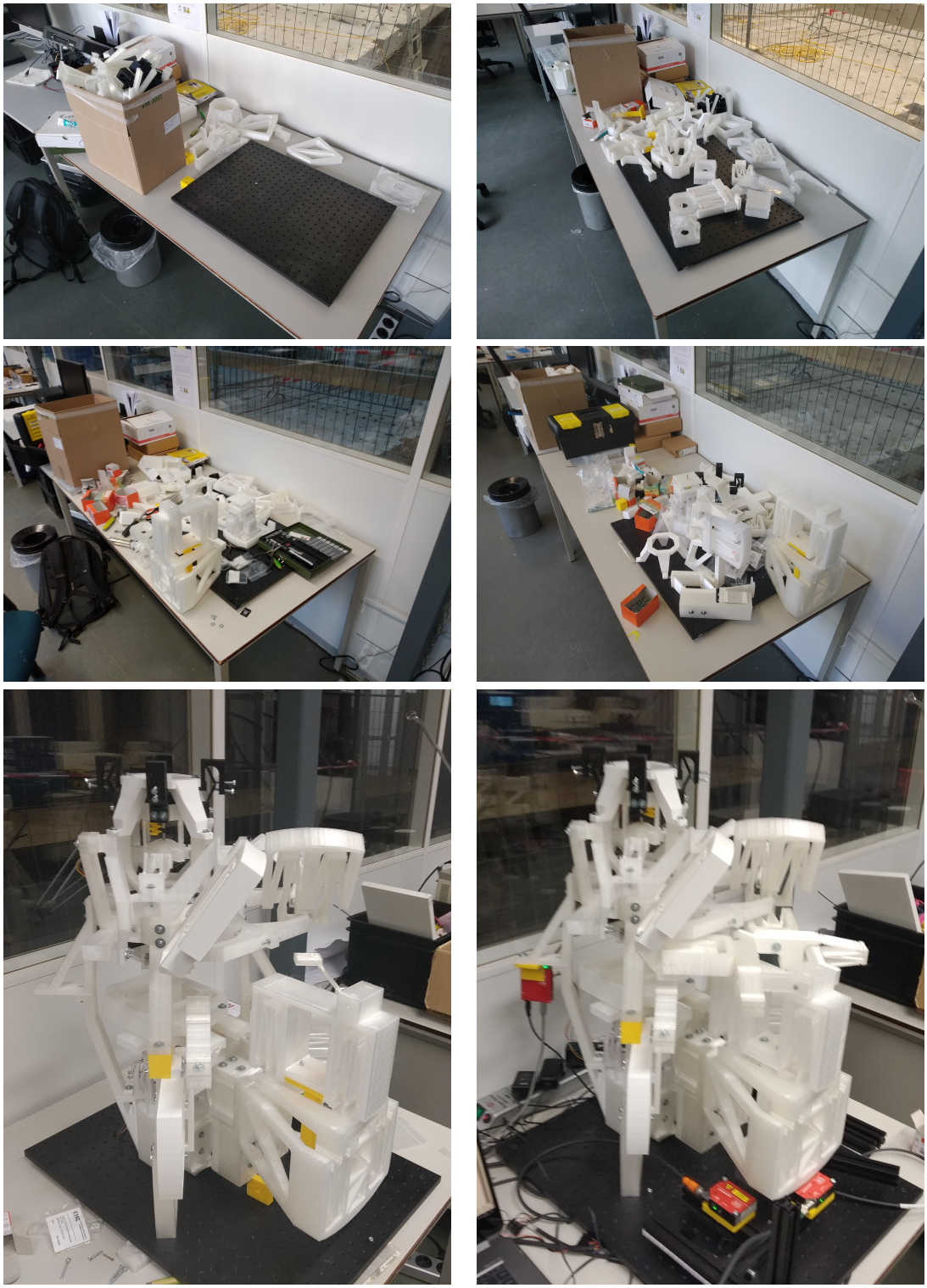

Table E.2: Pictures at different stages of the assembly process.

Appendix F

Measurement

F.1 Measurement procedure

The measurement setup is schematically described in fig. F.1. Every 3 seconds, a command was sent from the computer to the motor control system to increment the motor actuating IMG1 by a step of 7.2 degrees, resulting in a discretization of the full rotation into 50 steps. Every 50 steps, the stepper motor actuating IMG2 was incremented by the same amount. The motor control system consecutively powered the stepper motors, resulting in an increase in the angles α_1 and α_2 in the mechanism. With this change, a change in respectively the propulsion and angle β was generated. This new position was then recorded just before the computer sent the new command to increment. This happened through the system of sensors and the data acquisition system converting the values to computer readable format.
In more detail, the test protocol was made up out of the following steps.

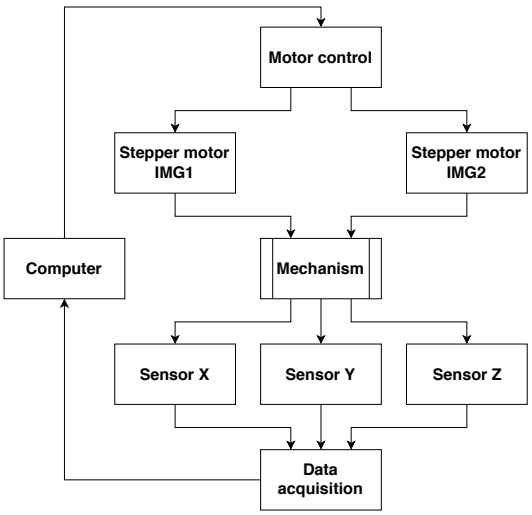

Figure F.1: Schematic of the measurement setup.

1. Set input angles α_1 and α_2 to their desired starting values manually
2. Power on stepper motors, fixing them in place
3. Verify and log the starting position of α_1 and α_2
4. Start automated measurement procedure
   (a) Record data
   (b) Increment α_1 by 7.2 degrees
   (c) Wait 3 seconds
   (d) If taken α_1 steps < 50 go to step 4a
      i. Increment α_1 by 7.2 degrees
      ii. If taken α_2 steps < 50 go to step 4a
   (e) End automated measurement procedure
5. Verify and log end position of α_1 and α_2

After having performed the above mentioned procedures five times, the data was analyzed. The results are presented in chapter 3. Next to the quantitative measurements of the displacements of the end effector, several time-lapse movies of the moving system were made as well. This provided a qualitative indication the behaviour of the subcomponents. The same actuation procedure as during the quantitative measurements was performed, except for the time delay, this was reduced to 2 seconds. A picture was taken after every increment and these were later merged into a time-lapse video providing insights in the overall behaviour of the system. The pictures were taken from multiple points of view to cover the entire machine.

F.2 Measurement setup

An overview of the test setup is given in fig. F.2. This shows the LabVIEW program running on the computer on the left, performing the automated measurement procedure. In the center the power supply for the motors and motor driver is situated, with on the right the mechanism and the laser triangulation displacement sensors attached to the base of the mechanism. A close up on the sensors is shown in fig. F.4, where the flattened aluminium measurement surfaces are also shown. These were glued onto the end effector to make sure the measurements were not influenced by the surface roughness of the 3D printed end effector. Furthermore, fig. F.2 also shows the vibration isolation table on which the device was measured. This was done to limit the disturbances due to vibrations. For the same reason, the measurement protocol had incorporated a 3 second delay between the displacement of the end effector and the measurement.
Figure F.3b shows a close up on the motor driver system. This board is an Arduino based CNC platform, the computer sent the information in the form of Gcode to the board, which transformed it into the rotation of the motors. The laser sensors were the optoNCDT ILD 1302-20 with a measurement resolution of 4μm for the X and Y direction, and the optoNCDT ILD1420-10 with a resolution of 0.5 μm for the Z direction. The angle α_2 was

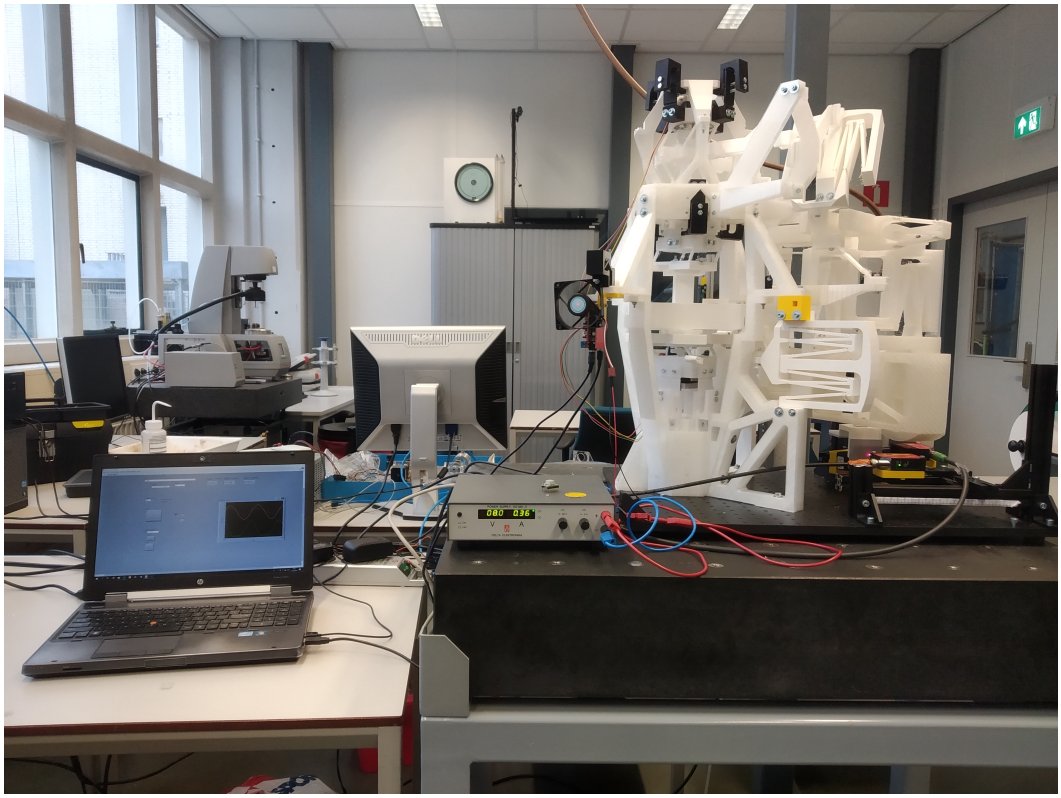

Figure F.2: Overview of the measurement setup.

measured at the start and endpoint of the measurement cycle by means of a pointer and protractor as indicated in fig. F.5. The angle α_1 was measured by measuring the distance of a similar pointer with respect to a fixed position of the frame by means of a caliper.

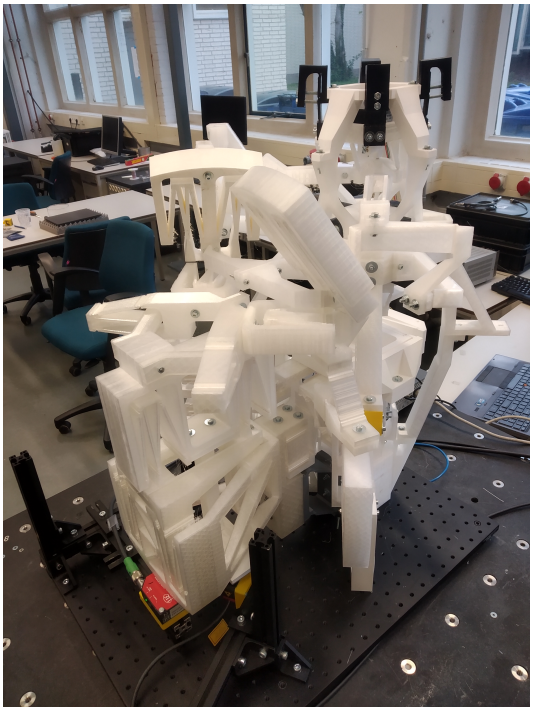

(a) Perspective view on the mechanism with sensors attached.

(b) Close up on the motor driver.

Figure F.3: Mechanism under testing and the motor driver.

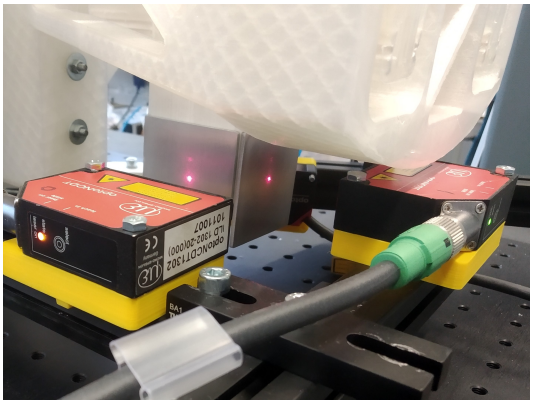

(a) Close up on the X and Y sensors.

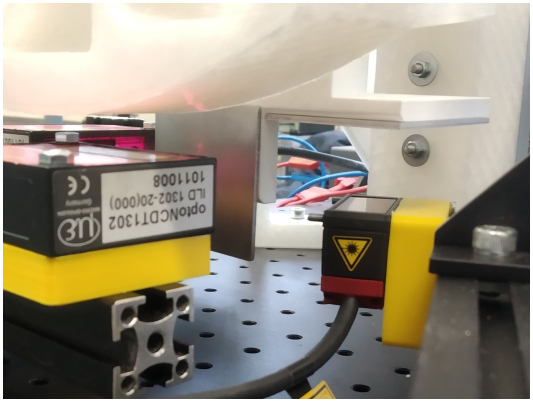

(b) Close up on the Y and Z sensors.

Figure F.4: Close up on the laser triangulation sensors.

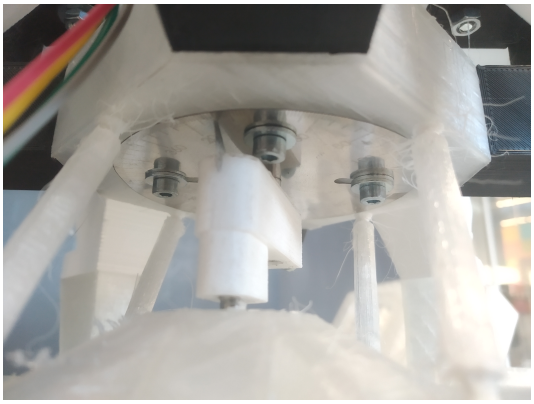

Figure F.5: Protractor for measuring α_2

Appendix G

Additional figures

G.1 Kinematic model

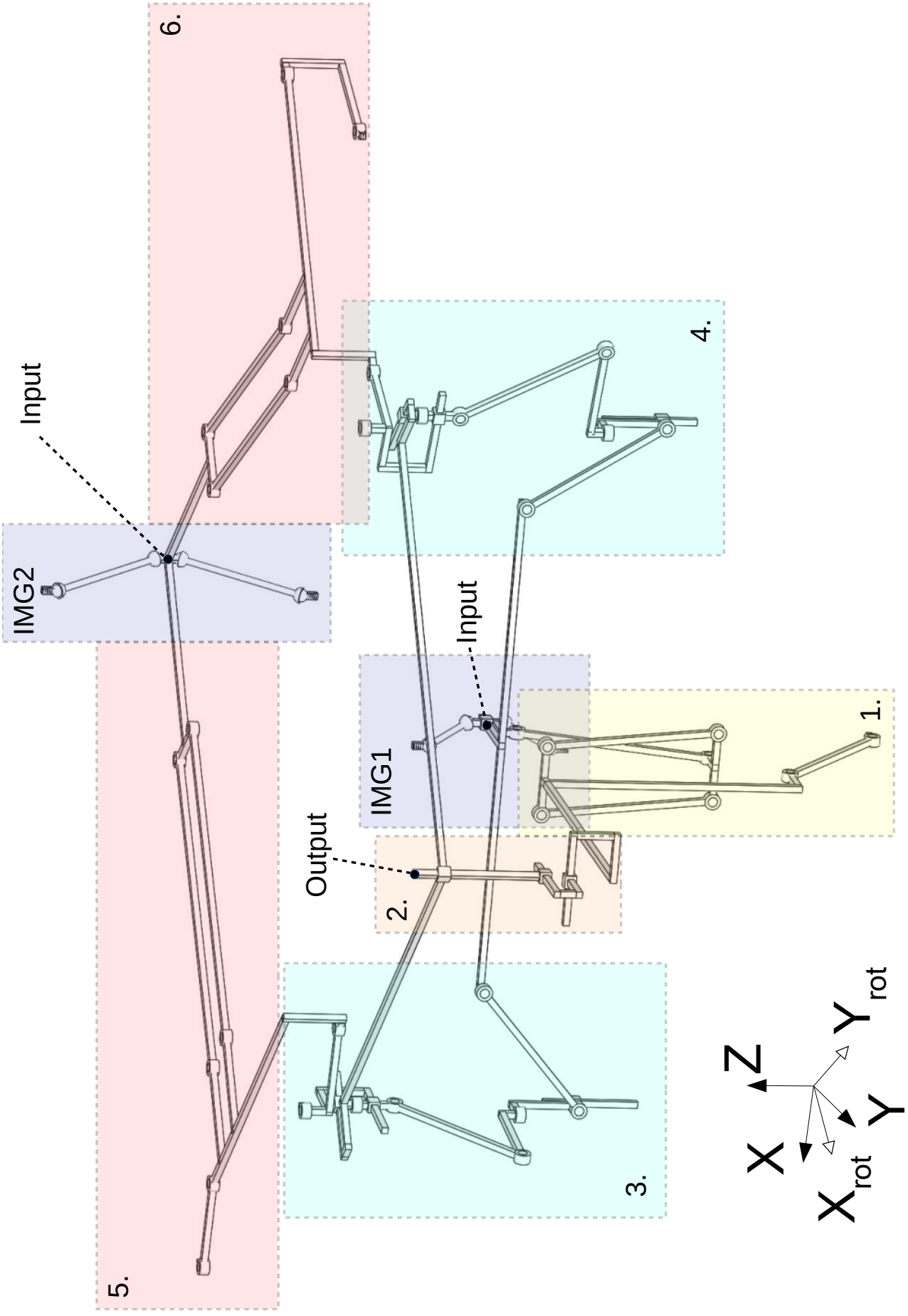

Figure G.1: View on overall kinematic model: (1.) Z transmission, (2.) Motion coupling mechanism, (3.) Y_{rot} transmission, (4.) X_{rot} transmission, (5.&6.) Direction setpoint mechanism.

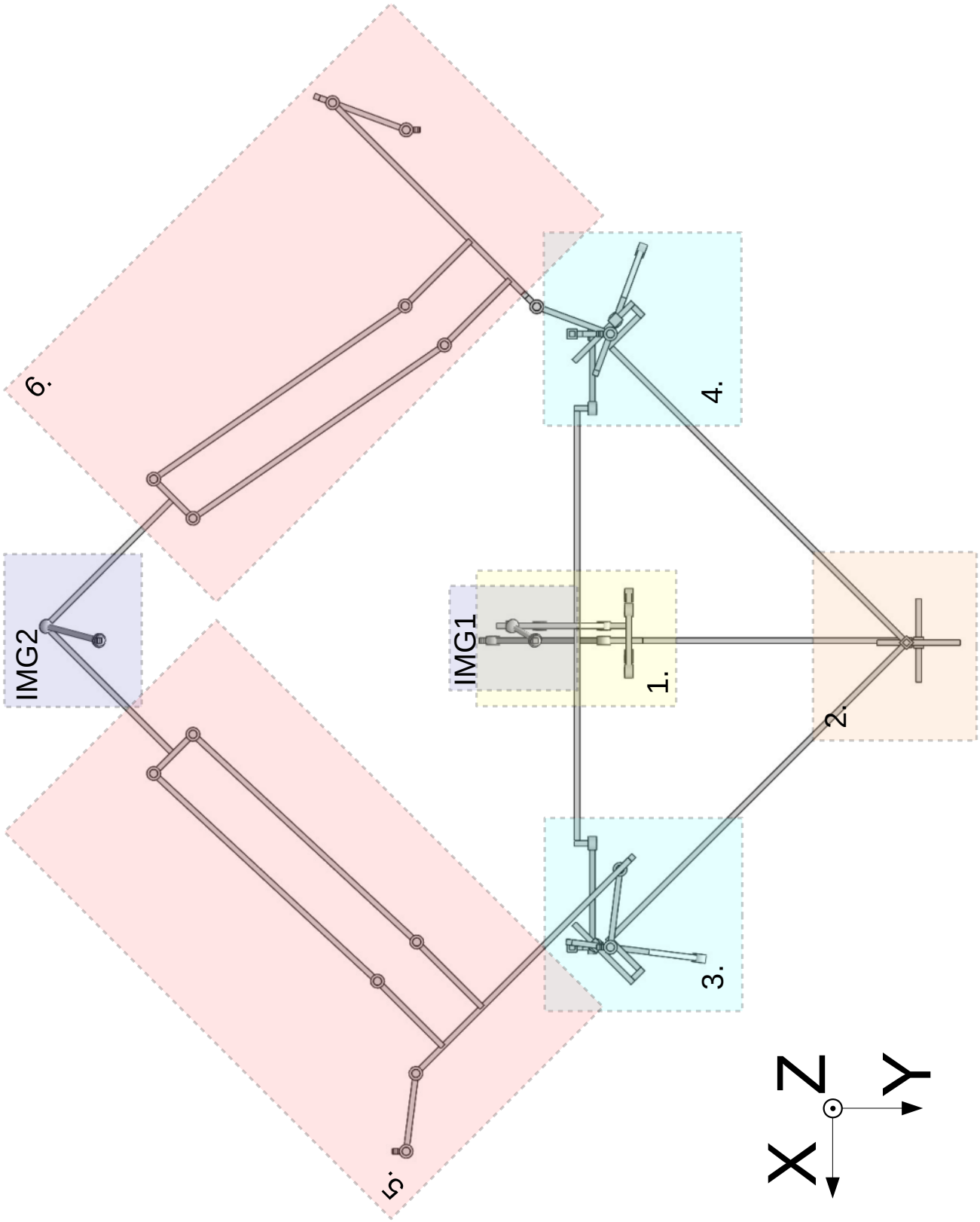

Figure G.2: Top view of the kinematic CAD model of the final design: (1.) Z transmission, (2.) Motion coupling mechanism, (3.) Y_{rot} transmission, (4.) X_{rot} transmission, (5.&6.) Direction setpoint mechanism.

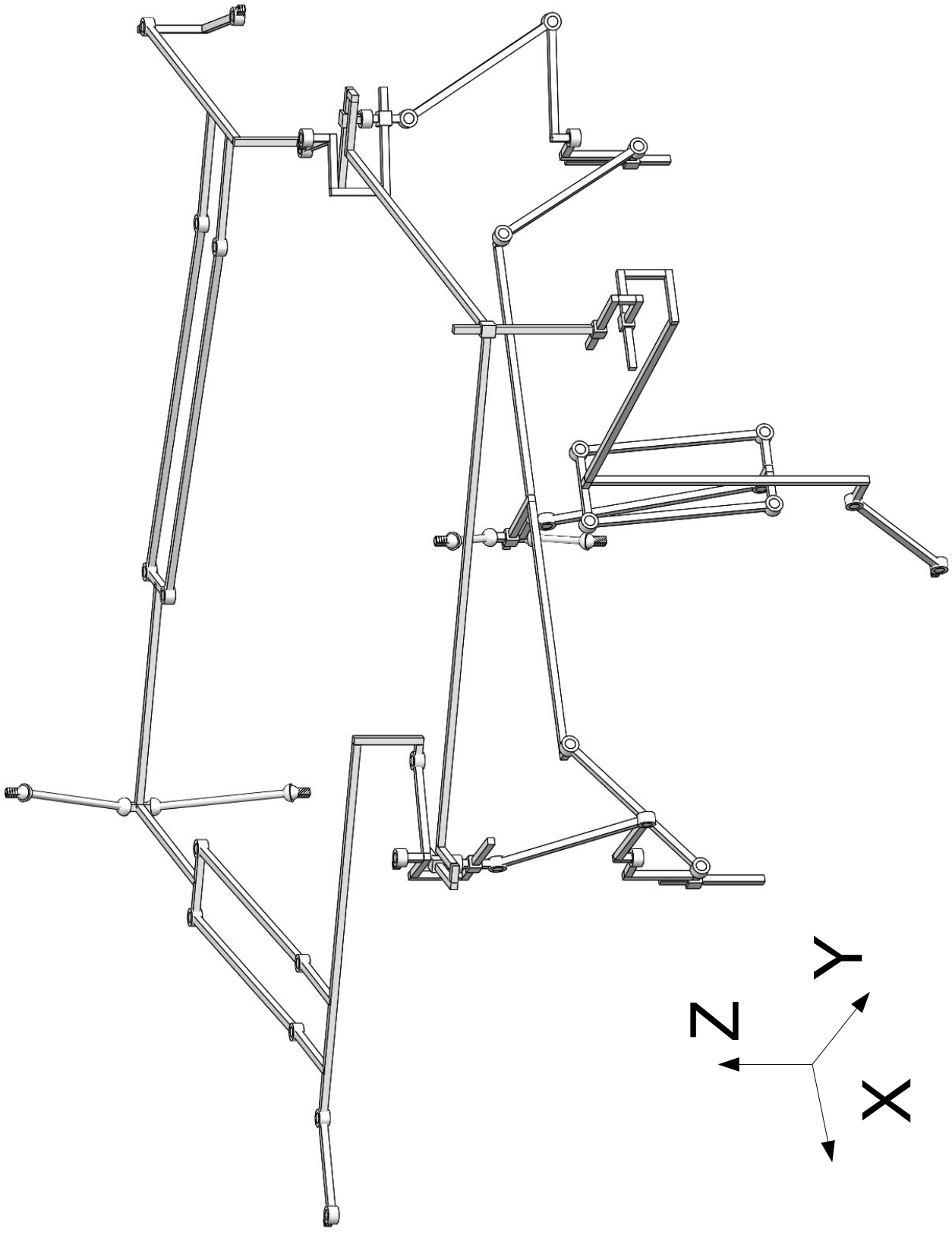

Figure G.3: 3D view of the kinematic CAD model of the final design.

G.2 Physical model

G.2.1 Views on 3D model

As a reference, the following figures provide close-ups on the resulting 3D model of the system as explained and shown in chapter 3. The subcomponents are indicated with their according colour as stated in table G.1.

	Colour
Sarrus Linkages	Green
Input motion generators	Purple
X and Y transmission	Blue
Z transmission	Yellow
Direction setpoint mechanism	Red
Motion coupling mechanism	Orange
End effector	Pink
Frame	Grey

Table G.1: Legend of colours.

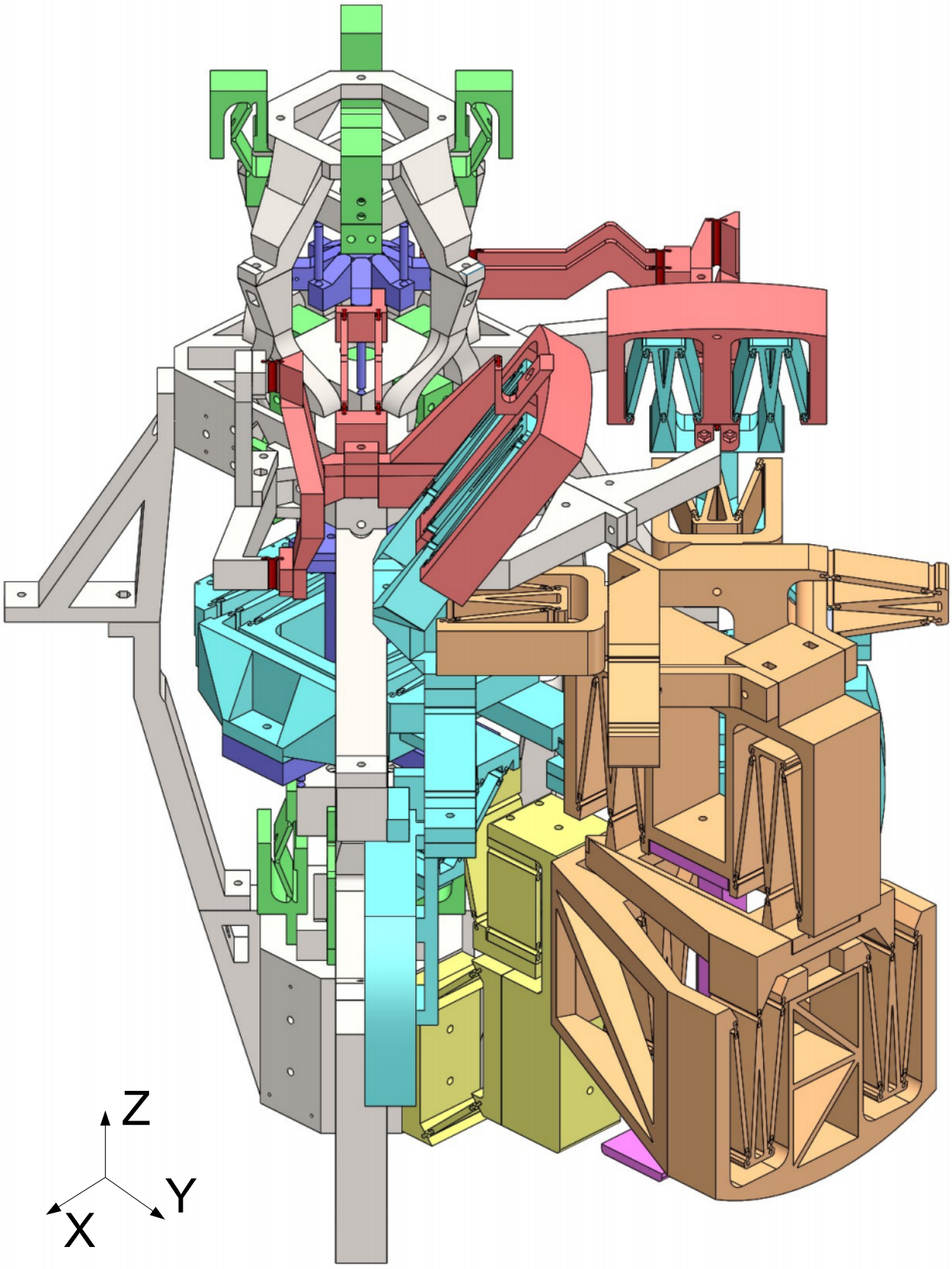

Figure G.4: 3D view of the CAD model of the final design.

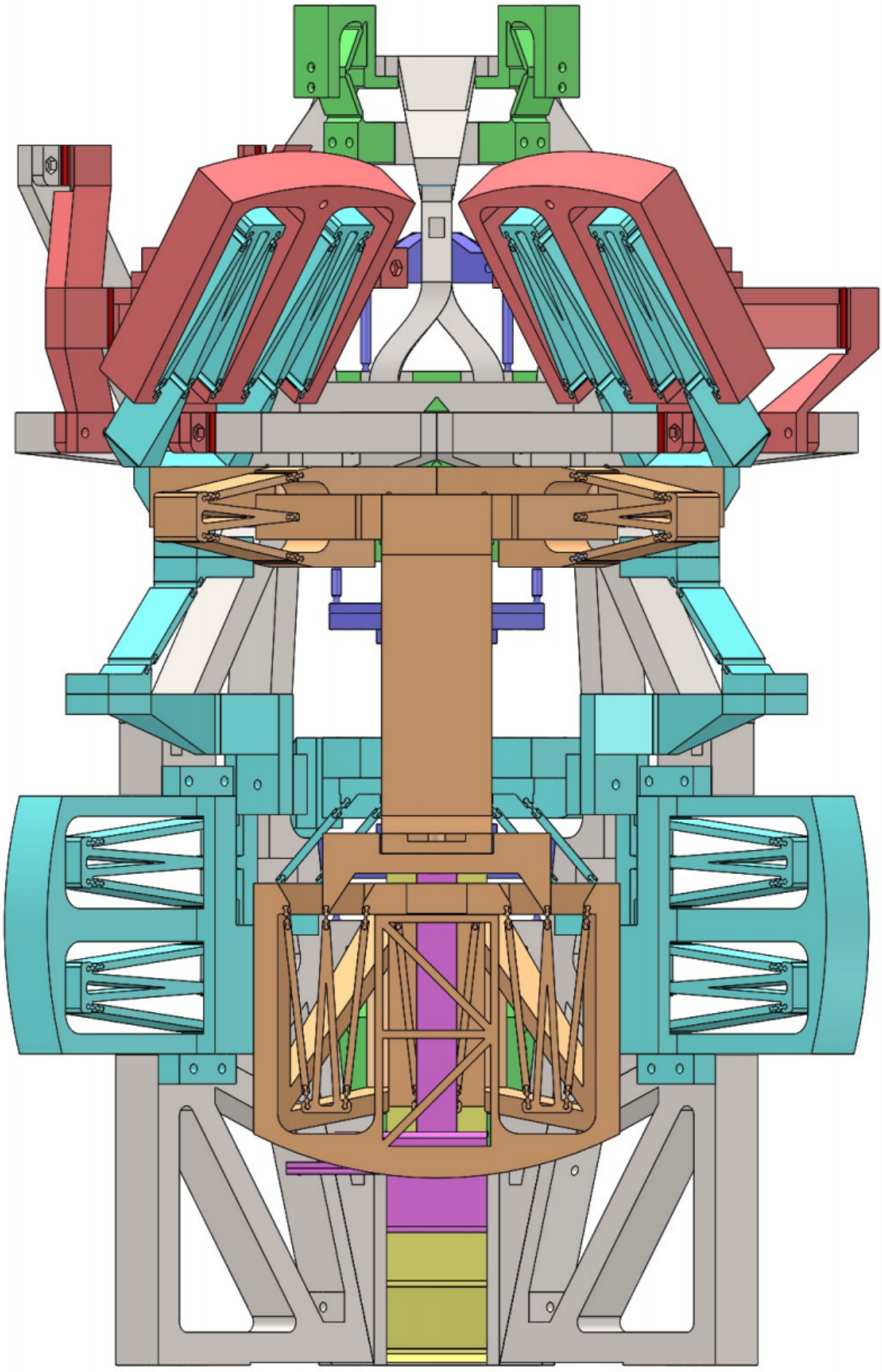

Figure G.5: Front view of the CAD model of the final design.

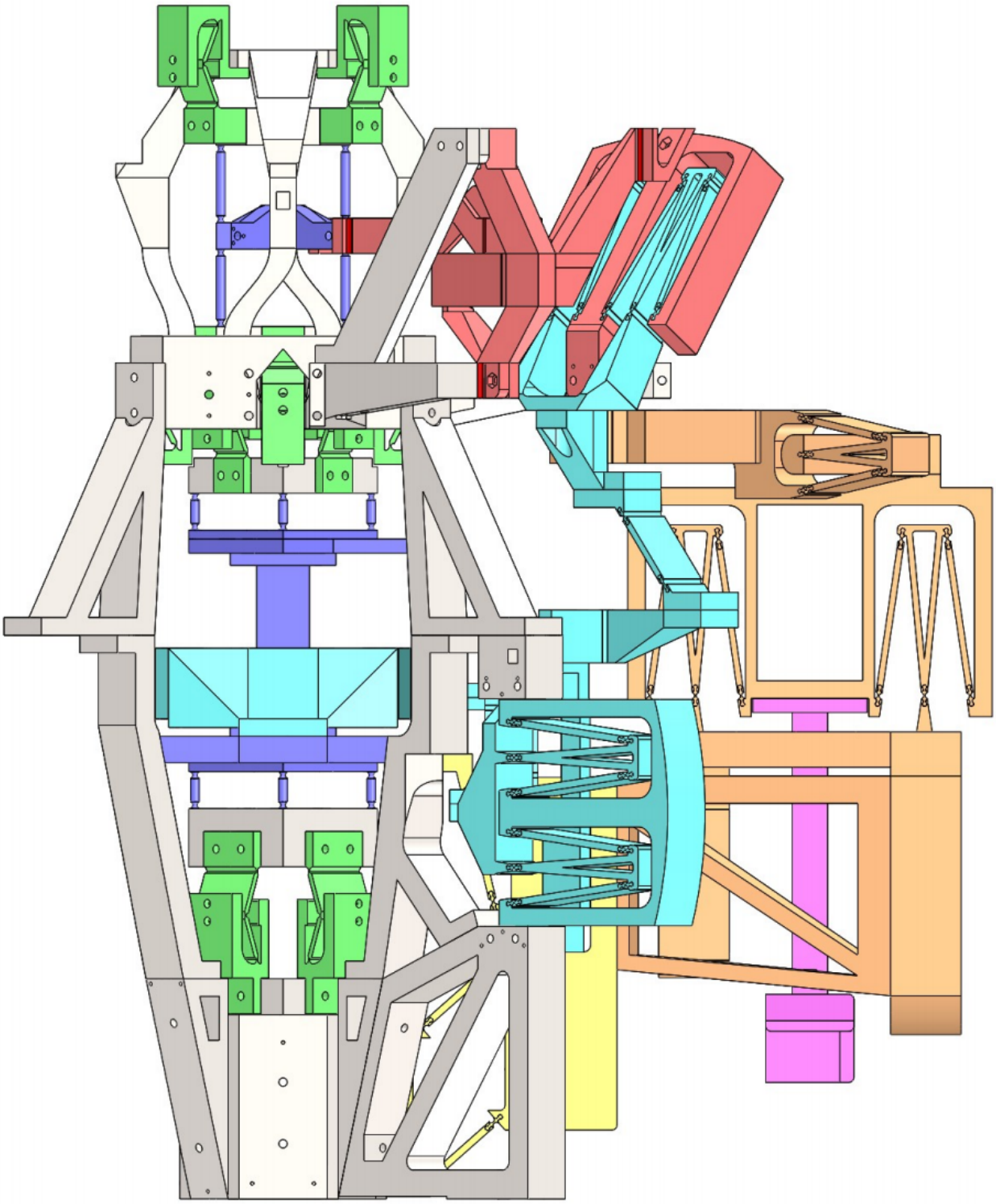

Figure G.6: Side view of the CAD model of the final design.

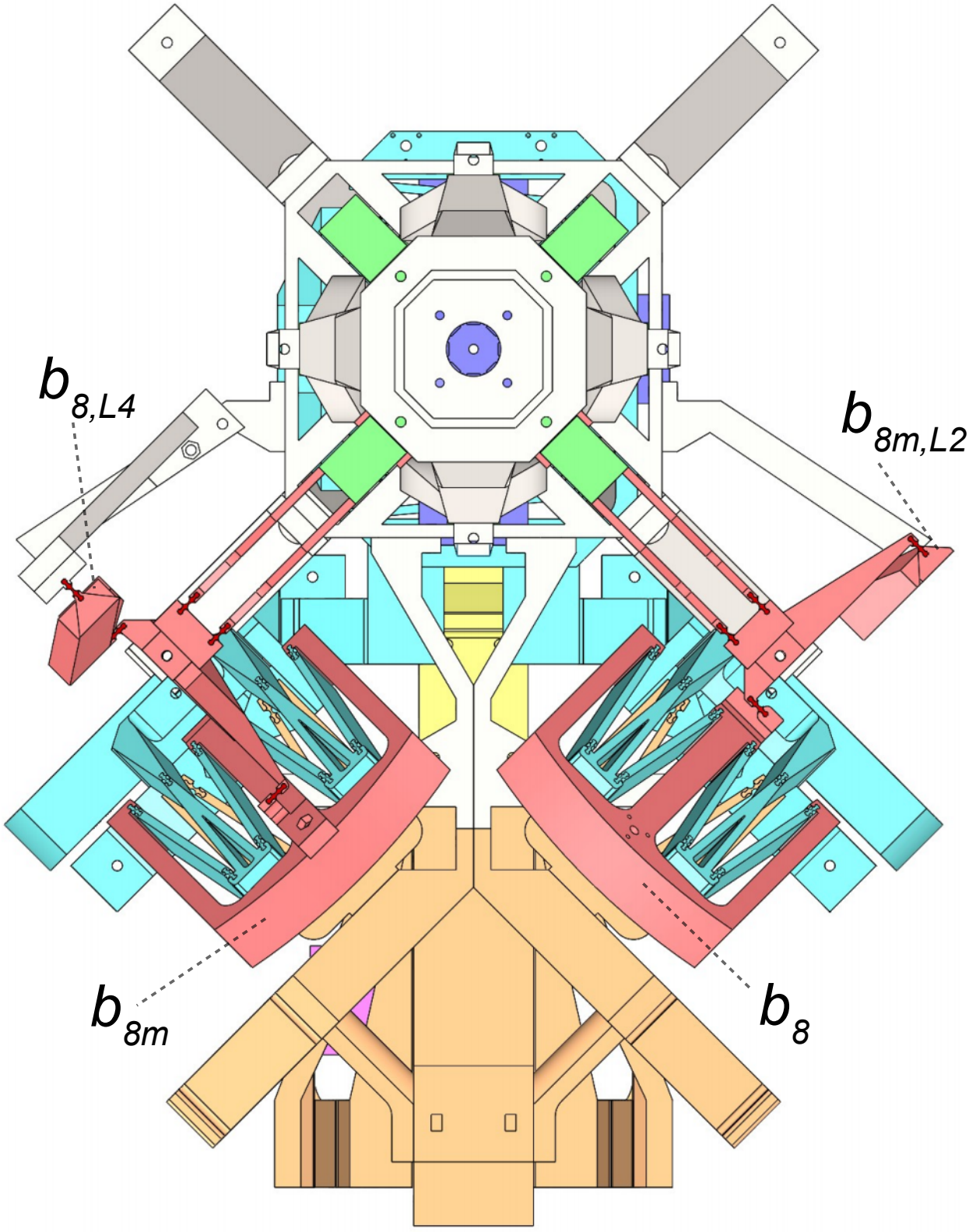

Figure G.7: Top view of the CAD model of the final design.

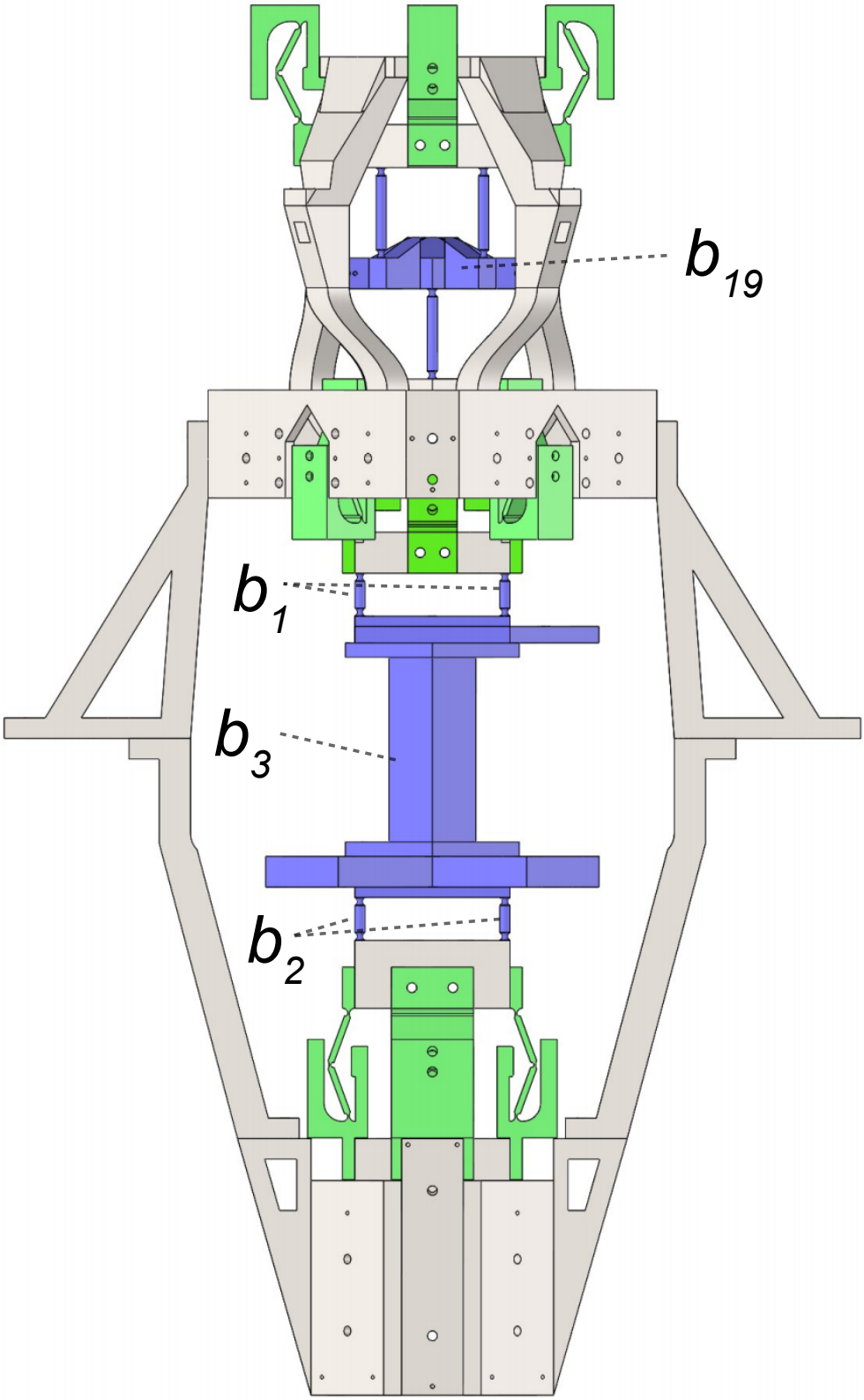

Figure G.8: Input motion generators and sarrus linkages of the final design.

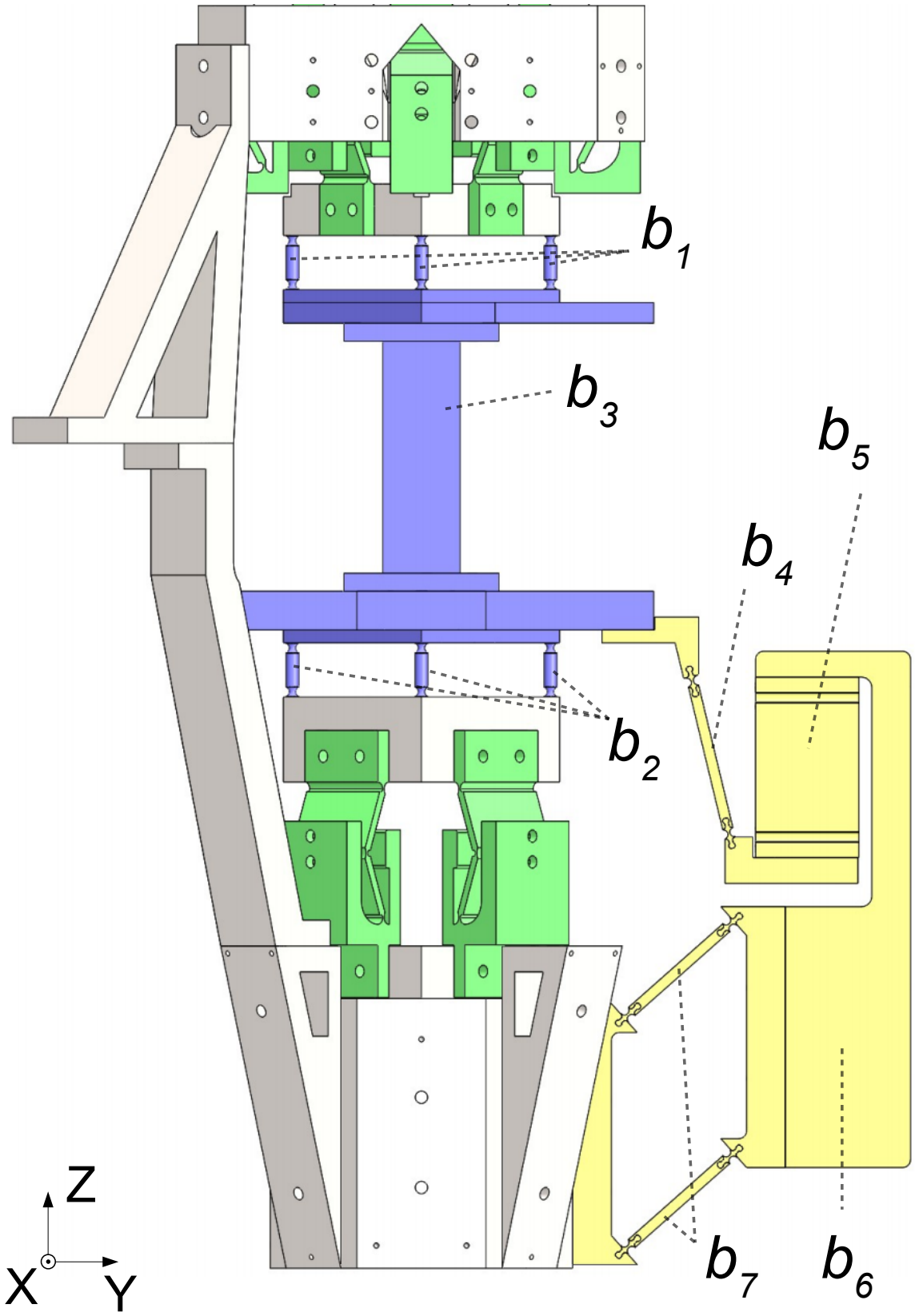

Figure G.9: Z transmission of the final design.

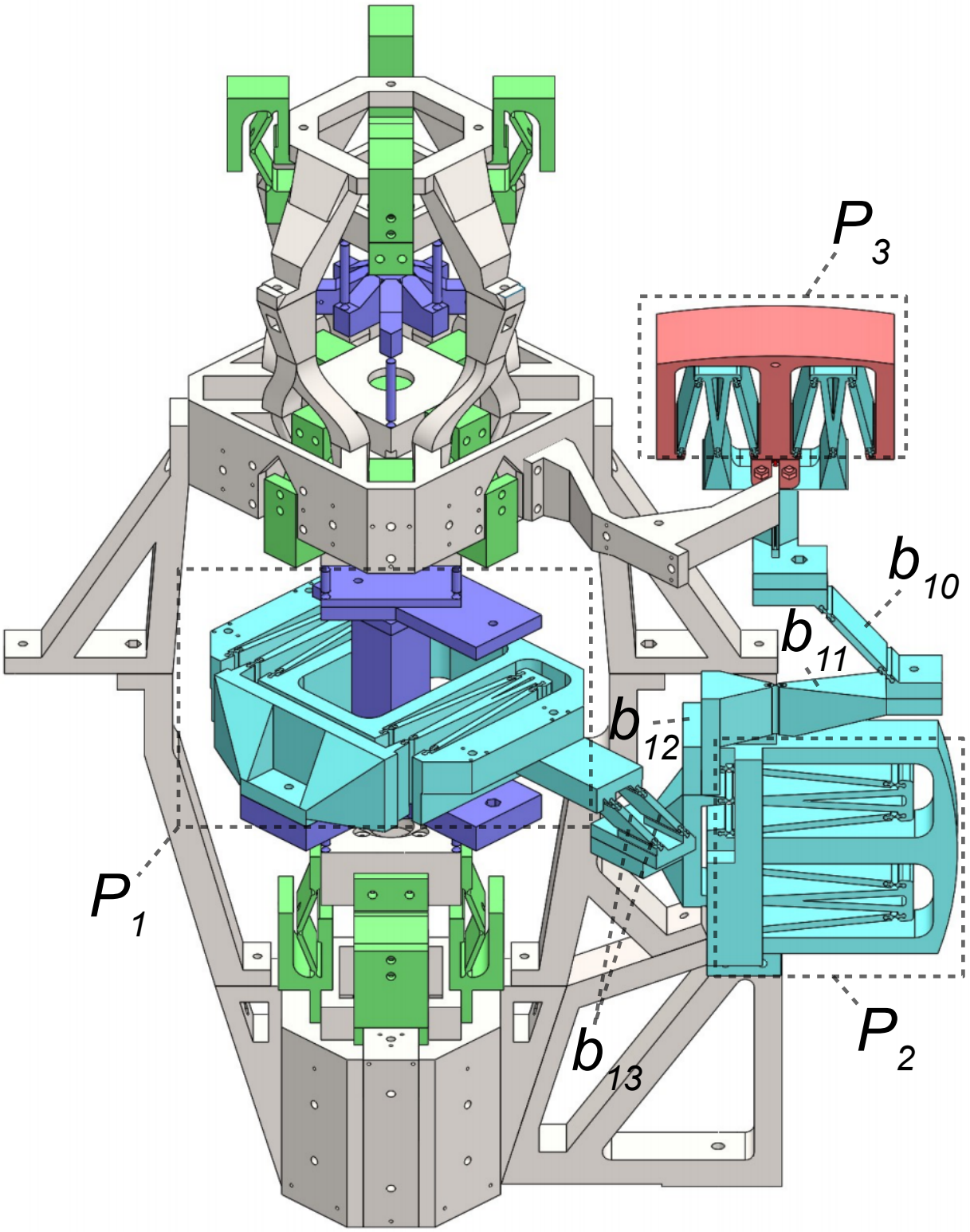

Figure G.10: View on X and Y transmission of the final design.

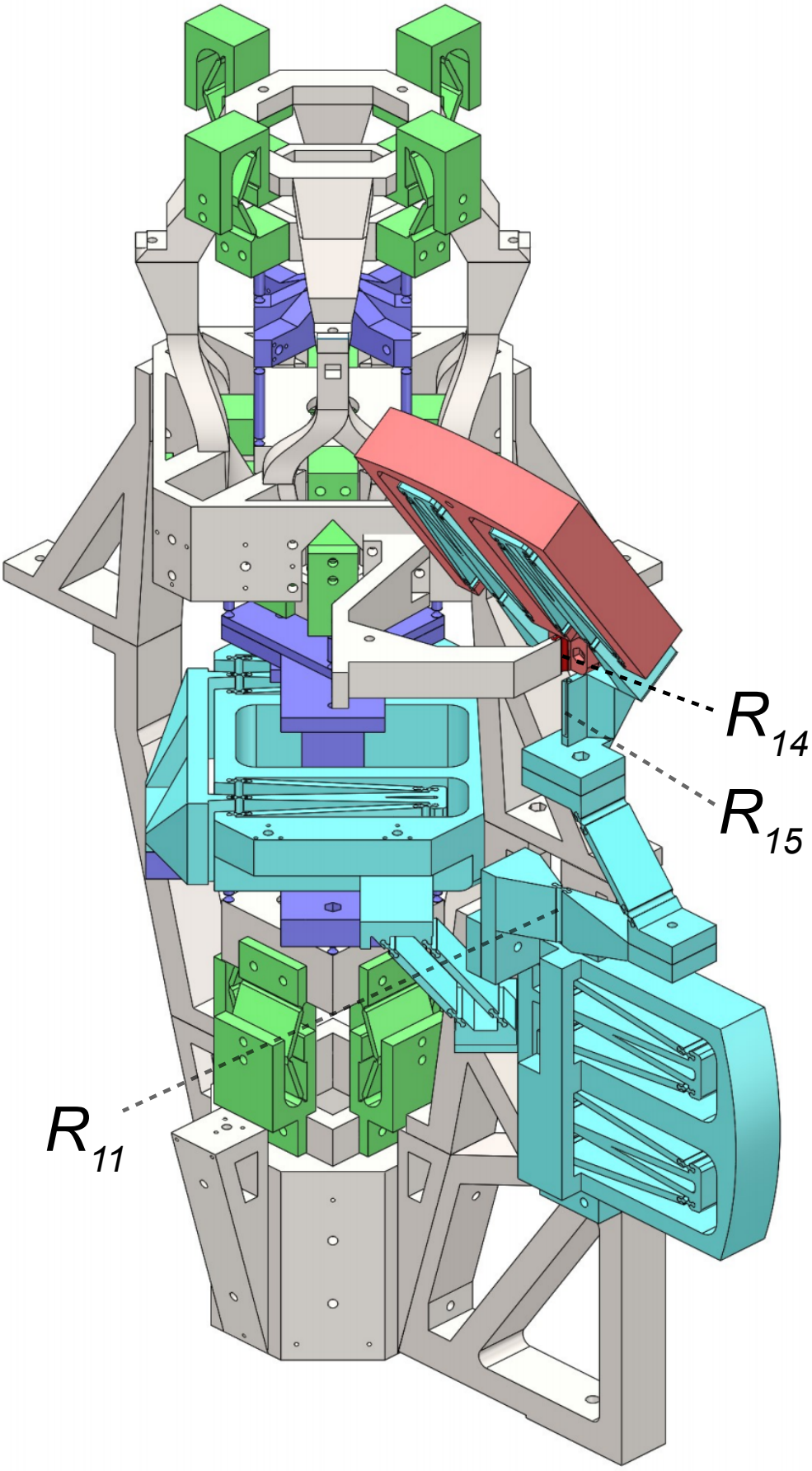

Figure G.11: View on X and Y transmission of the final design.

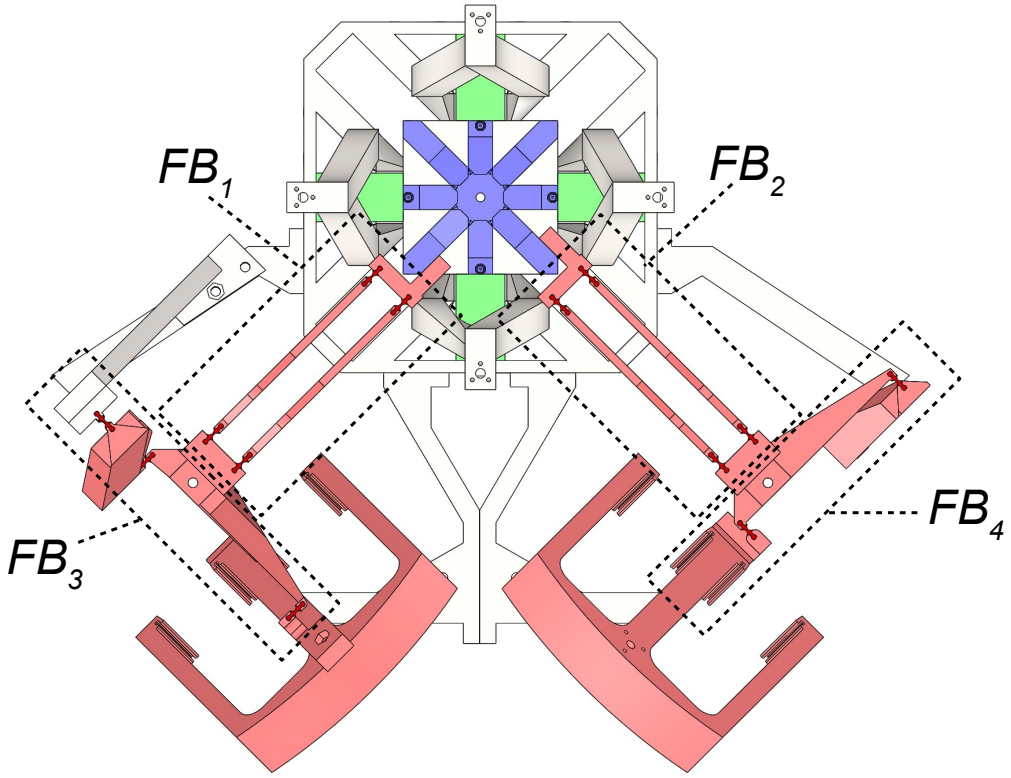

Figure G.12: Top view on the direction setpoint mechanism of the final design.

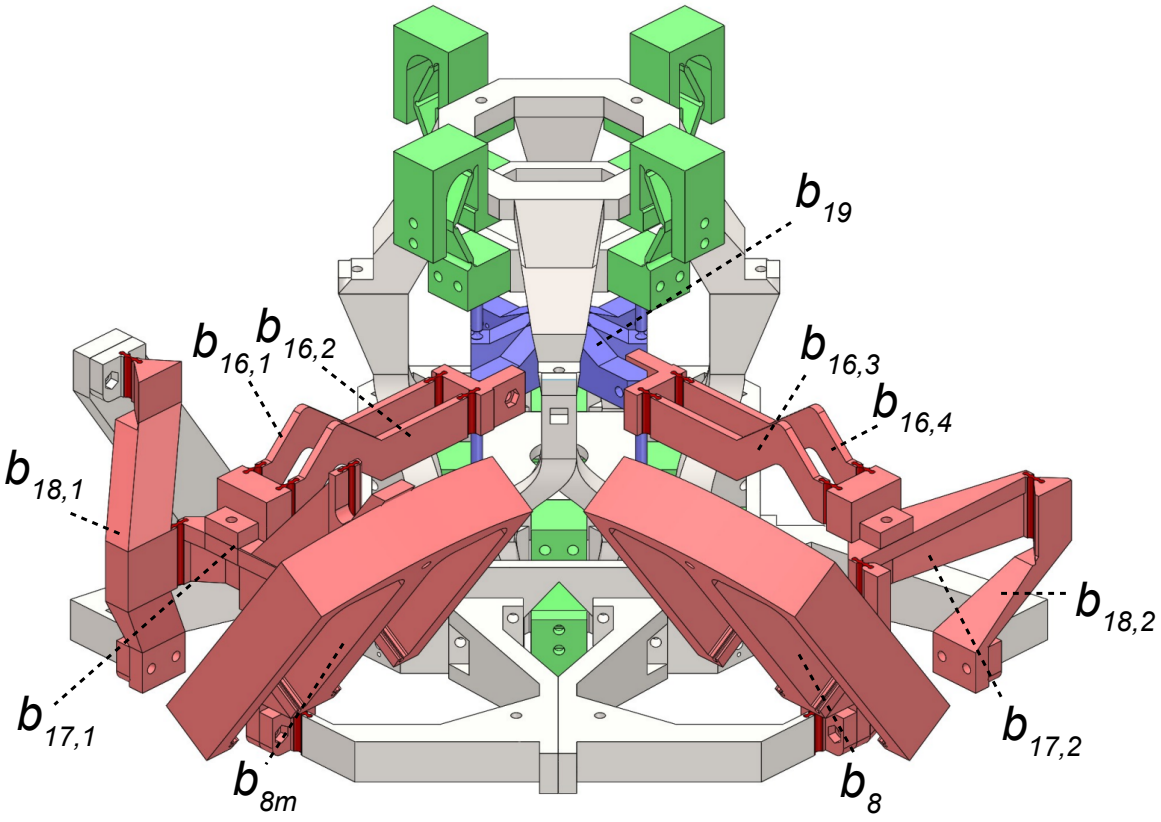

Figure G.13: View on the direction setpoint mechanism of the final design.

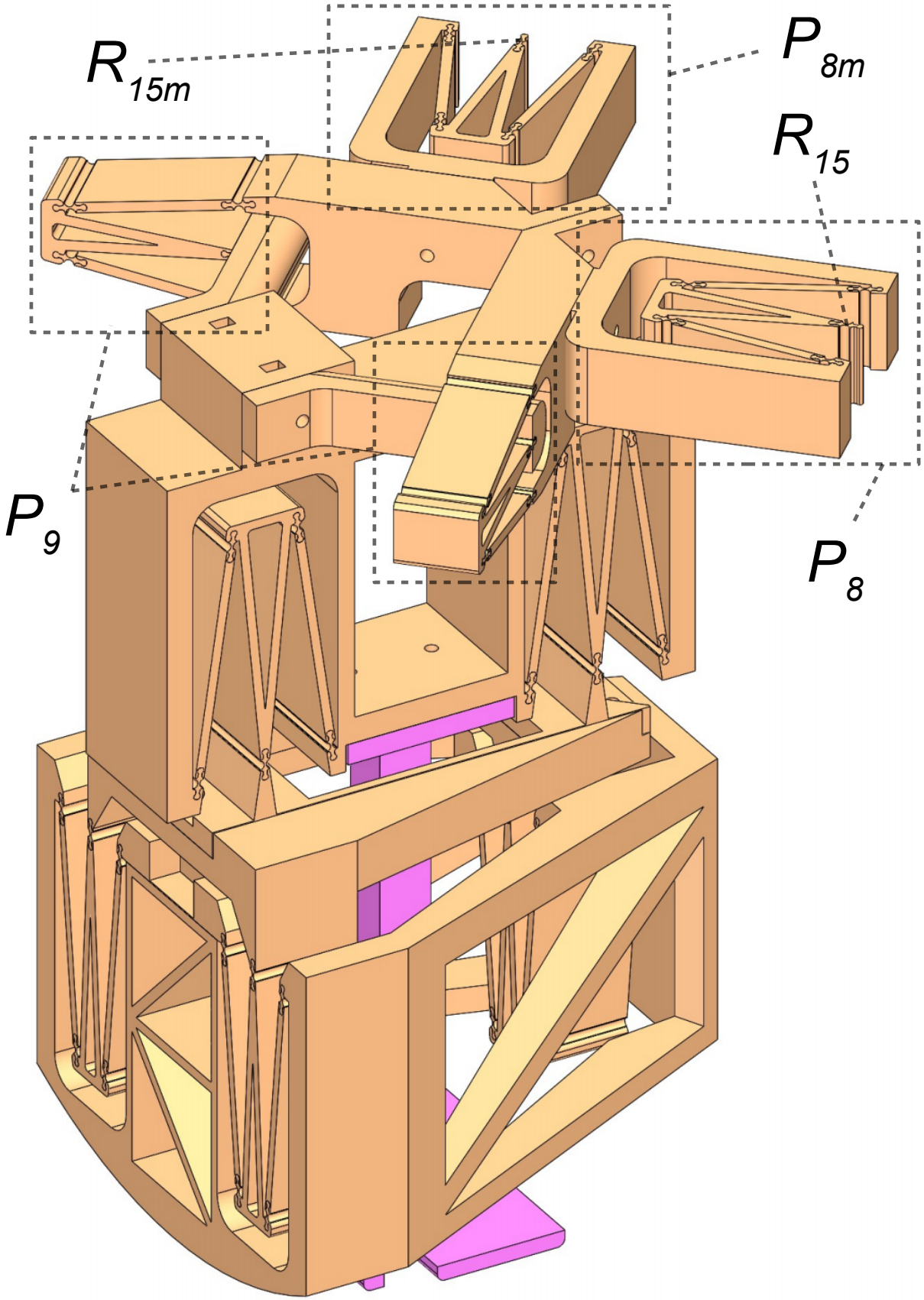

Figure G.14: 3D view on motion coupler of the final design.

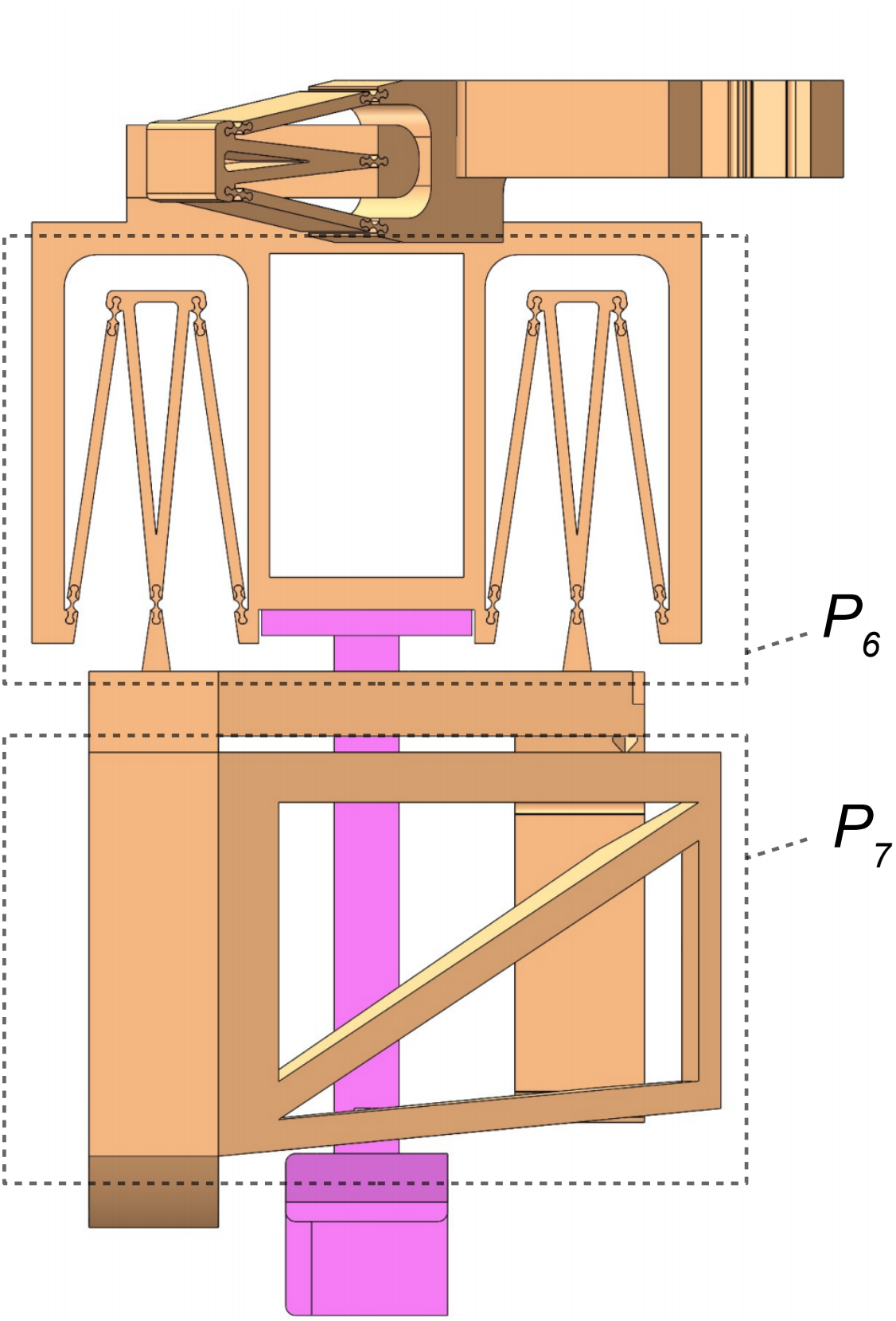

Figure G.15: Side view on motion coupler of the final design.

G.2.2 Pictures of the physical design

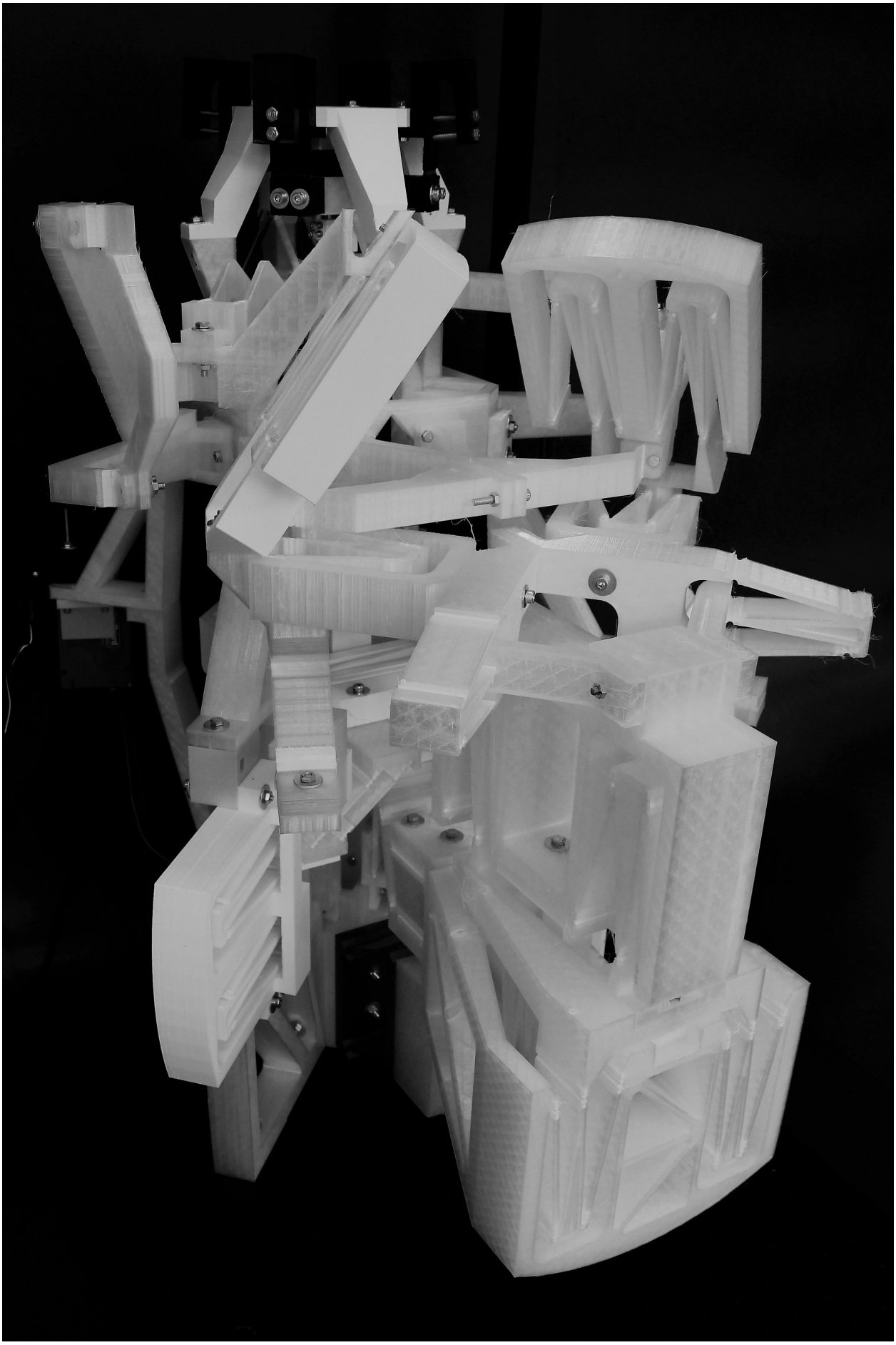

Figure G.16: Physical design, assembled.

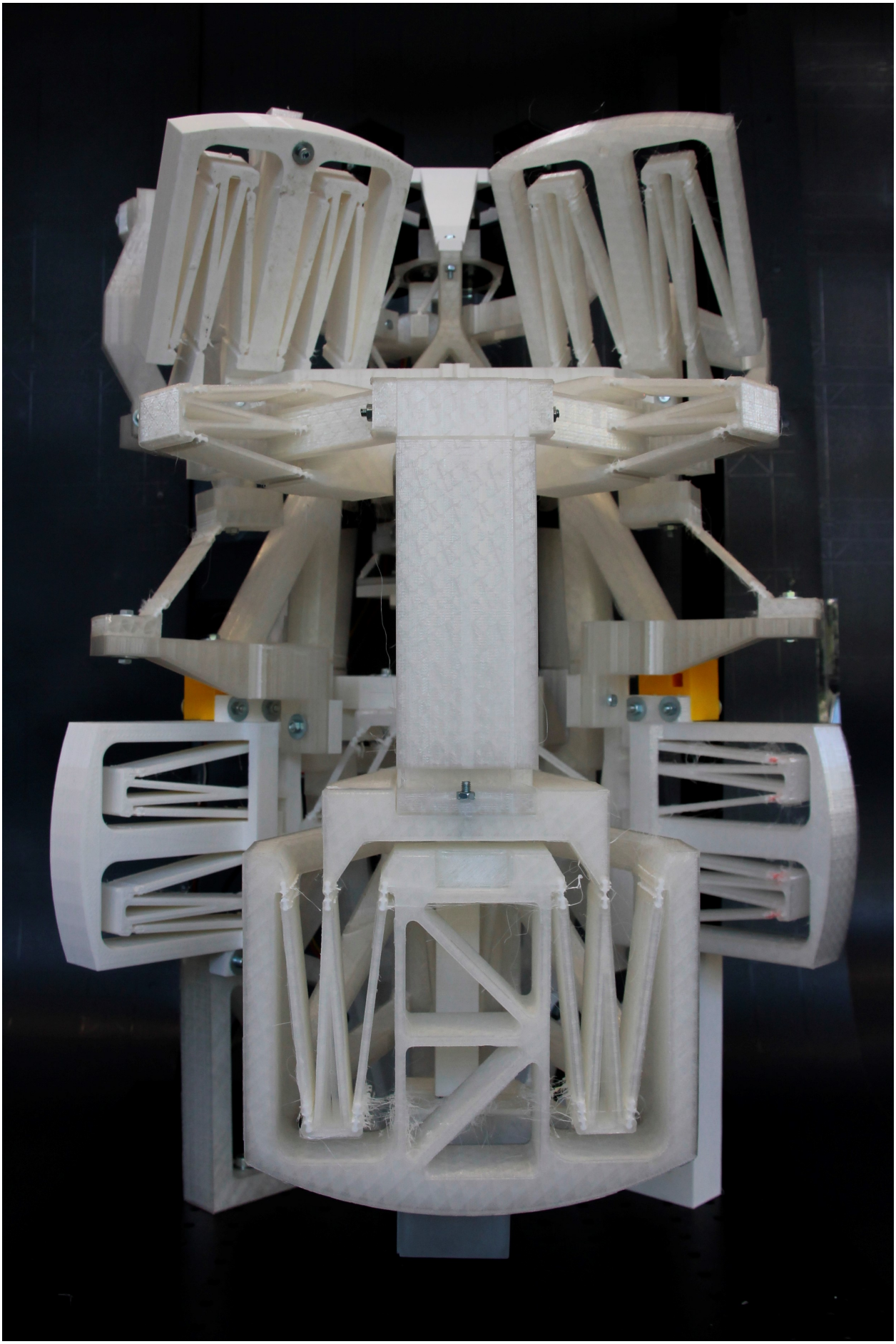

Figure G.17: Front view of physical design, assembled.

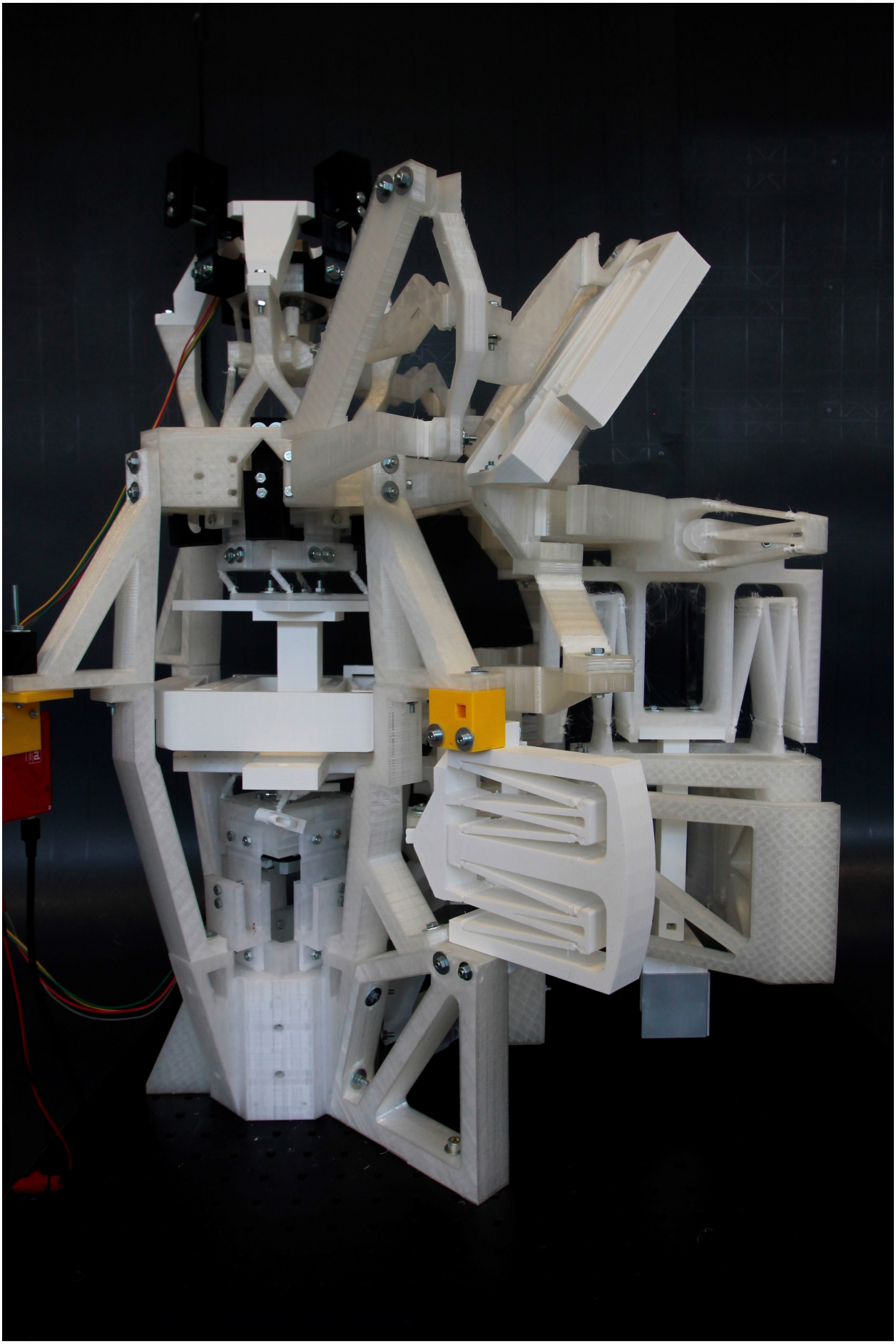

Figure G.18: Side view of physical design, assembled.

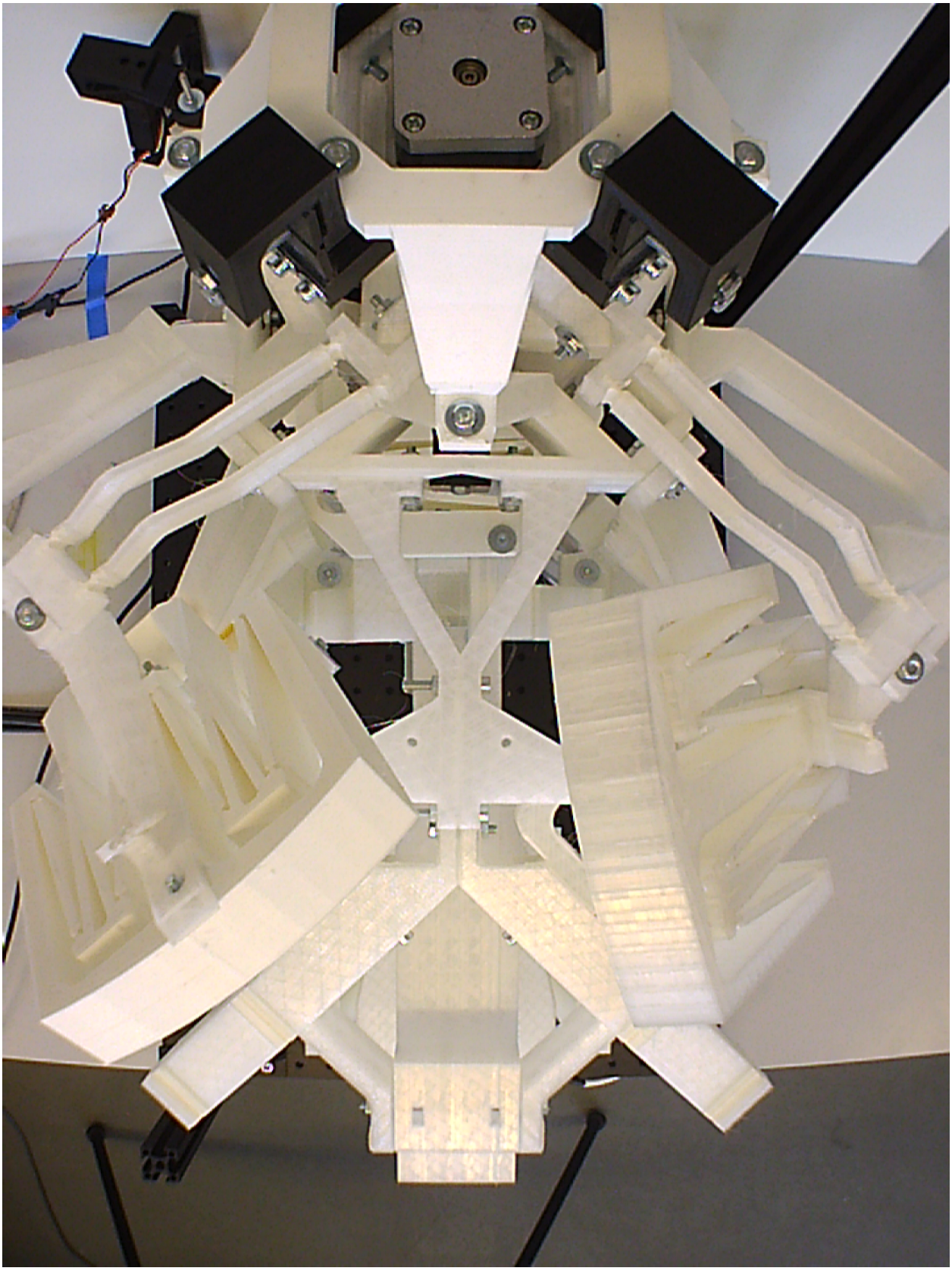

Figure G.19: Top view of physical design, assembled.